Torsional capacity of Lean Duplex Stainless Steel Semi-Elliptical Hollow Section members - a finite element study

A thesis submitted for the degree of

Doctor of Philosophy

by

Sanasam Vipej Devi

Department of Civil Engineering
Indian Institute of Technology Guwahati
Guwahati - 781 039, India

DECLARATION

I, Sanasam Vipej Devi, a PhD Scholar of Indian Institute of Technology Guwahati declare that the content of this thesis entitled "***Torsional capacity of Lean Duplex Stainless Steel Semi-Elliptical Hollow Section members - a finite element study***" submitted here is a partial fulfillment for the requirement of awarding the Degree for **Doctor of Philosophy** and submitted to Indian Institute of Technology Guwahati, India. This thesis is the documentation of the research work carried out by me at the institute in a period of **July, 2016 to September, 2019** under the supervision of ***Dr. Konjengbam Darunkumar Singh***, Professor, Department of Civil Engineering, Indian Institute of Technology Guwahati, India. I certify that the content of this thesis is the original one and has not been used for awarding any other degree. Moreover the thesis content has not been published by any other person. The published works done by others which I have consulted are always acknowledged in thesis by exact reference.

Date: (Sanasam Vipej Devi)

Place: IIT Guwahati Reg. No.: 166104041

CERTIFICATE

This is to certify that the work content in the thesis entitled by "***Torsional capacity of Lean Duplex Stainless Steel Semi-Elliptical Hollow Section members - a finite element study***" being submitted here by Ms**. Sanasam Vipej Devi** to Indian Institute of Technology Guwahati, India for the award of degree of **Doctor of Philosophy** is a record of genuine research work carried out by the aspirant as a PhD scholar under my supervision and guidance.

The Thesis work, in my opinion is worthy of considering for the award of degree of **Doctor of Philosophy** in accordance with the regulation of the Institute.

(Dr. **Konjengbam Darunkumar Singh**)
Professor
Department of Civil Engineering
Indian Institute of Technology Guwahati

Date:

Place: IIT Guwahati

Abstract

Lean Duplex Stainless Steel (LDSS) offers the combined benefit of low initial cost (due to low nickel content of ~ 1.5%) and relatively superior material property (high strength, good corrosion resistance, good weldability, fracture toughness etc.) and making LDSS as one of the promising grades of stainless steel family. It may be mentioned that, lean duplex stainless steel has been included for the first time in EN 1993-1-4 (2006) *via* a recent amendment (A1:2015). Adequate understanding of the LDSS material, its performance under various structural loadings and efficient design rules are vital to further disseminate the structural uses of lean duplex stainless steel members (such as LDSS tubular sections) among engineers and architects, in the construction domain.

Hence, in this thesis, a systematic parametric study was conducted on cold-formed lean duplex stainless steel (EN 1.4162 (LDX 2101) / UNS S32101) semi-elliptical hollow section members under torsion, using finite element (FE) analysis. Effects of geometric parameters of semi-elliptical hollow section *viz*. length of curve element, aspect ratio and size of section, and member length, on its torsional capacity were investigated. Based on the FE study, it was observed that, while higher curve length, higher section aspect ratio and lager section size were found to provide higher torsional capacity; member length was observed to affect the torsional capacity insignificantly. Based on the results obtained from the parametric study, torsion design equations were proposed, following the formats of EN 1993-

1-4: 2006+A1 (2015) and Direct Strength Method. Further, a new deformation based method (in line with Continuous Strength Method) was also proposed.

The study was extended to perforated cold-formed lean duplex stainless steel semi-elliptical hollow section members subjected to torsion. A single circular perforation at mid length of member, positioned either on flat or curve element of semi-elliptical hollow member, of varying perforation size were considered as parameters of the study. Influence of perforation on torsional capacity was assessed. Based on the parametric study, it was found that perforation on curve element is more deteriorating to member torsional capacity compared to the one on flat element. Additionally, the reduced torsional strength due to the influence of perforation was also seen to be dependent on perforation size and cross-section slenderness. Design equations were then proposed for perforated members (considering both perforation size and cross-section slenderness).

The study was supplemented by an investigation on the recovery of reduced torsional capacity (equivalent to that of unperforated torsional strength) for various stiffener patterns around perforation. Four different stiffener patterns (i.e. horizontal, vertical, square frame, ring) of various dimensions were adopted. Based on the study, it was found that, both square and ring stiffeners were able to achieve the unperforated strength, as compared to horizontal and vertical stiffeners. Based on the study for LDSS SEHS member, optimum stiffener dimensions capable of partial or full recovery of torsional capacity, were arrived.

Acknowledgement

This is to acknowledge all who has directly or indirectly supported me in any way through the course of my PhD work, without whose support, it would have been difficult to complete this thesis.

I would like to express my sincere gratitude to my supervisor **Prof. Konjengbam Darunkumar Singh**, Department of Civil Engineering, IIT Guwahati for his constant support throughout my PhD journey. His invaluable guidance, constant effort and encouragement has always been a great motivation to carry out and continue my research work. Besides, the lessons I have learned from him through the course of my research work will always help me in my future endeavours.

I am also thankful to Prof. Sudip Talukdar, Prof. K. S. R. Krishna Murthy, Dr. Amit Shelke, my doctoral committee members, for their invaluable guidance and suggestions from time to time that helped me shape my research work better.

I shall be thankful to Department of Civil Engineering, IIT Guwahati for allowing me to do research work and for providing me facilities.

My special thanks to my research group in IIT Guwahati - Gishan, Ricky, Narendra, Sukumar, Suman, Prashant and my seniors and friends - Devrani, Sophia, Rubi, Susma, for their companionship and emotional support during my stay at IIT Guwahati.

I am also thankful to my parents - Sanasam Mangi Singh and Lourembam Premabati Devi and my brothers - Sanasam Suvmanta Singh and Sanasam Mahesi Singh for their love, support and encouragement all the time.

Last, but not the least, I am thankful to the Almighty for the blessings and strength that led me continue my research work.

Sanasam Vipej Devi

Contents

Abbreviations and Notations

AISI	American Iron and Steel Institute
ARM	Arm Replacement Method
ASCE	American Society of Civil Engineers
AS/NZS	Australian/New Zealand Standard
ASTM	American Society for Testing and Materials
CHS	Circular Hollow Section
CSM	Continuous Strength Method
DBM	Deformation Based Method
DL	Dead Load
DSM	Direct Strength Method
EN	European Standard
FE	Finite Element
FEM	Finite Element Method
FEA	Finite Element Analysis

LDSS	Lean Duplex Stainless Steel
LL	Live Load
RP	Reference Point
SEHS	Semi-Elliptical Hollow Section
SFSM	Spline Finite Strip Method
SHS	Square Hollow Section
β	Target reliability index
ε	Strain
ε_{f}	Percentage strain at fracture
ε_{nom}	Engineering strain
$\varepsilon_{t0.2}$	Total strain at $\sigma_{0.2}$
ε_{true}^{pl}	True plastic strain
η	Shear area factor
θ	Twist
θ_{c}	Twist corresponding to critical torque
θ_{d}	Angle of diagonal tension field
θ_{u}	Twist corresponding to T_{u}
λ	Cross-section slenderness
$\bar{\lambda}_{p}$	Cross-section slenderness based on Continuous Strength Method

λ_T	Torsional slenderness
$\bar{\lambda}_w$	Cross-section slenderness based on European code
σ	Stress
$\sigma_{0.05}$	0.05% proof stress
$\sigma_{0.2}$	0.2% proof stress
$\sigma_{1.0}$	1.0% proof stress
σ_{true}	True stress
σ_{nom}	Engineering stress
σ_t	Tensile strength of plate
σ_u	Ultimate stress
τ_{cr}	Critical shear buckling stress
τ_t	Post buckling shear strength
τ_y	Shear yield stress
ν	Poisson's ratio
φ	Resistance factor
χ_w	Shear capacity reduction factor
A	Area enclosed by mid-line of section
b	Length of vertex from centre of semi-ellipse along minor axis
b_{eff}	Shear effective width

b_s	Width of stiffener
d_p	Diameter of circular perforation
$d_{p,f}$	Diameter of circular perforation on flat element
$d_{p,c}$	Diameter of circular perforation on curve element
E_0	Initial modulus of elasticity
$E_{0.2}$	Tangent modulus at 0.2% proof stress
f_y	Yield stress of steel material
F_M	Mean for fabrication factors
h	Length of vertex from centre of semi-ellipse along major axis
h_w	Clear distance between flanges
k	Shear buckling coefficient
l_c	Length of curve element of semi-elliptical hollow section
l_f	Length of flat element of semi-elliptical hollow section
l_f'	Length of flat element of non semi-elliptical hollow section
l_p	Length of plate
l_v	Anchorage length of stiffener
L	Length of member
M_M	Mean for material properties
n	Material non-linearity index

$n'_{0.2,1.0}$	Strain hardening exponent
R_f	Perforation reduction factor
$R_{f,f}$	Perforation reduction factor for perforation on flat element
$R_{f,c}$	Perforation reduction factor for perforation on curve element
R_t	Width-thickness parameter of single web panel
t	Thickness of semi-elliptical hollow section member
t_p	Thickness of plate
t_s	Thickness of stiffener
T	Twisting moment
T_{cr}	Elastic critical torsional buckling moment
T_u	Ultimate torsional capacity of unperforated member
T_{up}	Ultimate torsional capacity of perforated member
$T_{up\text{-}s}$	Ultimate torsional capacity of member with stiffened perforation
$T_{u,DSM}$	Design torsional capacity calculated using Direct Strength Method equation
$T_{u,DBM}$	Design torsional capacity calculated using Deformation Based Method equation
$T_{u,EN\text{-}modified}$	Design torsional capacity calculated using modified Eurocode equation
$T_{u,FE}$	Torsional capacity obtained from finite element model

T_y	Yield torque
V	Shear force
V_F	Coefficient of variation for fabrication factors
V_M	Coefficient of variation for material properties

List of figures

List of tables

CHAPTER 1

INTRODUCTION

1.1 Background

Application of stainless steel as a load bearing member in construction has increased considerably, despite its high initial cost, because of its structural advantages over carbon steel such as high strength to weight ratio leading to lighter construction, excellent corrosion resistance thus reducing maintenance requirement and associated cost, pleasing aesthetic appearance etc. Although its initial cost is relatively higher as compared to conventional carbon steel and other construction materials, total life cycle cost has been reported to be lower, thus making it an economical option for structural applications (Gardner, 2005). Moreover, recent development of Lean duplex stainless steel (LDSS) grade has curtailed the high initial cost of stainless steel, along with additional benefits of higher strength than commonly adopted austenitic stainless steel, good corrosion resistance and fracture toughness (Theofanous & Gardner, 2009). Further, good recycling and reuse potential of stainless steel is another favourable property, making it more sustainable, as compared to carbon steel (Rossi, 2014). Consequently, stainless steel becoming a viable alternative option as structural/construction material, has attracted attention of architects and engineers in the recent years.

Lean Duplex Stainless Steel (LDSS) is a family of duplex stainless steel with very low nickel content (~1.5%) and hence comparatively lower material cost (Theofanous & Gardner, 2009). It is characterised by relatively good mechanical properties, reduced cost (as compared to other grades of stainless steel) and comparable corrosion resistance with austenitic stainless steel (Baddoo, 2008; Theofanous & Gardner, 2009). Although it is comparatively new, LDSS grades (such as grade EN 1.4162 (LDX2101)) has seen applications in structural use and its demand has been growing (Baddoo, 2008; Huang & Young, 2014a). Application of LDSS can be seen in structures such as Kwandong Hockey Stadium in South Korea (exterior cover), Siena footbridge in Italy (girders and pylons), Doha International Airport in Qatar (roof), Likholefossen Bridge (all except concrete piers) in Norway, Sant Fruitos Bridge (all load bearing structural elements) in Spain and Sölvesborg Bridge (deck support, railing, arch) in Sweden as shown in Figure 1.1. Owing to its increased acceptance and hence necessity, LDSS grades have been recently introduced in the European design code EN 1993-1-4:2006+A1 (2015). Although study on LDSS sections are relatively scarce compared to other steels (such as carbon steel, austenitic steel etc.), attempts have been made by researchers to understand its structural behavior. Focus has been given by various researchers in the last decade to characterize its material properties and to understand its structural behavior under compression (Huang & Young, 2014b; Sachidananda & Singh, 2017; Theofanous & Gardner, 2009), bending (Hassanein & Silvestre, 2013; Sonu & Singh, 2017b; Theofanous & Gardner, 2010), combined loading (Huang & Young, 2014a) etc. However, it may be noted that as compared to other loading conditions, limited studies have been reported on torsion and hence its behavior is understudied. Study on torsional behavior of LDSS I beams (i.e. open section) was first reported by Lauwens et al. (2018). However, to the best of author's knowledge, no studies on torsional behavior of LDSS closed hollow section member have been reported yet.

In the structural engineering, torsional effects can arise due to eccentricity between centre of gravity and centre of resistance especially in asymmetric and irregular structures under ground motion, such as piers of curved and skewed bridges (Anumolu et al., 2016; Nie et al., 2012). Under eccentric lateral load and fluctuating wind forces, tall buildings are also susceptible to torsional load (Nadjai & Johnson, 1998; Tallin & Ellingwood, 1985). Under such structural configuration, component members or elements may come under the influence of torsion. Hence, studies have been conducted to understand the behavior of structural elements and members, such as hollow steel sections, concrete filled steel hollow members, steel I-section etc. under torsion (e.g. Beck & Kiyomiya, 2003; Lauwens et al., 2018; Ridley-Ellis, 2000).

Closed hollow sections are efficient torsional members because of its high torsional rigidity (approximately 200 times that of open section). Additionally, closed hollow sections offer advantages such as reduced protection requirement, low drag coefficient, potential of internal hollow void to be used for various purposes (Wardenier et al., 2002). Owing to its various advantages, closed hollow sections have found numerous structural applications in buildings, bridges, offshore structures, towers and masts etc. Possibility of achieving high strength and improved fire resistance by filling the internal void of hollow steel members by concrete has made it a suitable choice of architects and engineers in high rise constructions (Nie et al., 2012; Wardenier et al., 2002).

In the construction industry, traditionally, circular hollow section (CHS) and rectangular hollow sections (RHS) are being commonly adopted, essentially due to long experience and availability of codal design guidelines (Chan & Gardner, 2008). However, in recent years, relatively new and interesting section shapes with pleasing appearance such as elliptical (or oval), flat oval, semi-flat oval (also known as tunnel section) and semi-elliptical have also been introduced (see Figure 1.2). Being a closed section, they offer high torsional resistance and other typical

advantages of tubular sections mentioned above. In case of semi-elliptical hollow section (SEHS), the flat element makes it easier in establishing connections with other structural elements such as SHS, RHS etc. SEHSs also possess close major and minor bending moduli, thus, making them efficient when subjected to simultaneous bending moments about major and minor axes (Nowzartash & Mohareb, 2010). Although new, their applications can now be seen in the construction industry, particularly as exposed members e.g. Heathrow Airport (Figure 1.3a) and Stratford DLR Station (Figure 1.3b) in London, United Kingdom; and Garden City in Shenzhen, China (Figure 1.3c). Although an increasing interests on such sections can be seen in the literature (see e.g. Chan & Gardner, 2008; Nowzartash & Mohareb, 2010; Sachidananda & Singh, 2015; Zhu & Young, 2010), reported literature on their structural performances are relatively still limited.

Perforations (or cutouts or holes or openings), becomes inevitable on the structural members, for various reasons such as electrical and plumbing services, ease of maintenance, aesthetics, connections and other purposes (Hagen et al., 2009; Lawson et al., 2015; Yu & Davis, 1973). Perforations or openings may be of different shapes i.e. circular, rectangular, elliptical etc. Some applications of perforation in structural members are shown in Figures 1.4a - 1.4d. Introduction of these perforations have been reported to deteriorate the member capacity, depending on several factors *viz*. size, position, number of perforation etc., (Lawson et al., 2015; Moen & Schafer, 2008). However, it may be noted that studies reported on perforated torsional members are limited.

Where perforation is inevitable for reasons mentioned above, a common measure adopted to compensate the reduced capacity of member is to reinforce the perforation by using stiffeners (see e.g. Figures 1.4e and 1.4f with vertical and horizontal stiffeners) around the perforation. Investigations on the various patterns/configurations such as ring (e.g. Jiao et al., 2018), rectangular (e.g. Alsalah

et al., 2017), horizontal (e.g. Sivakumaran, 2008), vertical (e.g. Alsalah et al., 2017), inclined (e.g. Cheng & Li, 2012) etc., and types such as flat (e.g. Dimopoulos & Gantes, 2012; Alsalah et al., 2017), plate (e.g. Mahendran & Keerthan, 2013) etc. of stiffeners at the periphery of perforation, have been reported, under bending (e.g. Dimopoulos & Gantes, 2012), compression (e.g. Alsalah et al., 2017), shear (e.g. Cheng & Li, 2012) etc.

Ring stiffener is another type of stiffener arrangement which has been found to be commonly adopted (Jiao et al., 2018). It is important to study the effect of different stiffener parameters such as configuration, position, thickness etc. on its recovery capacity, and also determine the most effective stiffener and corresponding optimum size. However, it may be noted that study on stiffening effects on torsional capacity of perforated member has not been reported yet, to the best of author's knowledge.

1.2 Objectives

The main objective of the study is to investigate the torsional behaviour of lean duplex stainless steel (LDSS) unperforated and perforated semi-elliptical hollow section (SEHS) members under torsion, using finite element analyses. The study has been categorised into three main objectives as given below:

1. To study the torsional behaviour of unperforated LDSS SEHS members subjected to torsion, considering the effects of various geometrical parameters such as flat length, curve length, aspect ratio, size of cross section, member length etc. on its ultimate torsional capacity.
2. To assess the effects of perforation size and location, on the torsional behaviour of perforated LDSS SEHS members with single circular perforation.

3. To investigate the stiffening effect and effectiveness of different types of stiffeners *viz*. horizontal, vertical, square frame and ring on torsional capacity of single circular perforated LDSS SEHS members.

1.3 Thesis Outline

The research work presented in the thesis has been organised into 6 chapters, along with two appendices. Brief descriptions of the chapters are presented below:

Chapter 1 briefly introduces the background of the current study including the objectives of the work and a thesis outline. Relevant topics of this work *viz*. LDSS, Torsion, Closed hollow section and Perforation, concerning structural applications, are briefly introduced, to shape-up the research direction.

Chapter 2 provides the literature review pertinent to the present work. Literature review on various studies related to structural behaviour of LDSS members, torsion of steel members, perforated steel members, steel design provisions for torsion, and numerical modelling of thin walled metallic/steel members are presented. A summary of all the literature review is then provided at the end of the chapter.

A finite element study on LDSS SEHS member subjected to torsion is presented in **Chapter 3**. Results of the parametric study on the effects of various geometrical sectional parameters *viz*. length of curve element, aspect ratio and size of SEHS, and member length, on the ultimate torsional capacity of LDSS SEHS members are shown. Further, design rules have been developed, based on the formats of European code, Direct Strength Method and a Deformation Based Method.

The study was further extended in **Chapter 4** to perforated LDSS SEHS members under torsion, considering a single circular perforation at mid length of member, either on flat or curve element of SEHS. Effect of perforation size was assessed and

perforation reduction factors were proposed to determine torsional capacity of perforated LDSS SEHS members.

In **Chapter 5**, effectiveness of different stiffeners such as horizontal, vertical, square frame and ring stiffener in recovering reduced torsional capacity due to perforation was investigated, for LDSS SEHS members with perforation located at mid length. Optimum stiffener dimensions that can result in maximum recovery of torsional capacity was also determined.

The important conclusions of the thesis work are summarised in **Chapter 6**. Possible future scopes of study are also provided.

Sample calculations of proposed design torsional strength for unperforated and perforated LDSS SEHS members are provided in Appendices A and B respectively.

(a)

Kwandong Hockey Centre, South Korea
(www.worldstainless.org)

(b)

Siena Footbridge, Italy
(www.nickelinstitute.org)

(c)

Doha International Airport, Qatar
(www.imoa.info)

(d)

Likholefossen bridge, Norway
(www.outokumpu.com)

(e)

Sant Fruitos Bridge, Spain
(www.outokumpu.com)

(f)

Sölvesborg Bridge, Sweden
(www.outokumpu.com)

Figure 1.1: Application of LDSS seen in (a) Kwandong Hockey Centre, South Korea, (b) Siena Footbridge, Italy, (c) Doha International Airport, Qatar, (d) Likholefossen Bridge, Norway, (e) Sant Fruitos Bridge, Spain and (f) Sölvesborg Bridge, Sweden

Elliptical
(www.alibaba.com)

Semi-elliptical
(Nowzartash & Mohareb, 2010)

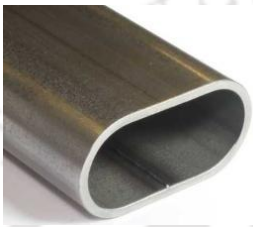

Flat oval

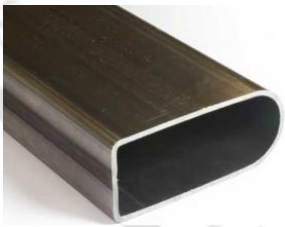

Semi-flat oval (or Tunnel)

(www. steeltubedirect.co.uk)

Figure 1.2: Relatively new structural steel sections available in construction industry

(a)

Heathrow Airport Terminal 5
(www.tboake.com)

(b)

Stratford DLR Station, London
(www.tboake.com)

(c)

Garden City in Shenzhen, China
(Chen & Young, 2018)

Figure 1.3: Elliptical hollow sections in (a) Heathrow Airport Terminal 5, London, (b) Stratford DLR Station, London and semi-flat oval (or tunnel) sections in (c) Garden City in Shenzhen, China

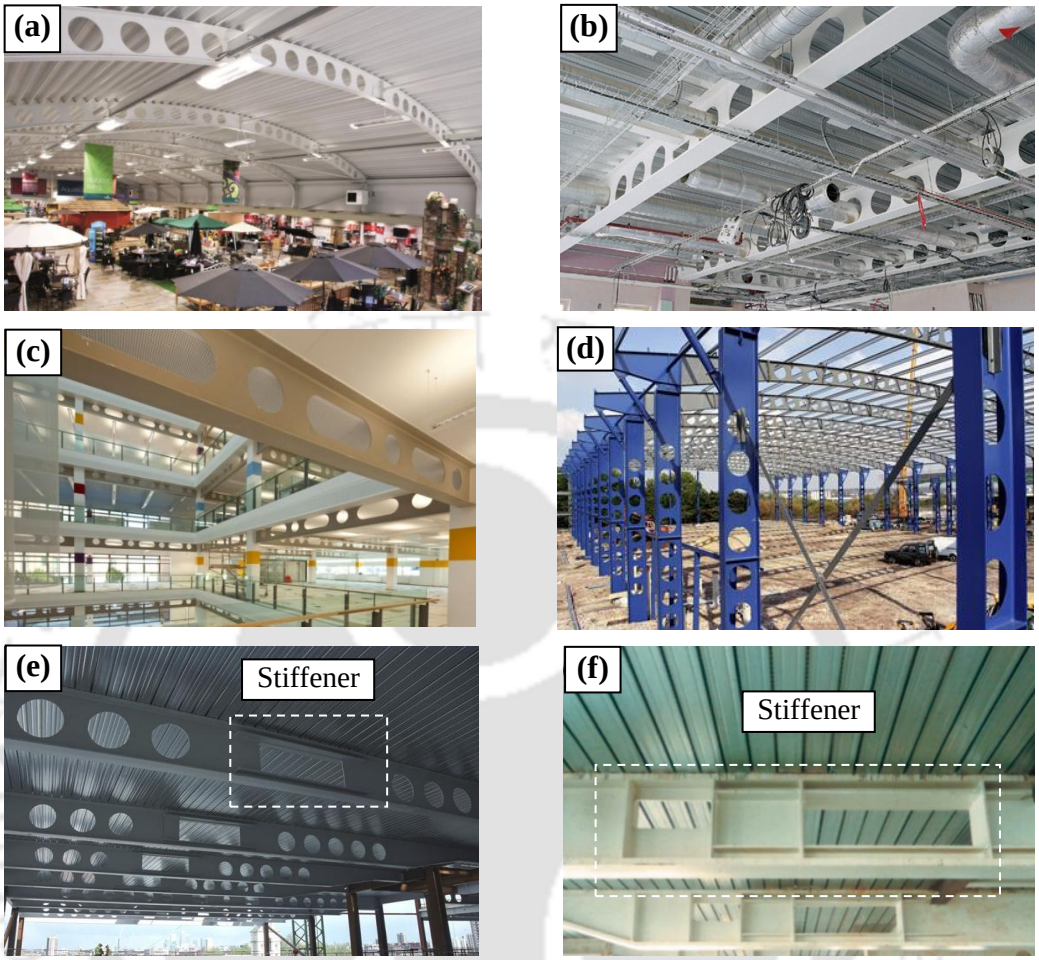

Figure 1.4: Structural members with perforation of varying configuration, without stiffeners (a-d) or with stiffeners (e, f) (www.steelconstruction.info)

CHAPTER 2

LITERATURE REVIEW

2.1 Introduction

This chapter provides a literature review on past investigations which are pertinent to the current research work on the torsional behavior of Lean Duplex Stainless Steel (LDSS) Semi-Elliptical Hollow Sections (SEHS) members under torsion. The literature review mainly focuses on the structural behavior, and is presented under the following sub-headings: a) LDSS members, b) torsion of steel members, c) perforated steel members, d) steel design provisions for torsion, and e) numerical modelling of thin walled metallic/steel members. Further, as the current study is on Semi-Elliptical Hollow Section (SEHS) members (i.e. closed hollow section), the literature review is primarily aimed at those investigations relevant to closed hollow steel sections.

An overview of studies on Lean Duplex Stainless Steel (LDSS) closed hollow section members is initially presented. This is followed by a review on investigations reported on torsional performance of structural steel members. Studies carried out on perforated steel members subjected to shear loading and torsion (also a case of shear loading) are presented next. Existing codified provisions, proposed design methods and equations including relatively new

method such as Direct Strength Method (DSM) for shear loading and torsion are briefly mentioned. A summary of all review is provided at the end of this chapter identifying present research directions.

2.2 Lean Duplex Stainless Steel hollow members

As stated earlier, although relatively new, lean duplex stainless steel (LDSS) has captured attention of engineers and architects because of its superior properties (mentioned in Section 1.1) over other grades of stainless steel and carbon steel. Consequently, there has been considerable progress in research work pertinent to LDSS in the last decade with attempts to understand the structural behavior of LDSS structural members) and also, to adapt existing design rules or propose new design equations for LDSS members (e.g. Huang & Young, 2013a; Saliba & Gardner, 2013a; Sonu & Singh, 2017b; Theofanous & Gardner, 2009). Structural behaviour of cold-formed LDSS closed hollow section members under compression has been investigated and reported by various researchers e.g. Anbarasu & Ashraf (2017); Huang & Young (2013b); Patton & Singh (2012); Sachidananda & Singh (2017); Theofanous & Gardner (2009). Performances of LDSS hollow section beams under flexure (e.g. Huang & Young, 2013a, Theofanous & Gardner, 2010) and shear (e.g. Sonu & Singh, 2017b), combined flexure and compression (e.g. Huang & Young, 2014a, Zhao et al., 2015) have been also been evaluated. However, it has been seen that studies on LDSS members under torsion are very limited. Lauwens et al. (2018) reported on the study of LDSS I section (i.e. on open section) subjected to pure torsion.

2.3 Torsion of steel members

Torsional behaviour studies of carbon steel members for both open (e.g. Basler, 1960; Bian et al., 2016; Chen & Trahair, 1992; Mohareb & Nowzartash, 2003) and closed sections (e.g. Aisyah Mohd Zaifuddin et al., 2017; Chen & Wierzbicki, 2000; Ridley-Ellis, 2000; Sezawa & Kubo, 1931) are available in literature. As mentioned in the previous section, very limited study has been reported on stainless steel (or LDSS) members subjected to pure torsion (e.g. Lauwens et al., 2018). Moreover, torsional performance of relatively newer cross-section such as elliptical, semi-elliptical, flat oval etc. has not been addressed yet.

Initial studies on buckling analysis of tubes under torsion were carried out by Schwerin (1924); Sezawa & Kubo (1931); Lundquist (1932) etc. Lundquist (1932) conducted experiments on thin-walled duralumin cylinders subjected to pure torsion and proposed a simple equation to calculate shear stress at failure. Donnell (1933) developed a theoretical formula to calculate critical shear stress for a thin-walled round tube under torsion, and compared it with experimental results performed earlier by other researchers (e.g. Lundquist, 1932; Sezawa & Kubo, 1931). Theoretical values of critical stress were found to be slightly higher than that of experimental values. Further studies to improve theoretical solution for buckling and post buckling behavior of thin cylinders under torsion were reported by Batdorf et al. (1947), Yamaki & Matsuda (1976) and Zhang & Han (2007) etc.

Mahendran & Murray (1990) carried out experimental study on steel box columns under pure torsion and torsion combined with other loads like axial compression. Test results were compared with ultimate strength prediction by available shear based plate girder theories and code provisions. The compared plate girder theories were found to overestimate ultimate torsional strength of box columns.

White et al. (1993) proposed equations to predict ultimate capacity of steel square hollow section subjected to torsion and bending using elastic and rigid-plastic

analysis approaches. Experiments were also conducted on closed-hat square section under pure torsion, bending and combined action of torsion and bending. The proposed theoretical ultimate strength was compared with the test results. Interaction equations for torsion and bending were also verified with the experimental results.

Ridley-Ellis (2000) conducted experimental and numerical studies on both hot rolled and cold formed unperforated and perforated (with single and double circular perforations) carbon steel rectangular hollow section members subjected to pure torsion. Failure mechanisms of perforated member under torsion loading were analysed. It was found that introducing perforation can significantly influence torsional capacity and stiffness of hollow rectangular members. Further, it was seen that the numerical (or finite element analysis) results provided relatively good agreement with the test data for smaller sections or small scale test, however for larger sections or large scale tests numerical models predicted higher values (ranging from ~ 1% - 20%). Based on the study, design recommendations were made for perforated rectangular hollow members under torsion.

Beck & Kiyomiya (2003) carried out experimental and numerical studies on circular hollow carbon steel, concrete and composite column under pure torsion. Based on the study, local buckling failure mode was seen in hollow steel column under pure torsion. Further, torsional capacity was found to be much higher in composite column than summation of individual capacity of steel and concrete column. Additionally, ductility of composite column was observed to be improved than hollow steel column. Comparison of the numerical and experimental results, showed fairly good agreement.

Han et al. (2007) investigated numerically hollow and concrete filled circular and square steel tubes subjected to pure torsion. Steel hollow tubes were observed to buckle outward along an angle of 45° to the axial direction under pure torsion, while no obvious buckling was seen in concrete filled tubes.

Huang et al. (2013) performed numerical and experimental investigations on hollow and concrete filled double skin carbon steel tubular members under pure torsion. At failure, inward buckling was found in the outer steel tube of double skin hollow tubular member. However, such buckling was observed to be absent in concrete filled double skin tubes due to confinement effect provided by the sandwiched concrete between the outer and the inner tubes.

Aisyah Mohd Zaifuddin et al. (2017) conducted a finite element study on multicorner tubes to evaluate its maximum torsional capacity. Based on the study, three different mechanisms of sectional collapse - elastic buckling, plastic yielding and plastic flattening of cross-section were identified. Elastic buckling was perceived in members having sufficiently small thickness to width ratio. For large thickness to width ratio and small strain hardening coefficient, plastic yielding dominated the failure mode while plastic flattening prevailed in cases of large thickness to width ratio and large strain hardening coefficient. Equations to estimate torsional capacity in each mode was also proposed.

2.4 Perforation in structural members

Structural behavior of perforated steel members have been investigated by several researchers to examine the effects of compression (e.g. Feng & Young, 2015; Moen & Schafer, 2008; Shanmugam, 1997; Singh & Singh, 2018), shear loadings (e.g. Lawson et al., 2015; Mahendran & Keerthan, 2013; Narayanan & Der Avanessian, 1984; Pham, 2017) etc. However, limited study has been reported on perforated steel tubular members under torsion. Further, most of the studies reported are on perforated carbon steel plates or open channel sections, with limited study on closed hollow section members or stainless steel members. In this section, investigations on perforated members (both open and closed sections) subjected to

shear loading or torsion only are presented. The literature on shear loadings is also included in the review, as torsional failure is due to shear effects.

Narayanan & Der-Avanessian (1984) presented a numerical investigation on elastic buckling behaviour of perforated square and rectangular plates subjected to shear loading. Various parameters such as shape (circular, square, rectangular), size and location (along tension and compression diagonal) of perforation on different plate dimensions and edge support conditions (simply supported and clamped) were monitored. Based on the study, a linear variation in shear buckling coefficient was observed with increasing size of central perforation irrespective of boundary condition. Approximate values of shear buckling coefficient of perforated plates were proposed based on the results obtained from the numerical study. Further, shear buckling coefficient was found to be improved when the perforation is located away from centre of plate along the compression diagonal, especially in case of clamped edge condition. However, along the tension diagonal, ~ 20% reduction in shear buckling coefficient was observed as perforation moved from centre towards corner for plates with clamped edge condition. Later, Narayanan & Der-Avanessian (1985) developed a method to calculate ultimate shear capacity of a plate girder having central circular perforation in the web.

Narayanan & Chow (1985) conducted experiments on thin webs with square and circular central and eccentrically placed perforation subjected to shear loading. Effect of perforation size (diameter ranging from 0.1 to 0.6 times web depth) and position (along tension and compression diagonal) on buckling and ultimate loads were examined. Both buckling coefficient and ultimate load were observed to reduce as perforation diameter increases. Further, perforation position/location was found to be insensitive to ultimate load in case of single perforation. However, location effects were seen to be higher when located in tension diagonal for the case of plates with two perforations on opposite sides of tension diagonal.

Theoretical equations to determine ultimate load and buckling coefficient for perforated plates were also proposed.

Cooper & Roychowdhury (1990) reported developed design equations for shear strength of plate girders with web rectangular perforation based on Basler's theory (Basler, 1960), wherein shear strength is determined by combination of web shear strength and shear contribution by tension field action. The proposed design equations were assessed with available test results. However, the proposed equations were found to provide a conservative estimate.

Ridley-Ellis (2000) conducted experiments on hot rolled and cold formed perforated carbon steel rectangular hollow section members subjected to pure torsion. Both single and double circular perforations of varying size were considered for the study. Failure mechanisms of perforated member under torsion loading were analysed. Based on the study, torsional capacity and stiffness were found to reduce with increasing perforation sizes. Additionally, design recommendations were proposed for perforated rectangular hollow section members under torsion.

Pellegrino et al. (2009) carried out a numerical study on perforated rectangular plates having different aspect ratio under shear loading. Parameters considered for the study were size, shape (circular and rectangular), position and orientation of perforation along main axes for different slenderness of panel. Based on the study, shear buckling coefficient was seen not to be particularly influenced by position and orientation of perforation, while diameter of perforation was observed to be a critical factor. For thicker panels, aspect ratio of plate was found to have insignificant effect on critical shear stress, while square plate was seen to have higher critical stress compared to rectangular plate in case of slender panels.

Keerthan & Mahendran (2013) investigated shear behaviour of perforated cold-formed lipped channel beams via experimental study. Test results were compared

with available shear design rules for perforated web in AS/NZS 4600 (2005), LaBoube et al. (1997), Keerthan & Mahendran (2012) and McMahon et al. (2008), and it was found that design equations were unsuitable for lipped channel beams with web perforation. Hence, new design proposals for shear capacity reduction factor were made and were found to be in good agreement with the experimental results.

Lawson et al. (2015) investigated experimentally and numerically stainless steel C section beams with multiple circular perforations subjected to shear and bending. Different failure modes were identified mainly based on spacing of perforations in the web. Based on the study, beams with widely spaced perforations were observed to fail by Vierendeel bending with local buckling, while web-post buckling dominated in closely spaced perforations. A method for calculating local normal and shear stress around perforation was also proposed for stainless steel C sections with web perforation.

Pham (2017) conducted buckling study on perforated square plates having central circular and square perforation subjected to uniform pure shear using Spline Finite Strip Method (SFSM) and Finite Element Method (FEM). Based on the study, reduction in shear buckling coefficient with increase in perforation size was found to be higher in square perforation as compared to circular ones. Using the results from the buckling analysis, equations to estimate shear buckling coefficient of perforated plate with square or circular perforation were proposed. Using similar approach, study was extended further to thin-walled channel sections with centrally located perforation subjected to shear loading. Design equations for shear buckling coefficient were then proposed for thin-walled channel sections containing central circular and square perforations.

Sonu & Singh (2017a) reported a numerical study on shear behaviour of perforated LDSS hollow rectangular beams. Effects of size and position of single circular perforation on shear behaviour of LDSS rectangular beam were investigated. From

the study, reduction in shear capacity with increase in perforation size was observed to be more pronounced in slender webs compared to stocky ones. Further, changing perforation position along longitudinal and transverse axes and tension diagonal seem to have insignificant effect on shear capacity. On the other hand, reduction in shear capacity was found to be maximum at the central position of compression diagonal and it gets smaller as perforation moved away from central region.

Wanniarachchi et al. (2017) carried out a numerical study on shear behaviour of cold-formed steel lipped channel beams with non-circular (elliptical, square and rectangular) web perforations. Effects of web yield stress, web thickness and perforation depth on ultimate shear capacity were examined. Results from the parametric study were compared with available design equations in LaBoube et al. (1997), AS/NZS 4600 (2005), Keerthan & Mahendran (2012). The compared equations were found to be conservative or unsafe. Hence, equations were proposed to determine shear capacity of cold-formed perforated members with non circular web opening based on a shear capacity reduction factor. Design equations for Direct Strength Method (DSM) were also proposed.

2.4.1 Stiffened perforation

Stiffening boundaries of perforation is a practical and economic measure adopted to compensate reduction in capacity due to perforation. Different types of simple (e.g. vertical, horizontal patterns) and complex (e.g. ring, square, doubler plate patterns) stiffeners around the perforation can be adopted (Alsalah et al., 2017; Hagen et al., 2009; Mahen Mahendran & Keerthan, 2013; Sonu, 2016). Examples of simple stiffener are shown in Figures 1.4e and 1.4f. However, such studies on the effects of stiffeners on perforated hollow steel member are found to be very limited, especially, to the best of author's knowledge, no studies have been reported for perforated stainless steel members under torsion. Hence, in this sub-

section, studies on stiffened perforation of both open and closed sections under shear loading are briefly reviewed.

Narayanan & Der Avanessian (1984) conducted a finite element analysis on shear buckling behaviour of square plates containing stiffened central circular or square perforation. Thickened plate elements were employed as reinforcement around the circular perforation and two strips of thickened element above and below the square perforation. From the analysis, it was observed that the critical shear buckling stress of unperforated plate can be easily achieved by the perforated plate with a small size of reinforcement around the opening. Larger size of perforation was seen to increase the shear buckling stress considerably than that of unperforated plate.

Sivakumaran (2008) performed experiments on perforated cold-formed steel joists with circular and square web opening, with perforation stiffeners. Three different schemes of reinforcement were adopted to check their efficiency in restoring shear capacity of joists i.e. (a) solid steel plate of same size and shape of opening extended beyond all edges of perforation, (b) cold-formed joist sections having same size and shape of opening and extended beyond edges of perforation and (c) two vertical and two horizontal joist section stiffeners around all edges of perforation. It was observed that reinforcement schemes (a) and (b) are incapable of restoring shear strength to the strength of unperforated joist. However, reinforcement scheme (c) was found efficient in restoring original shear strength of cold-formed steel joist section.

Hagen et al. (2009) investigated the stiffening effect of ring (or sleeve) stiffener and doubler plate stiffener on shear capacity of plate girders with web openings. Based on the study, ring stiffener was found to have a relatively higher stiffening capacity in larger opening as compared to small opening size. On the other hand, doubler plates were observed to provide relatively lesser improvement in shear capacity as compared to that of ring stiffener.

Cheng & Li (2012) carried out a numerical study on buckling behaviour of stiffened perforated steel plates subjected to shear loading, adopting three different types of stiffeners around a central circular perforation (ring, flat and strip stiffener oriented in different angles with respect to plate edge). From the numerical analyses, buckling strength was observed to be a function of plate slenderness ratio, perforation diameter to width ratio and type of stiffener. Out of all the stiffeners employed, strip stiffener oriented along compression diagonal was found to be the most effective in increasing elastic buckling strength, while ring stiffener, flat stiffener and strip stiffener oriented diagonally along compression diagonal increases the ultimate shear strength of perforated plate.

Mahendran & Keerthan (2013) reported an experimental investigation on shear behaviour of cold-formed LiteSteel beams (LSBs) with stiffened web openings. Different types of stiffeners (plate and stud stiffener) having different sizes and stiffener fastening systems were examined. Based on the study, suitable plate stiffener along with their dimensions and fastening arrangements to restore shear capacity to that of unperforated LSBs were proposed.

Sonu (2016) conducted a finite element study on shear behaviour of stiffened single perforated LDSS rectangular hollow beam, considering various stiffener types or orientations (vertical, horizontal, inclined, ring) and cross-sections (flat, angular, semi-circular). It was identified from the investigation that both vertical and horizontal stiffeners are not effective in improving shear capacity of the perforated beam. On the other hand, both inclined and ring stiffeners were observed to be capable of significantly improving shear capacity at higher stiffener width and thickness.

2.5 Design provisions for steel members subjected to torsion

This section provides a brief summary on codified guidelines enumerated in European standard for design of members under torsion, followed by a review on relatively new design approaches - Direct Strength Method and Continuous Strength Method. It may be worthwhile to mention that, codified provisions for torsional design are limited (e.g. EN 1993-1-1, 2005; ANSI/AISC 360, 2016), especially for tubular structural steel members. While design guidelines for torsion in ANSI/AISC 360 (2016) are specific to round (circular) and rectangular hollow structural steel sections, EN 1993-1-1 (2005) provides torsion design guidelines for closed (tubular) hollow section steel members in general. Hence, design provision for torsion members in EN 1993-1-1 (2005) is hereby reviewed.

2.5.1 European standard

Adequate codified guidelines for design of cold-formed stainless steel closed hollow members subjected to torsion are not available in stainless steel design codes (EN 1993-1-4:2006+A1, 2015), ASCE 8-02, 2002, AS/NZS 4673, 2001). However, EN 1993-1-1 (2005) recommends calculation of torsional resistance of closed hollow sections based on shear capacity of individual parts of cross-section (calculated as shear capacity of plate girder web). Design equations for shear capacity of stainless steel web plates are provided in EN 1993-1-4:2006+A1 (2015), in terms of shear buckling reduction factor (χ_w) (as a function of slenderness parameter $\bar{\lambda}_w$). Equations for shear buckling reduction factors provided in EN 1993-1-4:2006+A1 (2015) resulted from a study by Saliba et al. (2014), based on a large number of experimental data on stainless steel plate girders subjected to shear failure. Based on the recommendation by EN 1993-1-1 (2005), these equations for shear buckling reduction factors (χ_w) may be adapted to calculation of torsional capacity of stainless steel closed hollow section.

2.5.2 Design methods

In this section, literature on two new alternative design approaches/methods i.e. Direct Strength Method (DSM) and Continuous Strength Method (CSM), developed to provide a more rational and efficient design to structural metallic members are briefly reviewed. Both approaches eliminate the conventional system of classifying cross-section into discrete behavioural classes and employs gross cross-section properties. Interaction of cross-section elements has also been accounted for in these design approaches, rather than basing the design on an individual element of cross-section.

2.5.2.1 Direct Strength Method

Direct Strength Method (DSM) is a design method developed by Schafer & Pekoz (1998) for cold-formed steel members. The method employs elastic buckling solutions and strength curves on the entire member, wherein, slenderness of the member is determined by the lowest buckling stress. Requirement of cross-section classification and concept of effective properties are hence eliminated in this method, thus, providing flexibility to unusual cross-sectional and complex member geometries. DSM based design equations of stainless steel members under various loading conditions such as shear (e.g. Sonu & Singh, 2017b), compression (e.g. Becque et al., 2008) etc have been developed. Owing to its simplicity and flexibility for accommodating complex geometries, DSM has gained rapid acceptance and is now included in North American Specification for cold-formed steel structural members (AISI S100-16, 2016) and Australian/New Zealand Standard for cold-formed steel structures (AS/NZS 4600, 2005). An improvement in original DSM was proposed by Rossi & Rasmussen (2012) for cross-sections in low slenderness range, where stress is limited to yield stress in the original DSM, to avoid overly-conservative predictions in low slenderness range, especially for alloys exhibiting pronounced strain hardening e.g. stainless steel. Further, a unified full slenderness range DSM equation for stainless steel hollow section members

subjected to compression, bending and combined loading was proposed by Arrayago et al. (2017) based on strength curve for carbon steel members in AISI specifications, as an improvement over the earlier approach by Rossi & Rasmussen (2012). Although significant development in DSM approach has been made for loading conditions such as compression and bending, torsion based DSM design equations for stainless steel sections are not yet available. It may be noteworthy to mention that research on DSM for torsion has been initiated by Bian et al. (2016) for cold-formed steel lipped channels.

2.5.2.2 Continuous Strength Method

Continuous Strength Method (CSM) is a deformation based design approach developed by Gardner (2002), so as to exploit significant strain hardening in the design of stocky sections of non-linear metallic materials like stainless steel. The discrete system of design generally adopted in design standards (by cross section classification) is replaced by a continuous system of design (using a cross-section deformation capacity) in CSM. This method allows simple calculation of strength, based on a base curve relating a non dimensional deformation capacity with full cross-section slenderness (accounting for beneficial element interaction within the cross-section) and a material model representing material behavior which accounts for enhancement of strength due to strain hardening. The method was originally proposed for structural stainless steel and further extended to other metallic materials such as aluminium and high strength steels (Gardner & Ashraf, 2006). In literature, research work on CSM based design of stainless steel members has been reported by Afshan & Gardner (2013); Ahmed et al. (2016); Gardner & Ashraf (2006); Zhao et al. (2017) etc. Zhao et al. (2017) and Ahmed et al. (2016) extended the CSM design approach to slender stainless steel cross sections subjected to compression, bending and combined compression-bending loadings. It may be mentioned that CSM approach has not been reported for steel members subjected to torsion.

2.6 Numerical modelling of thin-walled members

Availability of analysis tool adopting numerical techniques such as Finite Element Analysis (FEA) has reduced the complexity involved in non-linear analysis of structural elements or members, thus, further widening scope of study. A wide range of parameters can be investigated using numerical analysis tools to generate large number of reliable results (which may be difficult to execute experimentally), when the finite element (FE) models are validated or calibrated against experimental results. Such analysis tools have been widely adopted by researchers and engineers to investigate structural behaviour of metallic thin-walled structures (e.g. Hassanein et al., 2013; Ridley-Ellis, 2000; Theofanous & Gardner, 2009). Accuracy and reliability of FE models for thin-walled metallic structures are influenced by several factors such as material modelling, boundary conditions, element types, FE mesh, geometric imperfections, residual stress etc. Sensitivity of the FE models in accurate calibration with experimental results is dependent on the above mentioned factors. A review on these factors adopted for modelling thin-walled members are briefly presented in the following sections.

2.6.1 Material modelling

An accurate material stress-strain model is vital to represent the actual behaviour of steel material considered. A material model generally referred to as compound Ramberg-Osgood material model has been adopted by several researchers for stainless steel (Anbarasu & Ashraf, 2017; Patton & Singh, 2012; Sachidananda & Singh, 2017; Saliba & Gardner, 2013b; Zhao et al., 2016) because of its suitability in accurate material modelling of non-linear metallic material exhibiting extensive strain hardening, like stainless steel. This stress-strain material model was originally developed by Ramberg & Osgood (1943) in terms of three parameters - Young's modulus and two secant yield strengths. Following the original Ramberg & Osgood, modifications have been made by several researchers (Gardner &

Ashraf, 2006; Gardner & Nethercot, 2004a; Hill, 1944; Mirambell & Real, 2000; Rasmussen, 2003), to provide improved equations suitable for non linear metallic materials. The representative compound Ramberg-Osgood stress-strain material model in the final modified form (Gardner & Ashraf, 2006), suitable for cold-formed stainless steel is given in Equations 2.1 and 2.2.

For $\sigma \leq \sigma_{0.2}$

$$\varepsilon = \frac{\sigma}{E_o} + 0.002\left(\frac{\sigma}{\sigma_{0.2}}\right)^n \tag{2.1}$$

For $\sigma \geq \sigma_{0.2}$

$$\varepsilon = \frac{(\sigma - \sigma_{0.2})}{E_{0.2}} + \left(0.008 - \frac{\sigma_{1.0} - \sigma_{0.2}}{E_{0.2}}\right)\left(\frac{\sigma - \sigma_{0.2}}{\sigma_{1.0} - \sigma_{0.2}}\right)^{n'_{0.2,1.0}} + \varepsilon_{t0.2} \tag{2.2}$$

where $\sigma_{0.2}$, E_0, n, $\varepsilon_{t0.2}$, $n'_{0.2,1.0}$ and $E_{0.2}$ are 0.2% proof stress, initial modulus of elasticity, material non-linearity index, total strain at $\sigma_{0.2}$, strain hardening exponent and tangent modulus at 0.2% proof stress respectively.

2.6.2 Element type

In numerical modelling, thin-walled metallic structures are generally discretised using FE shell elements in many studies available in literature. In most reported studies, general purpose FE element such as S4R (available in Abaqus, 2009) which is a four noded shell element with reduced integration having six degrees of freedom per node, shown to provide accurate results in comparison with experimental results, is adopted. S4R element has been reported to be reasonably accurate in modelling thin-walled members under various loading conditions including torsion (Bian et al., 2016; Ridley-Ellis, 2000; Shen et al., 2018) and shear (Hassanein, 2011; Sonu & Singh, 2017b).

2.6.3 Geometric imperfections and Residual stress

Geometric imperfections and residual stress are inherent in members, and are originated during its forming process, transportation, fabrication etc. Influence of geometric imperfections on member capacity has been reported in literature (Huang & Young, 2013a; Saliba & Gardner, 2013b; Theofanous & Gardner, 2009). Magnitude of initial local imperfection in cold-formed LDSS RHS sections has been measured experimentally by Huang & Young (2012) (2014a) and are found to be in the range of one-tenth to one-fiftieth of cross-section thickness. In the absence of experimental data, local geometric imperfections are incorporated in the FE modelling of LDSS thin walled-members using the lowest relevant elastic buckling mode shape with its magnitude calculated using a modified Dawson and Walker model (Gardner & Nethercot, 2004b) or local imperfection magnitude expressed in terms of thickness (t) such as t/100 (Saliba & Gardner, 2013b; Theofanous & Gardner, 2009). Effect of initial imperfection on members subjected to torsion was examined by Kim & Yoo (2008) and Wan & Mahendran (2015), wherein ultimate capacity was observed to be slightly reduced (~ 1.2% - 7%). The expected effect of residual stress on member behaviour is premature yielding and loss of stiffness. However, several studies have found that residual stress has insignificant effect on LDSS member response (e.g. Huang & Young, 2013a; Saliba & Gardner, 2013a, 2013b). In literature, most of the investigations on torsion did not consider initial imperfection and residual stress (e.g., Lauwens et al., 2018; Ridley-Ellis, 2000). However, it may be noteworthy to mention that insignificant effect of residual stress on ultimate capacity of members subjected to torsion was reported by Mahendran & Murray (1990), Wan & Mahendran (2015) etc.

2.7 Summary

A review of research work reported on torsional behaviour of unperforated and perforated structural steel members has been presented, with a major focus on tubular / hollow section members. A brief introduction of LDSS has also been made in the beginning of this chapter along with associated investigations reported on LDSS structural members till date. Further, since studies on torsion of steel members are very limited, researches carried out under shear loading (torsion being a case of shear) have also been additionally presented in this chapter for completeness, with a focus on closed hollow sections. Further, investigations reported on members with stiffened perforation subjected to shear loading are reviewed. This is followed by a brief summary of codified provisions for torsion design of stainless steel and relatively new design methods such as DSM and CSM. Design provisions for torsion in European standard and alternate design approaches such as DSM and CSM are also briefly reviewed.

Based on the literature review, it can be concluded that, although there is increased interest on research work related to LDSS structural sections/members, no study has yet been reported on torsional behaviour of LDSS closed hollow section members. Also, limited studies are available on pure torsional behaviour of cold-formed steel members. No investigation has yet been reported on torsional behaviour of relatively new cross section shapes such as elliptical, semi-elliptical, flat-oval etc. Further, so far, no studies have been available in the literature on steel members containing perforation (with or without perforation stiffeners) under torsional loading. Moreover, there are no adequate design provisions for stainless steel members (unperforated or perforated) subjected to torsion.

CHAPTER 3

UNPERFORATED LEAN DUPLEX STAINLESS STEEL SEMI-ELLIPTICAL HOLLOW SECTION MEMBERS SUBJECTED TO TORSION

3.1 Introduction

Torsion in structural members can occur in cases of eccentric members and irregular structures under the action of earthquake load (Nie et al., 2012), tall members under lateral loading (Han et al., 2007) etc. It has been highlighted in Chapter 2 that research on torsional loading is limited, unlike the case of compression and bending. Although studies on torsional behaviour of structural tubular members have been attempted in the past (e.g. Aisyah Mohd Zaifuddin et al., 2017; Beck & Kiyomiya, 2003; Donnell, 1933; Han et al., 2007; Mahendran & Murray, 1990; Ridley-Ellis, 2000), torsional behaviour of stainless steel (such as LDSS) closed hollow section (or tubular) members has not been reported in the literature, to the best of author's knowledge. Moreover, the aforementioned studies have been mainly concentrated on commonly available sections such as square hollow section (SHS) and circular hollow section (CHS), as outlined in Chapter 2. Further, it may be worthwhile to mention that, there is an apparent lack of explicit

codified provisions for torsional design, especially for tubular (stainless) steel members. Also, torsion design guidelines based on alternate design methods such as DSM (Schafer & Pekoz, 1998) and CSM (Gardner, 2002) are found to be very sparse. To the best of author's knowledge, DSM based equation for torsion design was first reported by Bian et al. (2016) for open (channel) sections which may need to be checked for its applicability in the design of other sections (such as semi-elliptical hollow sections) under torsion.

Hence, an attempt has been made in this chapter to investigate numerically, torsional behaviour of LDSS (grade EN 1.4162 (LDX2101)) SEHS members under torsion considering various key parameters such as curve length, flat length, cross-section slenderness, aspect ratio and length of member, along with an additional aim to develop design equations. A systematic parametric study on LDSS SEHS has been carried out using the commercial finite element software, Abaqus (Abaqus, 2009) considering the above mentioned parameters. First, finite element modelling approach was validated with experimental results (of YSt 210 and YSt 310 SHS members and those reported in the literature for torsion) and adopted for further study on LDSS SEHS members under torsion. It may be noted that the focus of the present study is only on the numerical (i.e. finite element) study of LDSS SEHS members under torsion, although experimental tests on SHS members have been presented in detail in this study for completeness of the FE modelling validation process.

3.2 Experimental investigation

As Lean Duplex Stainless Steel SEHS was not readily available in the Indian market, an ‘indirect’ approach has been employed herein to validate the finite element modelling approach (for metallic tubular members under torsion) that would be used for the present parametric study of SEHS under torsion. This has

been achieved by conducting torsional experiments on SHS members of carbon steel (YSt 210 and YSt 310 variety available in India) and comparing against developed FE models. Thus, an experimental investigation has been carried out on cold-formed thin-walled steel square hollow section members subjected to torsion. Specimens used for testing belongs to cold-formed carbon steel of material grade YSt 210 and YSt 310 having nominal yield stress of 210 MPa and 310 MPa respectively, manufactured by TATA Steel. Details of test carried out on SHS members under torsion and tensile coupon test are discussed in the subsequent sections.

3.2.1 Tensile test

To examine basic mechanical properties of YSt 210 and YSt 310 steel, tensile test was carried out on coupons extracted from flat and corner regions of SHS specimens. The SHS specimens from which coupons were extracted has section dimensions of outer width and depth of 50 mm, and thickness of 2.9 mm, designated herein as SHS 50 × 50 × 2.9 for YSt 210 steel and outer width and depth of 60 mm and thickness of 3.2 mm for YSt 310 steel designated as SHS 60 × 60 × 3.2. Flat coupons were extracted from the face opposite to weld containing face in the direction parallel to rolling. And corner coupon was extracted from a corner region, not adjacent to welded face. Dimensions of flat and corner coupons adopted were as per ASTM (ASTM, 2015). Procedure of tensile testing of coupon recommended by Huang & Young, 2014b for static mechanical property of metallic materials was considered for the present study. Basic material properties such as Young's modulus (E), 0.05% proof stress ($\sigma_{0.05}$), 0.2% proof stress ($\sigma_{0.2}$), 1% proof stress ($\sigma_{1.0}$), ultimate stress (σ_u), percentage strain at fracture (ε_f) obtained from test are given in Table 3.1.

3.2.2 Member test

Member test on cold-formed SHS members were conducted under applied axial torsion. Two repeated tests for each SHS specimen of YSt 210 and YSt 310 were carried out (with suffix -1 and -2 for Sample 1 and 2 respectively). The specimens were cut from 5 m long cold-formed steel tube using rotary hacksaw to achieve a nominal length of 600 mm and ends milled flat. Additional support fixtures were designed to fasten the specimen in the testing machine. Torsional testing arrangement along with schematic details of support fixtures are shown in Figure 3.1. The fixture arrangement is to ensure connectivity of sample with testing machine as well as to achieve required fixed boundary condition. Solid metal blocks were inserted at each end of hollow SHS tube to avoid local buckling in the interior of supports. The specimen ends were then inserted in a metal fixture having a cuboidal cut out of depth 72.5 mm. Metal fixture, SHS sample and metal block insert were bolted together using four bolts to restrict movement during testing. This whole arrangement was then mounted on the testing machine, aligned, bolted and tightened. With all support fixtures attached to specimen tubes, an effective length of ~ 455 mm is available which is free to twist.

A servo hydraulic torsion testing machine having a load cell of capacity 10,000 Nm and one rotating actuator having a stroke of ± 50 degrees (a total of 100 degrees) was used for member testing. One end of testing rig was held fixed while other end rotated. Rate of rotation adopted was ~ 9.68×10^{-4} radian/sec as reported in the literature (Ridley-Ellis, 2000). All specimens were loaded up to failure or up to limit of rotating actuator, whichever reach earlier. Torque-twist responses obtained from experimental tests are shown in Figures 3.2 and 3.3 for SHS 60 × 60 × 3.2 and SHS 50 × 50 × 2.9 respectively. A very close match in the response of specimens with corresponding repeat tests confirms the repeatability of the tests. Both Sample 1 and 2 were found to yield before failure with significant strain hardening.

3.3 Numerical modelling

3.3.1 General

Finite element (FE) software Abaqus (Abaqus, 2009) was used as a tool to carry out a systematic parametric study on behavior of thin-walled SEHS members under torsion. The following sections brief the steps followed in modelling SEHS member for the current parametric study. The FE modelling approach has been validated using an indirect approach (see Section 3.3.5), to evaluate its effectiveness to capture the response of a thin-walled structural steel members under torsion, accurately.

3.3.2 Geometry and boundary condition

Typical cross-section geometry of SEHS is shown in Figure 3.4. The parametric study (except for study of member length effect) was carried out considering a short member. Length of all short members was taken equal to three times that of the flat length (l_f) to meet the requirements of a stub column (Galambos, 1998). Curve length (l_c), aspect ratio (h/b), thickness (t) and member length (L) were varied from 270 - 540 mm; 0.5 - 2, 2.7 - 30 mm and from l_f - 30l_f respectively. To apply boundary conditions, two reference points each at bottom (RP-1) and top (RP-2) positioned at centroid of section (similar to the arrangement followed in Bian et al., 2016) were used to which all degrees of freedom were coupled through kinematic coupling (available in Abaqus, 2009). All degrees of freedom were restrained at bottom end while longitudinal displacement and rotational degree of freedom were released at the loaded top end (Figure 3.5a). Such boundary conditions are widely adopted in the literature for torsional study (see e.g. Zaifuddin et al., 2017; Shen et al., 2018). Using displacement control, rotation about longitudinal axis was applied through top reference point RP-2.

3.3.3 Finite element mesh and analysis technique

To discretise the FE model, general purpose shell element S4R (Abaqus, 2009) with reduced integration having four nodes with six degrees of freedom (3 translations and 3 rotations) at each node was employed. To check adequacy of mesh fineness, a mesh convergence study was conducted. Number of elements was determined from the mesh convergence study and ranges from ~7000 - 9000 for all short members and ranged upto ~20496 for long members. Aspect ratio of all elements was maintained ~1. A typical FE mesh with S4R elements is shown in Figure 3.5b. Initially, eigen buckling analysis was carried out to obtain buckling mode shapes used for incorporating imperfections in the FE models. Non-linear analysis was then carried out using *STEP Static, General available in Abaqus (Abaqus, 2009).

3.3.4 Material property and material model

Elastic and plastic properties of LDSS to be used for parametric study in Abaqus (Abaqus, 2009) were taken from the literature. Material property of LDSS given by Theofanous & Gardner (2009) for a flat compressive coupon has been adopted. The basic material properties used for developing stress strain relation are detailed in Table 3.2. To develop stress-strain relation, a two stage compound Ramberg-Osgood stress strain model was employed. The first stage of stress strain curve covers up to 0.2% proof stress which was originally developed by Ramberg & Osgood (1943) and modified by Hill (1944) as given in Equation 3.1. The second stage of the model originating at 0.2% proof stress and continued till ultimate stress was proposed by Mirambell & Real (2000) and additional parameters expressed in terms of original Ramberg-Osgood parameters ($\sigma_{0.2}$, E_0 and n) as described by Rasmussen (2003). Gardner & Nethercot (2004a) proposed that 1% proof stress be used in place of ultimate stress in the second stage of Ramberg-Osgood curve, thus leading to Equation 3.2. These equations were found to be in excellent agreement with experimental data for both tension and compression test. Same material

property was adopted for the whole model which may result in conservative results on account of negligence of strain hardening due to cold forming and strength enhancement in corner region.

$$\varepsilon = \frac{\sigma}{E_o} + 0.002\left(\frac{\sigma}{\sigma_{0.2}}\right)^n \tag{3.1}$$

$$\varepsilon = \frac{(\sigma - \sigma_{0.2})}{E_{0.2}} + \left(0.008 - \frac{\sigma_{1.0} - \sigma_{0.2}}{E_{0.2}}\right)\left(\frac{\sigma - \sigma_{0.2}}{\sigma_{1.0} - \sigma_{0.2}}\right)^{n'_{0.2,1.0}} + \varepsilon_{t0.2} \tag{3.2}$$

where $\sigma_{0.2}$, E_0, $\varepsilon_{t0.2}$, $n'_{0.2,1.0}$ and $E_{0.2}$ are 0.2% proof stress, initial modulus of elasticity, total strain at $\sigma_{0.2}$, strain hardening exponent and tangent modulus at 0.2% proof stress respectively. Poisson's ratio (ν) for the material was taken as 0.3. For use in Abaqus (Abaqus, 2009), the resulting stress strain was converted into true stress (σ_{true}) and true plastic strain (ε^{pl}_{true}) using following Equations 3.3 and 3.4.

$$\sigma_{true} = \sigma_{nom}\left(1 + \varepsilon_{nom}\right) \tag{3.3}$$

$$\varepsilon^{pl}_{true} = \ln\left(1 + \varepsilon_{nom}\right) - \frac{\sigma_{true}}{E_0} \tag{3.4}$$

where σ_{nom} = engineering stress and ε_{nom} = engineering strain.

3.3.5 Validation

As LDSS SEHS was not readily available in the Indian market, an 'indirect' approach has been employed herein to validate the finite element modelling approach (for metallic tubular members under torsion) that would be used for the present parametric study of SEHS under torsion. This has been achieved by comparing torque-twist (T-θ) response of FE model with test results of YSt 210 and YSt 310 SHS members from experimental investigation outlined in Section 3.2. Assessment of FE results was done in terms of T-θ curve, T_u and deformed shapes.

For validation with experimental results, material model detailed in Section 3.3.4 with material property provided in Table 3.1 were adopted in the FE model, along with similar boundary conditions, meshing and analysis technique described in Sections 3.3.2 and 3.3.3. The FE models were also checked with different values of initial geometric imperfection, *viz*. $t/10$, $t/50$ and $t/100$. No significant change in results was observed with change in imperfection. Hence, an imperfection value of $t/100$ was adopted for FE models as reported suitable for modelling thin-walled hollow sections (Theofanous & Gardner, 2009). Residual stress was not explicitly included in the models as it was reported not to have significant effect on the ultimate capacity of members subjected to torsion (Mahendran & Murray, 1990; Wan & Mahendran, 2015). Comparison of T-θ response from experiment and FE is shown in Figure 3.6. Overall T-θ curve given by FE was found to be in good agreement with that of experiment. Initial elastic stiffness and T_u were found to be closely matched with the experimental results. Figure 3.7 shows deformed shape of SHS 50 × 50 × 2.9 specimen from experiment at post peak rotation (Figure 3.7a) with respective deformed shape obtained from FE (Figure 3.7b). A similar failure mechanism of FE model (failure by yielding with significant strain hardening) with that of experiment was found and failure patterns were also closely comparable.

In addition, validation of FE modelling was assessed using T-θ response of thin-walled SHS (section with plated elements) and CHS (section with curve element) steel members under torsion available in the literature (Beck & Kiyomiya, 2003; Han et al., 2007; Ridley-Ellis, 2000) (see Figure 3.8). Details of sections used for validation from literature are provided in Table 3.3. In general, good agreement of the FE results with that of literature can be seen. The observed differences (T_u, θ_u) in experimental and FE observations may be associated with use of material properties from similar grade of steel (exact material property not reported in Beck & Kiyomiya, 2003; Han et al., 2007). Comparison of key parameters (T_u, θ_u, the initial slope of T - θ response) in terms of ratio of FE and test results are provided in Table 3.4 which gives mean value; coefficient of variation of 1.06;0.17, 0.84;

0.26 and 1.01;0.11 for T_u, θ_u and initial slope of T - θ response respectively. Hence it can be concluded that the present FE modelling approach discussed in this section can be satisfactorily adopted for modelling thin-walled hollow steel sections under torsion. It may be noteworthy to mention that, a torsional study on cold-formed steel lipped channel by Bian et al. (2016) has been reported using a similar FE modelling approach to assess torsional behaviour of thin-walled steel members. These FE modelling steps are then adopted for further parametric study of LDSS SEHS members under torsion.

3.4 Results and Discussion of parametric study

This section presents the results obtained from the parametric study on LDSS SEHS members under torsion, using Abaqus (Abaqus, 2009). Details of FE results generated from the investigation are provided in Tables 3.5 – 3.9. Observations from the parametric study are outlined and discussed in detail.

3.4.1 Eigen analysis

Linear eigen buckling analysis was carried out to observe buckling mode shapes for thin (slender) and thick (stocky) SEHS. Figures 3.9a and 3.9b show first buckling mode shapes for slender section (t = 2.7 mm) and stocky section (t = 17 mm) respectively. In case of slender section, local buckling was observed as fundamental mode with local buckling in flat element only. While for the stocky section, a mixture of local and distortional buckling was seen where local plate type buckling occurred in flat part and distortional buckling found in the curve part of the section.

3.4.2 Load deformation response

Figure 3.10a shows T-θ response of a slender LDSS SEHS section having t = 2.7 mm. Failure of the slender section is characterised by local buckling, which was

seen to be initiated in the flat part of member before reaching yield torque i.e. T_u/T_y < 1 (see Figure 3.10b). Initially, both flat and curve parts were observed to be subjected to high stress, showing their contribution to torsional capacity. At T_u, local buckling was found to be initiated in the flat part with a yielded zone band (signified by grey color in Von Mises stress contour where stress is greater than yield stress (f_y) of 560 MPa) oriented near diagonally, while the curve part showed no sign of local buckling (**A1**). Enhanced local buckling can be observed at member mid-length (i.e. $L/2$) and gradually diminishes towards supports, evident from transverse cross-section profiles shown in Figures 3.11a and 3.11b at T_u. Post T_u, local buckling in curve part was perceived to be triggered near flat-curve corner junction where local buckling in flat part meets the junction near support. As local buckling progresses in curve part, stress relaxation was found in other regions except at buckled zone (where higher stress was seen to be concentrated (**A2**)) which may be the reason of rapid drop in torque (T) at post T_u. Transverse cross-section profiles for **A2** at two different locations ($L/2$ and $L/4$) are shown in Figures 3.11c and 3.11d. Local buckling can be observed in both flat and curve parts with buckled zone in curve part prominently found near the supports. With further rotation, it was noticed that yielding spreads in both flat and curve parts. This may explain the stabilisation of T-θ curve at large twist of section ($\sim \theta > 0.15$ radian).

Unlike slender section, stocky sections have the capacity to reach its yield capacity and failure occurred due to yielding of section i.e. $T_u/T_y > 1$ (see Figure 3.12b). Prior to T_u (**B1**), curve part was observed to be almost fully yielded when other region in flat part has not reached yield torque. Hence, it may be inferred that development of initial sectional strength is primarily contributed by the curve part which is not so in the case of slender section. At T_u, initiation of local buckling was not identified anywhere and the member was seen to be fully yielded (**B2**) except at minor regions in the flat-curve corner junction. Significant strain hardening was found which was absent in slender section (see Figure 3.12a). A more gradual drop in T post T_u was perceived in all stocky sections considered. Twist at ultimate load

(θ_u) for stocky section was observed to be much higher than that of a slender section. Transverse cross-section profiles at two different positions along the length at $\theta = \theta_u$; and $\theta = 1.5\theta_u$ are provided in Figures 3.13a and 3.13b; and Figures 3.13c and 3.13d respectively. There was no sign of local buckling although cross-section deformation was noticed due to twisting. Stress relaxation was found in regions near the supports in both flat and curve parts (**B3**) leading to drop in T as twisting continues. But unlike a slender section, extent of stress relaxation was seen to be much lesser in the stocky section.

3.4.3 Cross-section classification

Slender sections are often restricted to reach its full yield capacity due to local buckling of its elements and hence results in lower strength. Cross sections can be classified into slender and stocky sections based on its capacity to reach full yield capacity. Slender sections are those which cannot attain its full yield capacity due to buckling and stocky sections are those which have the capacity to reach its yield strength. Although cross-section classification of stainless steel tubular sections under torsion has not been addressed to the best of author's knowledge, a similar approach of classification as that of a web under shear force given in EN 1993-1-4:2006+A1 (2015) may be used since stress distribution is very similar with that of closed cross-section under uniform torsion (Trahair et al., 2007). As per EN 1993-1-4:2006+A1 (2015), a cross-section slenderness limit of λ = 46.8 separates stocky and slender sections where $\lambda = \frac{h_w}{t}\sqrt{\frac{f_y}{235}\frac{210000}{E}}$, f_y is yield stress of material, h_w is clear distance between flanges ($h_w = l_f - 2t$ for SEHS in the present study). Figure 3.14 shows a plot of T_u/T_y versus cross-section slenderness calculated based on slenderness of flat element of SEHS. It was observed that a limit of λ = 46.8 (corresponding to $\bar{\lambda}_w = 0.542$ as in EN 1993-1-4:2006+A1, 2015; see Section 3.5.3) can be safely adopted for LDSS SEHS under torsion considering flat element

to be the critical element and thus governing failure.

3.4.4 Variation of buckling load

3.4.4.1 Effect of curve length (l_c)

In order to study effect of curve length (l_c) on the torsional response of SEHS, l_c was varied by considering a constant flat length (l_f = 2b = 223 mm) and varying l_c from ~ 270-540 mm. Curves for T - θ, T/T_y - θ for slender (t = 3mm) and stocky (t = 20 mm) sections are shown in Figures 3.15a; 3.15b and 3.16a; 3.16b respectively. For a slender section, angle made by buckled wrinkle with flat-curve junction was found to reduce with decrease in l_c (see **C1**, **C2** and **C3**). At T_u, for sections with longer l_c, curve element was noticed to have relatively higher stress over major portion compared to flat element signifying its significant contribution to ultimate torsional capacity. However as l_c decreases, stress level on the curve element was seen to reduce and both flat and curve parts were equally stressed. Hence, it can be concluded that effectiveness of curve element is more pronounced in members with higher value of l_c. Additionally, it was observed that θ_u decreases with increase in l_c. Figures 3.16a and 3.16b present T - θ and T/T_y - θ curves for a stocky section (t = 20 mm). Except for the difference in its failure mode (see Section 3.4.2), similar observations as mentioned above for a slender section in terms of drop in initial stiffness with decrease in l_c, significant contribution of curve part to sectional capacity for sections with longer l_c, reduction in θ_u with increase in l_c etc. were also made for stocky sections.

Figure 3.17 shows variation of T_u with l_c for t = 3 - 20 mm. A near-linear increase in T_u was observed with increase in l_c for all t considered. This may be explained by membrane analogy for thin-walled closed hollow sections. As l_c increases, volume enclosed by the membrane becomes larger and hence attributed to improvement in T_u. This improvement was seen to be higher in thicker sections (~ 373% for t = 3 mm and ~ 453% for t = 12 mm as l_c increases from 270 to 540 mm).

Variation of T_u/T_y with l_c for different t values is provided in Figure 3.18. There was no significant difference in values of T_u/T_y for different l_c, which may be due to similar rate of increase in T_u and corresponding T_y values.

3.4.4.2 Effect of aspect ratio (h/b)

In order to study the effect of aspect ratio (h/b), h/b = 0.5 - 2 were considered by keeping cross sectional area constant (ensuring same material consumption for a typical thickness of section). Figures 3.19a and 3.19b shows T-θ and T/T_y - θ response for slender section (t = 3.5 mm) with different h/b values. Increasing h/b ratio was found to enhance T_u, but not θ_u. Von Mises stress contour plot superimposed on deformed shapes at T_u are displayed in Figure 3.19c (**E1**, **E2** and **E3**). Prior to T_u, relatively higher stress was seen on sections of higher h/b ratio, in agreement with higher T_u. Significant reduction in initial stiffness of T - θ curve was also identified as h/b decreases. A sharper drop in T was observed for h/b = 2 but not for h/b = 1 and 0.5 at post T_u. This may be associated with increased difficulty in transferring local buckling from flat to curve as sharpness of junction between flat and curve increases as h/b decreases. At immediate post T_u, relatively flatter curve can be identified from Figure 3.19a for h/b = 1 and 0.5. This stabilisation may be related to spreading of yielded zone, although T reduces with progress of local buckling in the curve part. T - θ responses for stocky section of different h/b ratio are presented in Figures 3.20a and 3.20b. Deformed shapes and Von Mises stress contour on it at various locations on T - θ curve are provided in Figure 3.20c. Similar effect of h/b on overall response of stocky section was found similar to that of slender section (as mentioned above). Figure 3.21 shows the variation of T_u with h/b ratio for different t values. Higher rate of increase in T_u with increase in h/b ratio was identified for stockier section. Increase in T_u of corresponding sections with different t values (but same h/b) was observed to be more for higher h/b ratio.

3.4.4.3 Size effect

Variation of section size to study size effect was carried out considering two different cases. Case I is by using a scaling factor to change section size maintaining same h/b ratio. Case II is changing size of the same section by shifting flat length of SEHS away from its original position thus leaving a part of semi ellipse (non-SEHS). These two approaches are separately discussed below.

3.4.4.3.1 Case I

In this approach, size of section is varied maintaining same h/b ratio. Six different sizes of section were considered for three different values of h/b ratio, *viz*. 2, 1.5 and 1. Nomenclature of section is provided in such a manner that $h175b175$ indicates a SEHS having h = 175 mm and b = 175 mm. Figures 3.22a and 3.22b represents T-θ curves for three different sizes of slender and stocky section respectively having h/b = 1. Deformed shapes of SEHS at T_u are shown in Figure 3.22c. Local buckling at flat portion of slender section can clearly be seen at T_u (**G1**, **G2** and **G35**) which is extended from mid section towards supports. Section $h175b175$ with maximum section size out of all considered in this study was identified to carry maximum torque. For ~ 28% reduction of size with respect to $h175b175$, T_u was found to reduce by ~ 41% in case of slender section. For the same amount of reduction in size, stocky section was observed to lose more torsional strength as compared to slender section. For ~ 28% reduction in size with respect to $h175b175$, decrease in T_u was found to be ~ 54% in stocky section. Higher rate of drop in T-θ curve immediately post T_u was observed in larger size section.

Variation of T_y and T_u are plotted in Figures 3.23a and 3.23b for stocky and slender sections respectively. For stocky section, T_u was observed to increase at a higher rate than T_y (see Figure 3.23a) as opposed to slender section (Figure 3.23b). Figure 3.24 shows variation of T_u/T_y with l_f for slender and stocky sections. For all h/b

considered, T_u/T_y was seen to give consistent values for stocky section, while for slender section this ratio was found to decrease with increase in section size (~ 30% reduction as l_f changes from 223 mm to 250 mm for h/b = 2).

3.4.4.3.2 Case II

In the second approach, size of section was varied by taking a part of same SEHS and moving flat part away from its original position in a SEHS such that flat length of non-SEHS (l_f') is a fraction of l_f (*i.e* $l_f' = 0.7l_f$, $0.75l_f$, $0.8l_f$, $0.85l_f$, $0.9l_f$, $0.95l_f$). Figure 3.25a displays typical T-θ curves for a SEHS slender section (t = 3 mm, h/b = 2) and two non-SEHS derived from same SEHS having l_f' equal to $0.7l_f$ and $0.85l_f$. T_u was observed to decrease while θ_u improves with reduction in section size. It was found that relatively larger portions of the curve part are yielded in non-SEHS (**N2, N3**) compared to SEHS (**N1**). There was no rapid drop in T at post T_u for non-SEHS, leading to a flatter curve (see Figure 3.25a). This may be linked with relative stiffening effect provided by reduced length of curve and flat parts, although T_u is lesser than that of SEHS due to reduction in size. T - θ responses for SEHS and non-SEHS stocky sections are plotted in Figure 3.25b. Non-SEHS sections of smaller section size were observed to be more ductile although T_u decreases. Initial elastic stiffness of curve was found to be considerably affected by section size, which decreases with reduction in size. Non-SEHS sections were observed to be fully yielded at T_u (**M2** and **M3**) while SEHS section has minor unyielded regions at flat-curve junction (**M1**). Post T_u, a sharper drop in T was noticed in case of SEHS while it was more gradual for non-SEHS.

Variation of T_u with l_f' is provided in Figures 3.26a and 3.26b for slender and stocky sections respectively. T_u was seen to be highest for h/b = 2 out of all corresponding sections of similar size but different h/b ratio. Difference in T_u for corresponding sections of different h/b ratio was found to be less significant for sections of smallest size considered herein. In slender section, a rapid drop in T_u was observed from SEHS to non-SEHS section (T_u lowers by ~ 35% for ~ 5%

reduction in size) which was not so for stocky section.

3.4.4.4 Effect of length

Effect of length on torsional capacity of SEHS was studied considering different length of member (L) ranging from 1 to 30 times of l_f, with fixed value of h/b = 2. T-θ curve for t = 6 mm having different L and deformed shapes of member are shown in Figures 3.27a and 3.27b respectively. T_u was found not to be significantly affected by L in contrast to θ_u. Also, initial stiffness of T-θ curve reduces with increase in L. Members was seen to be yielded at T_u (**L2**, **L5** and **L8**). For section with L/l_f = 3, local buckling in both curve and flat part was found to be initiated at immediate post T_u. For L/l_f = 10, a sharp drop in T_u was noticed which was more rapid than that of L/l_f = 3. Although local buckling was not identified anywhere at the section at T_u (**L5**), it was seen to be initiated at curve part at immediate post T_u near support where twist is applied. As θ increases, local buckling was observed in flat part as well (**L6**). For longer member i.e. L/l_f = 20, sudden drop in T was found as in intermediate long member (L/l_f = 10). Section was seen to undergo large twist before reaching T_u. At immediate post T_u, local buckling was perceived to be initiated in flat part of section near fixed end. Further as θ increases, curve part was also found to subject to local buckling near fixed end (**L9**).

Variation of T_u with L has been plotted in Figure 3.28. Significant reduction of T_u was not observed with increase in L for all t considered. As L increases, T_u was seen to become consistent after certain value of L. Similar observations were made by Omidvari & Hematiyan (2015) for rectangular tubes under torsion. For stocky sections, stabilization of T_u was found to occur after L/l_f value of 3 while for slender section, the same was observed after L/l_f value of 10.

3.5 Design rules

Although design rules for torsion members are not readily available, design provisions for plated members under shear loading have been reported in the literature (Aisyah Mohd Zaifuddin et al., 2017; EN 1993-1-4:2006+A1, 2015; Nakai et al., 1990; Vilnay & Burt, 1988). Since stress distribution in a closed hollow section under torsion is similar to that in a web plate subjected to shear loading (Trahair et al., 2007), shear design equations available in literature for web plates have been checked for SEHS sections under torsion, following similar approaches in the literature (Aisyah Mohd Zaifuddin et al., 2017; EN 1993-1-4:2006+A1, 2015; Nakai et al., 1990; Vilnay & Burt, 1988). Some available design rules that have been checked for LDSS SEHS in the present work for estimation of torsional strength are briefly summarised in this section.

3.5.1 Aisyah Mohd Zaifuddin et al. (2017)

Taking analogy of torsional buckling of a thin-walled plated tube to elastic buckling problem of a plate subjected to shear loading, Aisyah Mohd Zaifuddin et al. (2017) applied the analytical equation developed by Basler (1960) to estimate ultimate torsional moment (T_u) due to elastic collapse, as shown in Equation 3.5.

$$\frac{T_u}{T_y} = \frac{\tau_{cr}}{\tau_y} + \frac{\sqrt{3}}{2}\frac{1-\tau_{cr}/\tau_y}{\sqrt{1+\alpha^2}} \tag{3.5}$$

$$T_y = 2\tau_y A t_p \tag{3.6}$$

where T_y = yield torque , τ_y = yield shear stress, τ_{cr} = critical shear stress, $\alpha = l_p/b_p$, t_p = thickness of plate, b_p = width of plate, l_p = length of plate and A = area enclosed by mid line of section. Critical shear stress (τ_{cr}) is given by

$$\tau_{cr} = k\frac{\pi^2 E}{12\left(1-\upsilon^2\right)}\left(\frac{t_p}{b_p}\right)^2 \tag{3.7}$$

where k is shear buckling coefficient and for simply supported rectangular plate, k is given by

$$k = 5.35 + 4.00\left(\frac{b_p}{l_p}\right)^2 \tag{3.8}$$

Equation 3.5 was found to give satisfactory results for elastic failure of thin tubes consisting of plate elements irrespective of cross-section shape (*viz*. rectangular, hexagonal tubes). Whereas, for thicker tubes which fail due to plastic yielding, Equation 3.5 was observed to give conservative results since strain hardening effects were not accounted for.

3.5.2 Nakai et al. (1990)

Nakai et al. (1990) proposed an analytical expression to determine T_u (Equation 3.9) of thin-walled stiffened box girder, governed by shear buckling of single panel of web plate. T_u consisted of two components i.e. shear buckling strength (τ_{cr}) and post buckling strength (τ_t).

$$\frac{T_u}{T_y} = \frac{\tau_{cr} + \tau_t}{\tau_y} \tag{3.9}$$

Shear buckling strength (τ_{cr}) is given by Equation 3.10.

$$\begin{aligned} \tau_{cr} &= \tau_y && R_t \le 0.6 \\ &= \left[1 - 0.614\left(R_t - 0.6\right)\right]\tau_y && 0.6 < R_t \le 2 \\ &= \left(1/R_t^2\right)\tau_y && R_t > 2 \end{aligned} \tag{3.10}$$

where R_t = width-thickness parameter of single panel and is given by

$$R_t = \frac{b_p}{t_p}\sqrt{\frac{12\left(1-\upsilon^2\right)\tau_y}{k\pi^2 E}} \tag{3.11}$$

Shear buckling coefficient (k) of plate can be determined by Equation 3.12.

$$\begin{aligned} k &= 5.34+4\left(\frac{b_p}{l_p}\right)^2 && \frac{l_p}{b_p}\geq 1 \\ &= 4+5.34\left(\frac{b_p}{l_p}\right)^2 && \frac{l_p}{b_p}<1 \end{aligned} \tag{3.12}$$

The post buckling strength (τ_t) of plate can be computed by

$$\tau_t = \sigma_t\left(\sin\theta_d\cos\theta_d - \left(l_p/b_p\right)\sin^2\theta_d\right) \tag{3.13}$$

where σ_t is tensile strength and θ_p is angle of diagonal tension field, given by

$$\sigma_t = \left[1-\left(\tau_{cr}/\tau_y\right)^{1.2}\right]\sigma_y \tag{3.14}$$

$$\theta_d = \frac{1}{2}\tan^{-1}\left(\frac{b_p}{l_p}\right) \tag{3.15}$$

The developed Equation 3.9 was checked by the authors (Nakai et al., 1990) for stiffened and unstiffened box girders subjected to torsion and was found to give satisfactory results.

3.5.3 European code

As per EN 1993-1-1: 2005, torsional capacity of a closed hollow section may be determined by considering shear strength of individual elements of the cross-

section. Taking analogy of shear stress in web plate under shear force with that of shear stress in closed hollow section under pure torsion, Equation 3.16 may be used to predict T_u for stainless steel closed section under torsion as per EN 1993-1-4: 2006 + A1 (2015).

$$T_u = \chi_w T_y \tag{3.16}$$

where χ_w is reduction factor in shear capacity due to shear buckling and is given by Equation 3.17 (which results after substitution of value of η = 1.2 as per EN 1993-1-4:2006+A1, 2015).

$$\chi_w \begin{cases} = 1.2 & \bar{\lambda}_w \le 0.542 \\ = \dfrac{0.65}{\bar{\lambda}_w} & 0.542 < \bar{\lambda}_w < 0.65 \\ = \dfrac{1.56}{0.91 + \bar{\lambda}_w} & \bar{\lambda}_w \ge 0.65 \end{cases} \tag{3.17}$$

where $\bar{\lambda}_w = \sqrt{\dfrac{\tau_y}{\tau_{cr}}}$.

3.5.4 Effective width method

Vilnay & Burt (1988) used the concept of effective width method (originally developed by Von Karman, 1932 for compression members) to estimate capacity of aluminium plate under shear loading. Based on strain distribution at edges of a rectangular plate at failure, shear effective width was proposed which is in line with effective width equation of plate under uniaxial compression. Shear effective width proposed by Vilnay & Burt (1988) is given by Equation 3.18.

$$b_{eff} = b_p \sqrt{\frac{\tau_{cr}}{\tau_y}} \left(2 - \sqrt{\frac{\tau_{cr}}{\tau_y}} \right) \tag{3.18}$$

where b_{eff} is shear effective width and b_p is width of plate. Shear force in the plate is then calculated as

$$V = \tau_y t_p b_{eff} \tag{3.19}$$

Extending this concept to torsion, T_u may be determined using Equation 3.20.

$$\frac{T_u}{T_y} = \sqrt{\frac{\tau_{cr}}{\tau_y}} \left(2 - \sqrt{\frac{\tau_{cr}}{\tau_y}} \right) \tag{3.20}$$

3.6 Reliability analysis

For assessment of reliability of various design equations used in the current study, a reliability analysis was carried out as elaborated in AISI S100-16-C (2016); ASCE 8-02 (2002) for design of cold-formed steel structural members. A target reliability index (β) of 2.5 for structural steel members was adopted as a lower limit, as specified by AISI S100-16-C (2016). A resistance factor (φ) of 0.8 was adopted for DSM as stated by AISI S100-16 (2016) and also adopted by Zhu & Young (2012) for sections not considered as pre-qualified sections with a load combination of 1.2DL+1.6LL (DL - dead load, LL - live load). To maintain consistency, a resistance factor of 0.8 has been adopted for all design rules. Ratio of DL/LL is taken as 1/5 as recommended by AISI S100-16-C (2016). The statistical parameters M_M, V_M, F_M, and V_F (mean and coefficient of variation for material properties and fabrication factors) are taken as 1.10, 0.03, 1.00 and 0.05 respectively as enumerated in Afshan et al. (2015) for duplex stainless steel.

3.7 Comparison of FE results with design strength

Torsional capacity obtained from FE analysis ($T_{u,FE}$) for SEHSs were compared with design strengths predicted by Equations 3.5, 3.9, 3.16 and 3.20 ($T_{Eqn3.5}$, $T_{Eqn3.9}$, $T_{Eqn3.16}$ and $T_{Eqn3.20}$) as detailed in Section 3.5. Figure 3.29 shows comparison of FE and predicted results in terms of normalized T_u/T_y ratio and slenderness parameter λ_T or $\bar{\lambda}_w$, where $\lambda_T = \sqrt{T_y/T_{cr}} = \sqrt{\tau_y/\tau_{cr}}$ and $\bar{\lambda}_w$ as defined in EN 1993-1-4:2006+A1 (2015) (T_{cr} is elastic critical buckling torque). Prediction based on Equation 3.5 was found to be conservative for SEHS at lower values of torsional slenderness (λ_T < 0.55) due to non consideration of strain hardening in thicker sections while it over predicts strength at higher torsional slenderness value (λ_T > 2.86). Similar observations were also made for prediction using Equation 3.9 but with higher extent of conservatism. Although it was observed to provide reasonable values of T_u for very high values of λ_T (λ_T > 5.2), in overall, these equations were seen to give conservative results. Strain hardening for stocky sections has been neglected in both approaches which lead to conservative results. Shear design strength based on EN 1993-1-4:2006+A1, 2015 (Equation 3.16 in this paper) was also checked for LDSS SEHS sections under torsion. For sections of high value of λ_T (λ_T > 2) and low values of λ_T (λ_T < 0.7), prediction by Equation 3.16 was found to overestimate FE strength. While for sections with 0.7 < λ_T < 2, it was observed that Equation 3.16 gives good prediction of torsional strength of SEHS. Equation 3.20 was found to underpredict torsional strength for λ_T < 0.55 while it overpredicts when λ_T > 0.55.

Values of mean, COV and reliability index (β) were calculated for all design equations and presented in Table 3.10. Target reliability of 2.5 is not met by design equations 3.16 and 3.20 mentioned here and hence are not recommended for design of SEHS. On the other hand, although Equations 3.5 and 3.9 met the target reliability, higher extent of conservatism can be seen and needs to be modified for

design of SEHS members. However, it is to be noted that all these equations were developed based on failure of a flat plate under shear loading. This may explain the observed conservatism of these equations for SEHS members since significant contribution of curve part to its torsional capacity (see Section 3.4.4) is not considered. Hence, further improvement of EN 1993-1-4:2006+A1 (2015) equation is proposed (see Section 3.8.2).

3.8 Modified and proposed design rules

Since the available design rules as explained in Section 3.5 were found to give unreliable results for design of LDSS SEHS member under torsion, new and modified design rules were proposed based on a lower bound curve. Although SEHS sections of higher aspect ratio were found to have comparatively higher T_u, the proposed design equations may conservatively be used for design of SEHS sections with h/b up to a value of 2 (since a lower bound curve was fitted). Moreover, these equations will be applicable to short and long SEHS members as well, since length of member was found to affect T_u insignificantly.

3.8.1 Direct Strength Method (DSM)

Direct Strength Method is an alternate design method developed by Schafer and Pekoz (Schafer & Pekoz, 1998) for cold-formed steel structures which is less cumbersome and non iterative compared to traditional effective width method. Since then, various researches have been carried out by several authors (e.g., Arrayago et al., 2017; Becque et al., 2008; Pham & Hancock, 2012; Rossi & Rasmussen, 2012) to develop DSM based equations for sections under different types of loading such as compression, bending, shear and combined loading. The method requires determining elastic buckling stress and by using a strength curve, capacity can be calculated. Initially, all DSM equations were developed for sections of high slenderness value keeping traditional value of normalised load

ratio equal to 1 for sections of low slenderness, which was found to yield conservative results. As an improvement, to harness benefits of strain hardening particularly for non-linear metallic materials such as stainless steel, Rossi and Rasmussen (Rossi & Rasmussen, 2012) developed DSM equations for low section slenderness. Arrayago et al. (2017) recently proposed design equations for full range of section slenderness for stainless steel, which takes into account effect of strain hardening (in line with Rossi & Rasmussen, 2012) for various loading conditions such as compression, bending and combined loading. Development of DSM design equations for cold-formed steel structures under torsion has been initiated by Bian et al. (2016) which was developed based on lipped channel sections dominated by warping and is also checked for applicability in the current case. All the present FE results were plotted as T_u/T_y vs λ_T and existing DSM equation for torsion (Bian et al., 2016) was checked for LDSS SEHS member. Elastic critical torsional buckling moment (T_{cr}) for calculation of λ_T in this study is obtained from Finite element method using Abaqus (Abaqus, 2009). The existing DSM equation (Bian et al., 2016) was found to overestimate torsional capacity for sections of low λ_T while it underpredicts for higher value of λ_T (see Figure 3.30). This may be associated with variation in torsional response of open section (for which existing DSM equation (Bian et al., 2016) was developed) from that of closed SEHS members. Hence, a new design equation to predict T_u for closed hollow section members based on DSM was proposed in this paper.

A lower bound curve was fitted on data available from parametric study by using regression analysis. A three stage expression based on non-linear regression analysis using least square method to predict torsional strength ($T_{u,DSM}$) was then proposed as given in Equation 3.21, also accounting for benefits of strain hardening effects particularly in stocky sections.

$$T_{u,DSM}/T_y = 1 + \left(0.13 - 0.27\lambda_T\right) \qquad \lambda_T \le 0.548 \tag{3.21}$$

$$= 1.18 - 0.35\lambda_T \qquad 0.548 < \lambda_T \leq 0.91$$

$$= \frac{3.42}{\lambda_T^{0.38}} - \frac{2.61}{\lambda_T^{0.27}} \qquad \lambda_T > 0.91$$

Comparison of FE results with T_{DSM} in terms of T_{FE}/T_{DSM} ratio gives a mean value of 1.127 and COV of 0.111 as shown in Table 3.10. Reliability index (β) was found to be 3.29 which is higher than 2.5 (i.e. target value) and hence, these proposed DSM equations can be safely adopted for design of LDSS SEHS under torsion.

3.8.2 Modified Eurocode design equation

Existing shear design curve in Eurocode (EN 1993-1-4:2006+A1, 2015) for stainless steel plates under shear loading was checked for its applicability in design of LDSS SEHS under torsion. The comparison was given in Section 3.7 and was found to give unreliable results. Hence, a modified equation for χ_w based on Eurocode (EN 1993-1-4:2006+A1, 2015) was proposed by a non-linear regression analysis using a lower bound curve. The ultimate capacity can then be calculated using Equation 3.16 and modified χ_w (χ_w is as defined in EN 1993-1-4:2006+A1, 2015). The proposed equations for modified χ_w are given as follows.

$$\chi_w \quad = 1.2 \qquad \bar{\lambda}_w \leq 0.14$$

$$= \frac{0.883}{\bar{\lambda}_w^{0.155}} \qquad 0.14 < \bar{\lambda}_w < 0.72 \qquad (3.22)$$

$$= \frac{1.023}{0.377 + \bar{\lambda}_w} \qquad \bar{\lambda}_w \geq 0.72$$

The proposed predicted strength ($T_{u,EN\text{-}modified}$) is plotted in Figure 3.31. A check on reliability of proposed design equation was done. Mean, COV and β were found to be 1.146, 0.118 and 3.32 respectively. The target reliability of 2.5 is met (Table

3.10) and hence, the proposed equation may be safely adopted for design of LDSS SEHS members under torsion.

3.8.3 Deformation Based Method (DBM)

A simple design method based on deformation capacity of section was developed which is in line with Continuous Strength Method (CSM). CSM is a deformation based design rule recently proposed so as to harness significant strain hardening in stocky sections of non-linear metallic material like stainless steel. The method was originally proposed for structural stainless steel (Gardner, 2002) and further extended to other metallic materials such as aluminium and high strength steel (Gardner & Ashraf, 2006). Generally, available stainless steel design guidelines such as EN 1993-1-4: 2006, ASCE 8-02: 2002 and AS/NZS 4673: 2001 restrict the strength of a structural member to yield strength which under predicts its strength in case of a stocky section where there is significant strain hardening and often makes the design guidelines conservative. This method allows simple calculation of strength based on a base curve relating a non dimensional deformation capacity with full cross-section slenderness (accounts for beneficial element interaction within the cross-section) and a material model representing material behavior (accounts for beneficial strain hardening). A common upper limit of full cross-section slenderness $\bar{\lambda}_p$ = 0.68 was adopted for stainless steel, carbon steel and aluminium (Afshan & Gardner, 2013) (where $\bar{\lambda}_p = \sqrt{f_y / f_{cr}}$). Ahmed et al. (2016) and Zhao et al. (2017) further extended this method to slender cross sections ($\bar{\lambda}_p$ > 0.68) which facilitates design equations over whole range of cross-section slenderness. The same slenderness $\bar{\lambda}_p$ limit of 0.68 was adopted for the proposed method herein. Instead of strain ratio like in CSM, ratio of rotation capacity (θ_c/θ_y) was used in the present method proposed. Rotation capacity is defined in terms of torsional slenderness (λ_T) over full range which in turn is related to its ultimate strength. An expression for θ_c/θ_y for slender section ($\lambda_T > 0.68$) similar to that of

CSM base curve for stainless steel slender section as derived by Zhao et al. (2017) was adopted as it was found to match well with the FE results, which was not so for stocky section and hence an expression for θ_c/θ_y has been proposed for $\lambda_T \leq 0.68$ (see Equation 3.23). Figure 3.32 shows a continuous relationship between proposed normalized rotation capacity (θ_c/θ_y) with torsional slenderness λ_T which can be expressed as

$$\begin{aligned} \theta_c / \theta_y &= \frac{0.581}{\lambda_T^{1.41}} && \lambda_T \leq 0.68 \\ &= \frac{1}{\lambda_T^{1.05}}\left(1-\frac{0.222}{\lambda_T^{1.05}}\right) && \lambda_T > 0.68 \end{aligned} \tag{3.23}$$

Once rotation capacity (θ_c) for the section is known, ultimate strength can be determined by using an established relation between strength and rotation capacity. Figure 3.33 shows variation of T_u/T_y with θ_c/θ_y from FE analysis in this study. A lower bound regression curve was fitted with an initial linear curve and a power law second curve to determine relation between section ultimate capacity and rotation capacity. The ultimate capacity ($T_{u,DBM}$) can then be calculated by using proposed relation given by Equation 3.24.

$$\begin{aligned} T_{u,DBM}/T_y &= \left(\theta_c/\theta_y\right) && \theta_c/\theta_y < 1 \\ &= \left(\theta_c/\theta_y\right)^{0.1} && \theta_c/\theta_y \geq 1 \end{aligned} \tag{3.24}$$

The proposed design curve was checked for reliability using reliability analysis detailed in Section 3.6. A reliability index (β) of 3.01 was obtained (see Table 3.10) which is higher than the target reliability index (β = 2.5). Hence, the proposed design method may be reliably adopted for design of LDSS SEHS under torsion.

3.9 Conclusion

A systematic numerical based (using finite element analysis) parametric study was conducted on lean duplex stainless steel semi-elliptical hollow tubular members under torsion. Effect of various parameters such as curve length, aspect ratio and section size on ultimate torsional capacity was studied for sections with different cross-section slenderness. The following observations were made from the study:

1. Increase in curve length was found to increase the torque carrying capacity in a near linear manner. Also, rate of increase in T_u was seen to be more for stocky sections.
2. Sections of higher aspect ratio were found to carry more torque. But on the other hand, twist at maximum torque was seen to be more for sections of lower aspect ratio. Initial stiffness in T - θ curve was observed to be affected to a great extent by aspect ratio, which reduces as aspect ratio lowers in case of both slender and stocky sections.
3. Reduction in member size decreases its torque carrying capacity. For SEHS sections of different size, similar behaviour of T-θ response was observed in contrast to non-SEHS sections. Section size was also seen to have considerable effect on initial stiffness of T-θ response.
4. Member length was found not to have significant effect on T_u although θ_u was found to increase significantly with increase in member length. Minor reduction in T_u was seen for short members which becomes stable after a certain length of member.

Shear design equations available for plated members were checked for its applicability in torsion design of LDSS SEHS members. The equations were found to give unreliable results and hence new design equations were proposed for design of LDSS semi-elliptical hollow section members under torsion. The proposed design equations were adapted to three different formats – Direct Strength Method,

Eurocode and Deformation Based Method. The proposed equations were assessed by a reliability analysis and were found to satisfy the target reliability index. It may be noted that, further improvement in the design equations could be obtained, as experimental torsional data on LDSS SEHS become available in future.

Table 3.1: Tensile test result on SHS YSt 210 and YSt 310 flat and corner coupons

Section	E (MPa)	$\sigma_{0.05}$ (MPa)	$\sigma_{0.2}$ (MPa)	$\sigma_{1.0}$ (MPa)	σ_u (MPa)	ε_f (%)
SHS 50×50×2.9 - f	1,97,311	328	354	362	368	17.1
SHS 50×50×2.9 - c	1,83,393	365	450	493	510	6.78
SHS 60 × 60 × 3.2 - f	1,95,482	387	412	429	452	17.01
SHS 60 × 60 × 3.2 - c	1,84,322	420	582	640	645	3.73

Table 3.2: Compressive flat material property (Theofanous & Gardner, 2009) for LDSS

Cross-section	E (MPa)	$\sigma_{0.2}$ (MPa)	$\sigma_{1.0}$ (MPa)	Compound R-O coefficient	
				n	$n'_{0.2,1.0}$
100×100×4	198200	560	642	8.3	2.6

Table 3.3: Cross section details of circular and square hollow section (from literature) used for FE validation

Section	B or D (mm)	t (mm)
SHS, CHS (Han et al., 2007)	400.0	9.30
CHS (Beck & Kiyomiya, 2003)	139.8	3.50
SHS (Ridley-Ellis, 2000)	38.00	1.43

B = side length of SHS, D = diameter of CHS, t = thickness

Table 3.4: Comparison of response from FE models and experimental results

	FE/Test							
	Present experimental study				Literature		Mean	COV
	YSt 210		YSt 310		(Ridley-Ellis, 2000)	(Beck & Kiyomiya, 2003)		
	Sample 1	Sample 2	Sample 1	Sample 2				
Ultimate torque (T_u)	0.99	0.99	0.98	0.97	1.01	1.45	1.06	0.17
Twist corresponding to T_u (θ_u)	0.89	0.79	0.89	0.91	1.10	0.43	0.84	0.26
Initial slope of T-θ response	0.85	0.97	1.08	0.94	1.01	1.19	1.01	0.11

Table 3.5: Details of SEHS cross-section geometry and FE results generated for parametric study on effect of curve length

Section	h (mm)	b (mm)	t (mm)	l_c (mm)	$T_{u,FE}$ (kNm)
*h*55.7-*b*111.5-*t*3	55.7	111.5	3	270	13.82
*h*74.7-*b*111.5-*t*3	74.7	111.5	3	295	20.13
*h*92.5-*b*111.5-*t*3	92.5	111.5	3	321	25.93
*h*111.5-*b*111.5-*t*3	111.5	111.5	3	350	32.04
*h*133.8-*b*111.5-*t*3	133.8	111.5	3	386	39.15
*h*167.2-*b*111.5-*t*3	167.2	111.5	3	442	49.45
*h*203-*b*111.5-*t*3	203	111.5	3	504.5	60.12
*h*223-*b*111.5-*t*3	223	111.5	3	540	65.36
*h*55.7-*b*111.5-*t*6	55.7	111.5	6	270	32.03
*h*74.7-*b*111.5-*t*6	74.7	111.5	6	295	46.11
*h*92.5-*b*111.5-*t*6	92.5	111.5	6	321	59.38
*h*111.5-*b*111.5-*t*6	111.5	111.5	6	350	73.58
*h*133.8-*b*111.5-*t*6	133.8	111.5	6	386	90.5
*h*167.2-*b*111.5-*t*6	167.2	111.5	6	442	116.2
*h*203-*b*111.5-*t*6	203	111.5	6	504.5	143.1
*h*223-*b*111.5-*t*6	223	111.5	6	540	155.8
*h*55.7-*b*111.5-*t*12	55.7	111.5	12	270	58.78
*h*74.7-*b*111.5-*t*12	74.7	111.5	12	295	88.46
*h*92.5-*b*111.5-*t*12	92.5	111.5	12	321	117.19
*h*111.5-*b*111.5-*t*12	111.5	111.5	12	350	148.29
*h*133.8-*b*111.5-*t*12	133.8	111.5	12	386	185.37
*h*167.2-*b*111.5-*t*12	167.2	111.5	12	442	241.06
*h*203-*b*111.5-*t*12	203	111.5	12	504.5	297.45
*h*223-*b*111.5-*t*12	223	111.5	12	540	325.1
*h*74.7-*b*111.5-*t*20	74.7	111.5	20	295	130.35
*h*92.5-*b*111.5-*t*20	92.5	111.5	20	321	177.76
*h*111.5-*b*111.5-*t*20	111.5	111.5	20	350	228.69
*h*133.8-*b*111.5-*t*20	133.8	111.5	20	386	288.61
*h*167.2-*b*111.5-*t*20	167.2	111.5	20	442	377.77
*h*203-*b*111.5-*t*20	203	111.5	20	504.5	470.29
*h*223-*b*111.5-*t*20	223	111.5	20	540	519.82

Table 3.6: Details of SEHS cross-section geometry and FE results generated for parametric study on effect of aspect ratio

Section	h (mm)	b (mm)	t (mm)	h/b	$T_{u,FE}$ (kNm)
*h*82.3-*b*164.6-*t*25	82.3	164.6	25	0.5	239.7
*h*103.9-*b*155.1-*t*25	103.9	155.1	25	0.67	326.1
*h*122.1-*b*147.1-*t*25	122.1	147.1	25	0.83	392.3
*h*139.4-*b*139.4-*t*25	139.4	139.4	25	1	447.3
*h*157.7-*b*131.4-*t*25	157.7	131.4	25	1.2	494.1
*h*203-*b*111.5-*t*25	203	111.5	25	1.8	560.9
*h*213.6-*b*106.8-*t*25	213.6	106.8	25	2	564.9
*h*82.3-*b*164.6-*t*20	82.3	164.6	20	0.5	206.2
*h*139.4-*b*139.4-*t*20	139.4	139.4	20	1	374.8
*h*157.7-*b*131.4-*t*20	157.7	131.4	20	1.2	413.8
*h*203-*b*111.5-*t*20	203	111.5	20	1.8	470.3
*h*213.6-*b*106.8-*t*20	213.6	106.8	20	2	473.5
*h*82.3-*b*164.6-*t*17	82.3	164.6	17	0.5	183.2
*h*103.9-*b*155.1-*t*17	103.9	155.1	17	0.67	241.7
*h*122.1-*b*147.1-*t*17	122.1	147.1	17	0.83	286.6
*h*139.4-*b*139.4-*t*17	139.4	139.4	17	1	325.5
*h*157.7-*b*131.4-*t*17	157.7	131.4	17	1.2	359.7
*h*203-*b*111.5-*t*17	203	111.5	17	1.8	409.8
*h*213.6-*b*106.8-*t*17	213.6	106.8	17	2	412.4
*h*139.4-*b*139.4-*t*14.2	139.4	139.4	14.2	1	275.3
*h*157.7-*b*131.4-*t*14.2	157.7	131.4	14.2	1.2	304.5
*h*203-*b*111.5-*t*14.2	203	111.5	14.2	1.8	348.9
*h*213.6-*b*106.8-*t*14.2	213.6	106.8	14.2	2	350.6
*h*82.3-*b*164.6-*t*12.5	82.3	164.6	12.5	0.5	142.6
*h*139.4-*b*139.4-*t*12.5	139.4	139.4	12.5	1	243.2
*h*157.7-*b*131.4-*t*12.5	157.7	131.4	12.5	1.2	268.8
*h*203-*b*111.5-*t*12.5	203	111.5	12.5	1.8	309.4
*h*213.6-*b*106.8-*t*12.5	213.6	106.8	12.5	2	310.5
*h*82.3-*b*164.6-*t*10	82.3	164.6	10	0.5	116.2
*h*103.9-*b*155.1-*t*10	103.9	155.1	10	0.67	148.8
*h*122.1-*b*147.1-*t*10	122.1	147.1	10	0.83	173.3
*h*139.4-*b*139.4-*t*10	139.4	139.4	10	1	194.4
*h*157.7-*b*131.4-*t*10	157.7	131.4	10	1.2	214.0
*h*203-*b*111.5-*t*10	203	111.5	10	1.8	247.5
*h*213.6-*b*106.8-*t*10	213.6	106.8	10	2	247.9

*h*82.3-*b*164.6-*t*8	82.3	164.6	8	0.5	92.63
*h*139.4-*b*139.4-*t*8	139.4	139.4	8	1	154.0
*h*157.7-*b*131.4-*t*8	157.7	131.4	8	1.2	169.2
*h*203-*b*111.5-*t*8	203	111.5	8	1.8	195.7
*h*213.6-*b*106.8-*t*8	213.6	106.8	8	2	196.1
*h*82.3-*b*164.6-*t*7	82.3	164.6	7	0.5	80.1
*h*139.4-*b*139.4-*t*7	139.4	139.4	7	1	133.6
*h*157.7-*b*131.4-*t*7	157.7	131.4	7	1.2	146.5
*h*82.3-*b*164.6-*t*6	82.3	164.6	6	0.5	67
*h*103.9-*b*155.1-*t*6	103.9	155.1	6	0.67	86.4
*h*122.1-*b*147.1-*t*6	122.1	147.1	6	0.83	100.8
*h*139.4-*b*139.4-*t*6	139.4	139.4	6	1	112.8
*h*157.7-*b*131.4-*t*6	157.7	131.4	6	1.2	123.8
*h*203-*b*111.5-*t*6	203	111.5	6	1.8	143.1
*h*213.6-*b*106.8-*t*6	213.6	106.8	6	2	143.8
*h*82.3-*b*164.6-*t*5	82.3	164.6	5	0.5	53
*h*139.4-*b*139.4-*t*5	139.4	139.4	5	1	91.6
*h*157.7-*b*131.4-*t*5	157.7	131.4	5	1.2	100.8
*h*203-*b*111.5-*t*5	203	111.5	5	1.8	115.8
*h*213.6-*b*106.8-*t*5	213.6	106.8	5	2	117.0
*h*82.3-*b*164.6-*t*4	82.3	164.6	4	0.5	37.9
*h*103.9-*b*155.1-*t*4	103.9	155.1	4	0.67	50.5
*h*139.4-*b*139.4-*t*4	139.4	139.4	4	1	69.2
*h*157.7-*b*131.4-*t*4	157.7	131.4	4	1.2	76.5
*h*203-*b*111.5-*t*4	203	111.5	4	1.8	88.8
*h*213.6-*b*106.8-*t*4	213.6	106.8	4	2	89.9
*h*82.3-*b*164.6-*t*3.5	82.3	164.6	3.5	0.5	30.5
*h*139.4-*b*139.4-*t*3.5	139.4	139.4	3.5	1	56.3
*h*157.7-*b*131.4-*t*3.5	157.7	131.4	3.5	1.2	63.1
*h*203-*b*111.5-*t*3.5	203	111.5	3.5	1.8	75.1
*h*213.6-*b*106.8-*t*3.5	213.6	106.8	3.5	2	76.5
*h*82.3-*b*164.6-*t*3	82.3	164.6	3	0.5	23.6
*h*139.4-*b*139.4-*t*3	139.4	139.4	3	1	45.3
*h*157.7-*b*131.4-*t*3	157.7	131.4	3	1.2	50.8
*h*203-*b*111.5-*t*3	203	111.5	3	1.8	60.1
*h*213.6-*b*106.8-*t*3	213.6	106.8	3	2	61.3
*h*82.3-*b*164.6-*t*2.5	82.3	164.6	2.5	0.5	17.7
*h*157.7-*b*131.4-*t*2.5	157.7	131.4	2.5	1.2	39.4
*h*203-*b*111.5-*t*2.8	203	111.5	2.8	1.8	54.6
*h*82.3-*b*164.6-*t*2	82.3	164.6	2	0.5	12.4
*h*157.7-*b*131.4-*t*2	157.7	131.4	2	1.2	28.7
*h*213.6-*b*106.8-*t*2	213.6	106.8	2	2	31.2

*h*82.3-*b*164.6-*t*1.4	82.3	164.6	1.4	0.5	6.36
*h*82.3-*b*164.6-*t*1	82.3	164.6	1	0.5	2.80
*h*213.6-*b*106.8-*t*1.6	213.6	106.8	1.6	2	20.4
*h*139.4-*b*139.4-*t*1.3	139.4	139.4	1.3	1	12.3
*h*213.6-*b*106.8-*t*1.3	213.6	106.8	1.3	2	12.6
*h*213.6-*b*106.8-*t*1.2	213.6	106.8	1.2	2	10.1
*h*157.7-*b*131.4-*t*1	157.7	131.4	1	1.2	7.7
*h*213.6-*b*106.8-*t*1	213.6	106.8	1	2	6.50
*h*139.4-*b*139.4-*t*0.9	139.4	139.4	0.9	1	5.50
*h*213.6-*b*106.8-*t*0.8	213.6	106.8	0.8	2	4.20
*h*157.7-*b*131.4-*t*0.7	157.7	131.4	0.7	1.2	3.56

Table 3.7: Details of SEHS cross-section geometry and FE results generated for parametric study on effect of section size (Case I)

Section	*h* (mm)	*b* (mm)	*t* (mm)	$T_{u,FE}$ (kNm)
*h*50-*b*50-*t*3	50	50	3	7.4
*h*111.5-*b*111.5-*t*3	111.5	111.5	3	32.1
*h*125-b125-*t*3	125	125	3	38.1
*h*139.4-*b*139.4-*t*3	139.4	139.4	3	47.1
*h*150-*b*150-*t*3	150	150	3	50.8
*h*175-*b*175-*t*3	175	175	3	64.6
*h*50-*b*50-*t*30	50	50	30	51.2
*h*111.5-*b*111.5-*t*30	111.5	111.5	30	301.5
*h*125-b125-*t*30	125	125	30	394.1
*h*139.4-*b*139.4-*t*30	139.4	139.4	30	508.9
*h*150-*b*150-*t*30	150	150	30	602.2
*h*175-*b*175-*t*30	175	175	30	853.4
*h*75-*b*50-*t*3	75	50	3	11.8
*h*167.2-*b*111.5-*t*3	167.2	111.5	3	49.7
*h*187.5-b125-*t*3	187.5	125	3	59.7
*h*209.1-*b*139.4-*t*3	209.1	139.4	3	71.3
*h*225-*b*150-*t*3	225	150	3	80.1
*h*262.5-*b*175-*t*3	262.5	175	3	102.5
*h*75-*b*50-*t*30	75	50	30	69.3
*h*167.2-*b*111.5-*t*30	167.2	111.5	30	511.8
*h*187.5-b125-*t*30	187.5	125	30	664.4
*h*209.1-*b*139.4-*t*30	209.1	139.4	30	850.8
*h*225-*b*150-*t*30	225	150	30	1001.6
*h*262.5-*b*175-*t*30	262.5	175	30	1406.7
*h*100-*b*50-*t*3	100	50	3	15.8

*h*223-*b*111.5-*t*3	223	111.5	3	65.7
*h*250-b125-*t*3	250	125	3	78.4
*h*278.8-*b*139.4-*t*3	278.8	139.4	3	91.3
*h*300-*b*150-*t*3	300	150	3	99.3
*h*350-*b*175-*t*3	350	175	3	113.7
*h*100-*b*50-*t*30	100	50	30	95.2
*h*223-*b*111.5-*t*30	223	111.5	30	714.1
*h*250-b125-*t*30	250	125	30	924.3
*h*278.8-*b*139.4-*t*30	278.8	139.4	30	1178.9
*h*300-*b*150-*t*30	300	150	30	1384.0
*h*350-*b*175-*t*30	350	175	30	1932.3

Table 3.8: Details of SEHS cross-section geometry and FE results generated for parametric study on effect of section size (Case II)

Section	*h*' (mm)	*b*' (mm)	*t* (mm)	*h*/*b*	l_f'/l_f	$T_{u,FE}$ (kNm)
h'139.4-*b*'139.4-*t*3	139.4	139.4	3	1	1.00	47.16
h'96.4-*b*'132.6-*t*3	96.4	132.6	3	1	0.95	27.67
h'79.4-*b*'125.8-*t*3	79.4	125.8	3	1	0.90	21.38
h'66.4-*b*'118.8-*t*3	66.4	118.8	3	1	0.85	17.05
h'54.4-*b*'110.5-*t*3	54.4	110.5	3	1	0.80	13.36
h'47.4-*b*'104.8-*t*3	47.4	104.8	3	1	0.75	11.54
h'39.4-*b*'97.2-*t*3	39.4	97.2	3	1	0.70	9.37
h'139.4-*b*'139.4-*t*12	139.4	139.4	12	1	1.00	300.5
h'96.4-*b*'132.6-*t*12	96.4	132.6	12	1	0.95	190.9
h'79.4-*b*'125.8-*t*12	79.4	125.8	12	1	0.90	150.6
h'66.4-*b*'118.8-*t*12	66.4	118.8	12	1	0.85	121.1
h'54.4-*b*'110.5-*t*12	54.4	110.5	12	1	0.80	95.52
h'47.4-*b*'104.8-*t*12	47.4	104.8	12	1	0.75	81.36
h'39.4-*b*'97.2-*t*12	39.4	97.2	12	1	0.70	65.98
h'139.4-*b*'139.4-*t*20	139.4	139.4	20	1	1.00	374.8
h'96.4-*b*'132.6-*t*20	96.4	132.6	20	1	0.95	371.6
h'79.4-*b*'125.8-*t*20	79.4	125.8	20	1	0.90	298.2
h'66.4-*b*'118.8-*t*20	66.4	118.8	20	1	0.85	244.6
h'54.4-*b*'110.5-*t*20	54.4	110.5	20	1	0.80	197.3
h'47.4-*b*'104.8-*t*20	47.4	104.8	20	1	0.75	170.7
h'39.4-*b*'97.2-*t*20	39.4	97.2	20	1	0.70	141.6
h'181.4-*b*'120.9-*t*3	181.5	120.9	3	1.5	1.00	56.58
h'121.4-*b*'114.1-*t*3	121.4	114.1	3	1.5	0.95	34.27
h'101.4-*b*'108.6-*t*3	101.4	108.6	3	1.5	0.90	27.46
h'85.4-*b*'102.6-*t*3	85.4	102.6	3	1.5	0.85	22.68

h′72.4-*b*′96.7-*t*3	72.4	96.7	3	1.5	0.80	18.58
h′61.4-*b*′90.7-*t*3	61.4	90.7	3	1.5	0.75	15.00
h′51.4-*b*′84.4-*t*3	51.4	84.4	3	1.5	0.70	11.92
h′181.4-*b*′120.9-*t*12	181.5	120.9	12	1.5	1.00	284.4
h′121.4-*b*′114.1-*t*12	121.4	114.1	12	1.5	0.95	212.7
h′101.4-*b*′108.6-*t*12	101.4	108.6	12	1.5	0.90	169.3
h′85.4-*b*′102.6-*t*12	85.4	102.6	12	1.5	0.85	136.3
h′72.4-*b*′96.7-*t*12	72.4	96.7	12	1.5	0.80	111.0
h′61.4-*b*′90.7-*t*12	61.4	90.7	12	1.5	0.75	90.8
h′51.4-*b*′84.4-*t*12	51.4	84.4	12	1.5	0.70	73.4
h′181.4-*b*′120.9-*t*30	181.5	120.9	30	1.5	1.00	451.6
h′121.4-*b*′114.1-*t*30	121.4	114.1	30	1.5	0.95	403.4
h′101.4-*b*′108.6-*t*30	101.4	108.6	30	1.5	0.90	325.4
h′85.4-*b*′102.6-*t*30	85.4	102.6	30	1.5	0.85	265.9
h′72.4-*b*′96.7-*t*30	72.4	96.7	30	1.5	0.80	219.7
h′61.4-*b*′90.7-*t*30	61.4	90.7	30	1.5	0.75	182.3
h′51.4-*b*′84.4-*t*30	51.4	84.4	30	1.5	0.70	150.0
h′213.6-*b*′106.8-*t*3	213.6	106.8	3	2	1.00	61.3
h′145.6-*b*′101.2-*t*3	145.6	101.2	3	2	0.95	39.8
h′120.6-*b*′96.1-*t*3	120.6	96.1	3	2	0.90	32.2
h′100.6-*b*′90.6-*t*3	100.6	90.6	3	2	0.85	25.4
h′85.6-*b*′85.5-*t*3	85.6	85.5	3	2	0.80	20.5
h′72.6-*b*′80.2-*t*3	72.6	80.2	3	2	0.75	16.5
h′60.6-*b*′74.5-*t*3	60.6	74.5	3	2	0.70	13.0
h′213.6-*b*′106.8-*t*12	213.6	106.8	12	2	1.00	298.2
h′145.6-*b*′101.2-*t*12	145.6	101.2	12	2	0.95	231.7
h′120.6-*b*′96.1-*t*12	120.6	96.1	12	2	0.90	182.1
h′100.6-*b*′90.6-*t*12	100.6	90.6	12	2	0.85	144.3
h′85.6-*b*′85.5-*t*12	85.6	85.5	12	2	0.80	114.4
h′72.6-*b*′80.2-*t*12	72.6	80.2	12	2	0.75	95.4
h′60.6-*b*′74.5-*t*12	60.6	74.5	12	2	0.70	76.3
h′213.6-*b*′106.8-*t*30	213.6	106.8	30	2	1.00	473.5
h′145.6-*b*′101.2-*t*30	145.6	101.2	30	2	0.95	428.9
h′120.6-*b*′96.1-*t*30	120.6	96.1	30	2	0.90	340.7
h′100.6-*b*′90.6-*t*30	100.6	90.6	30	2	0.85	273.6
h′85.6-*b*′85.5-*t*30	85.6	85.5	30	2	0.80	225.5
h′72.6-*b*′80.2-*t*30	72.6	80.2	30	2	0.75	185.7
h′60.6-*b*′74.5-*t*30	60.6	74.5	30	2	0.70	150.8

Table 3.9: Details of SEHS cross-section geometry and FE results generated for parametric study on effect of member length

Section	h (mm)	b (mm)	t (mm)	L (mm)	L/l_f	$T_{u, FE}$ (kNm)
*h*213.6-*b*106.8-*t*3	213.6	106.8	3	213.6	1	68.52
*h*213.6-*b*106.8-*t*3	213.6	106.8	3	641.0	3	61.35
*h*213.6-*b*106.8-*t*3	213.6	106.8	3	1068	5	57.48
*h*213.6-*b*106.8-*t*3	213.6	106.8	3	2136	10	53.99
*h*213.6-*b*106.8-*t*3	213.6	106.8	3	4272	20	54.28
*h*213.6-*b*106.8-*t*3	213.6	106.8	3	6408	30	53.10
*h*213.6-*b*106.8-*t*6	213.6	106.8	6	213.6	1	152.3
*h*213.6-*b*106.8-*t*6	213.6	106.8	6	641.0	3	143.6
*h*213.6-*b*106.8-*t*6	213.6	106.8	6	1068	5	143.4
*h*213.6-*b*106.8-*t*6	213.6	106.8	6	2136	10	144.0
*h*213.6-*b*106.8-*t*6	213.6	106.8	6	4272	20	144.2
*h*213.6-*b*106.8-*t*6	213.6	106.8	6	6408	30	144.2
*h*213.6-*b*106.8-*t*8	213.6	106.8	8	213.6	1	207.3
*h*213.6-*b*106.8-*t*8	213.6	106.8	8	641.0	3	195.9
*h*213.6-*b*106.8-*t*8	213.6	106.8	8	1068	5	196.3
*h*213.6-*b*106.8-*t*8	213.6	106.8	8	2136	10	196.6
*h*213.6-*b*106.8-*t*8	213.6	106.8	8	4272	20	197.0
*h*213.6-*b*106.8-*t*10	213.6	106.8	10	641.0	3	247.8
*h*213.6-*b*106.8-*t*10	213.6	106.8	10	1068	5	248.1
*h*213.6-*b*106.8-*t*10	213.6	106.8	10	2136	10	248.1

Table 3.10: Comparison of FE and design strengths

	$T_{u,FE}/T_{Eqn3.5}$	$T_{u,FE}/T_{Eqn3.9}$	$T_{u,FE}/T_{Eqn3.16}$	$T_{u,FE}/T_{Eqn3.20}$	$T_{u,FE}/T_{DSM}$	$T_{u,FE}/T_{EN\text{-}modified}$	$T_{u,FE}/T_{DBM}$
Mean	1.130	1.295	0.986	0.915	1.127	1.146	1.117
COV	0.228	0.284	0.283	0.204	0.111	0.118	0.154
Resistance factor	0.800	0.800	0.800	0.800	0.800	0.800	0.800
Reliability index	2.62	2.69	1.97	2.08	3.29	3.32	3.01

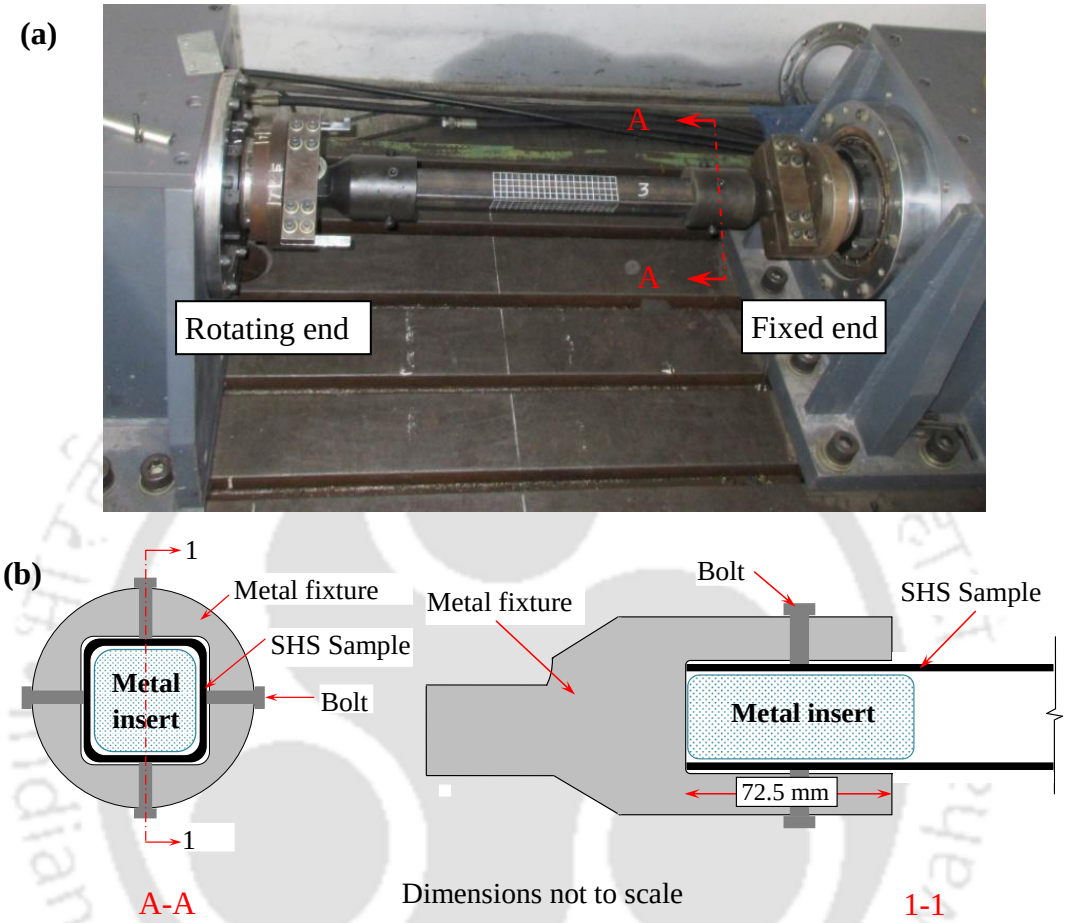

Figure 3.1: (a) Torsional testing arrangement and (b) Schematic details of support fixtures

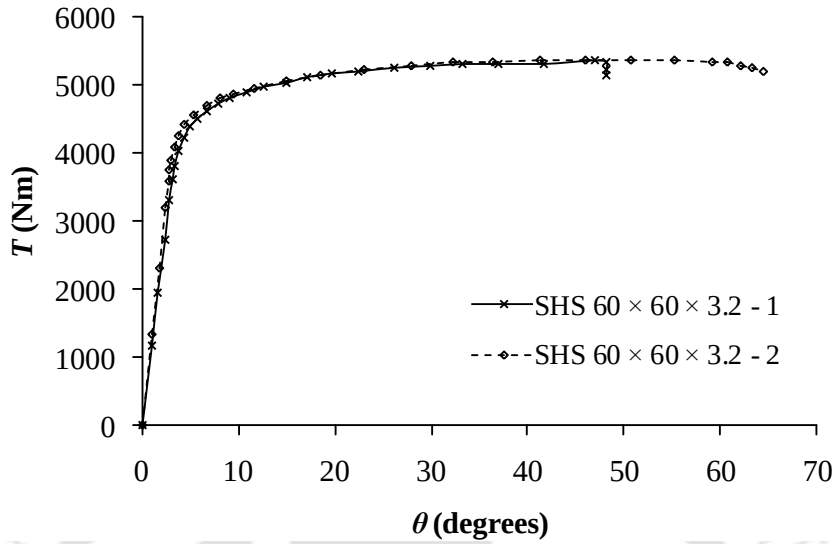

Figure 3.2: Typical experimental *T*-θ curve for SHS 60 × 60 × 3.2 specimens

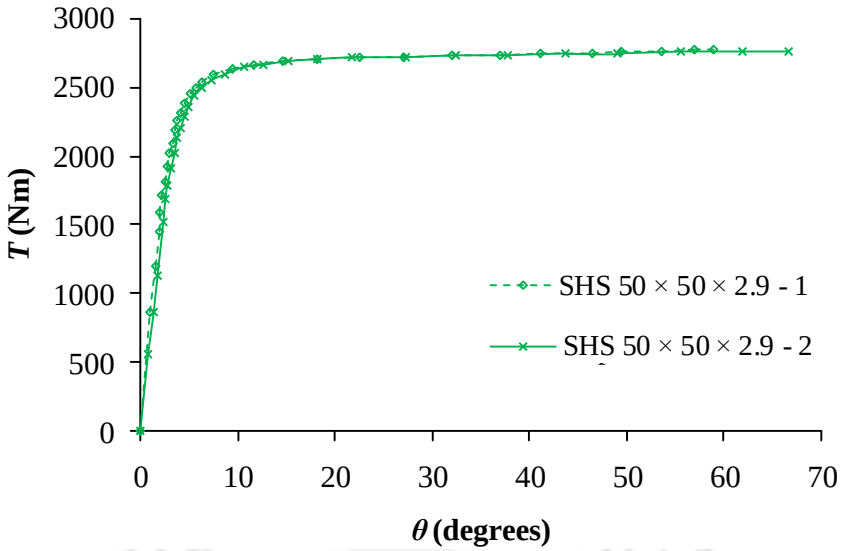

Figure 3.3: Typical experimental *T*-θ curve for SHS 50 × 50 × 2.9 specimens

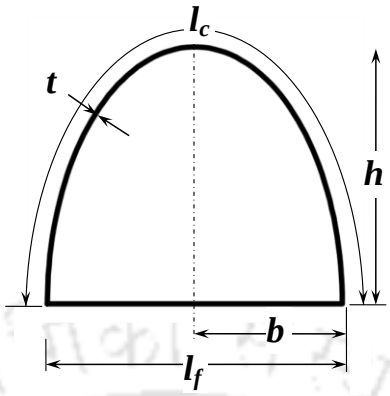

Figure 3.4: Cross-section geometry of semi-elliptical hollow section

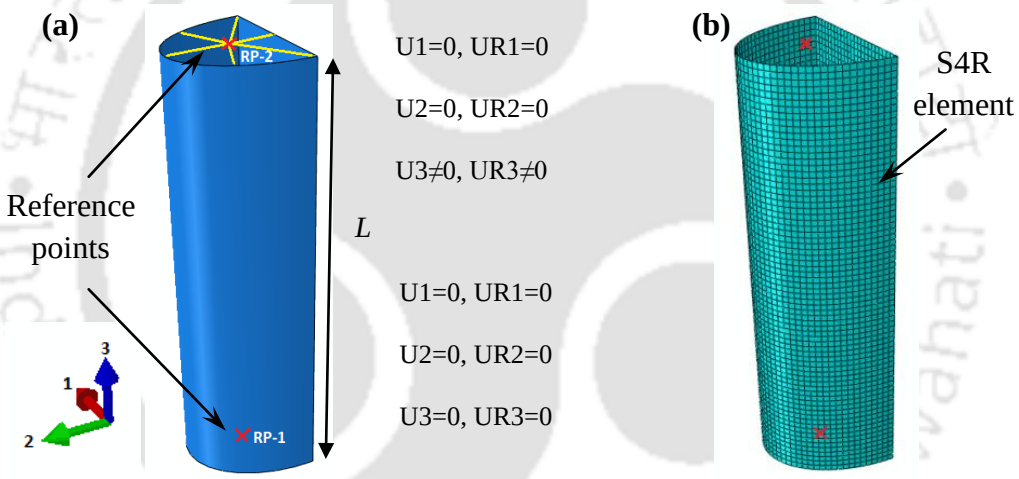

Figure 3.5: (a) Reference points and applied boundary conditions (b) Typical FE mesh

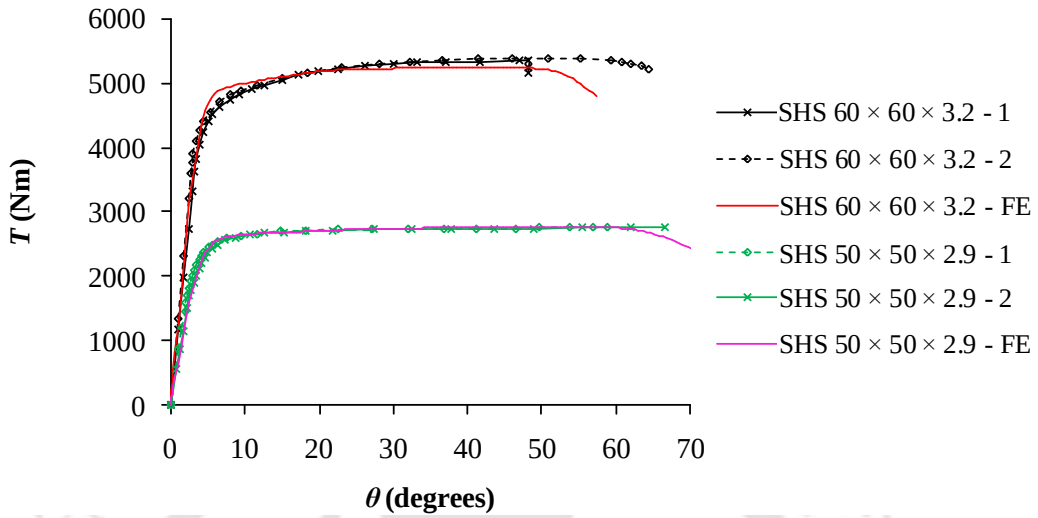

Figure 3.6: Comparison of experimental and FE T-θ responses for SHS specimens

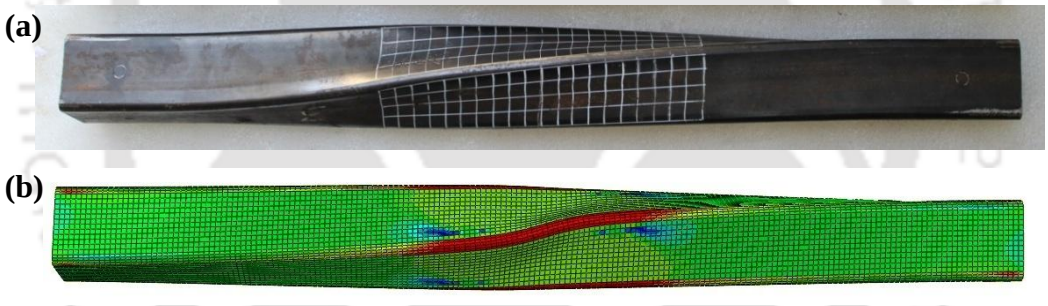

Figure 3.7: Comparison of (a) experimental and (b) FE deformed shapes at post peak rotation of SHS 50 × 50 × 2.9 specimens

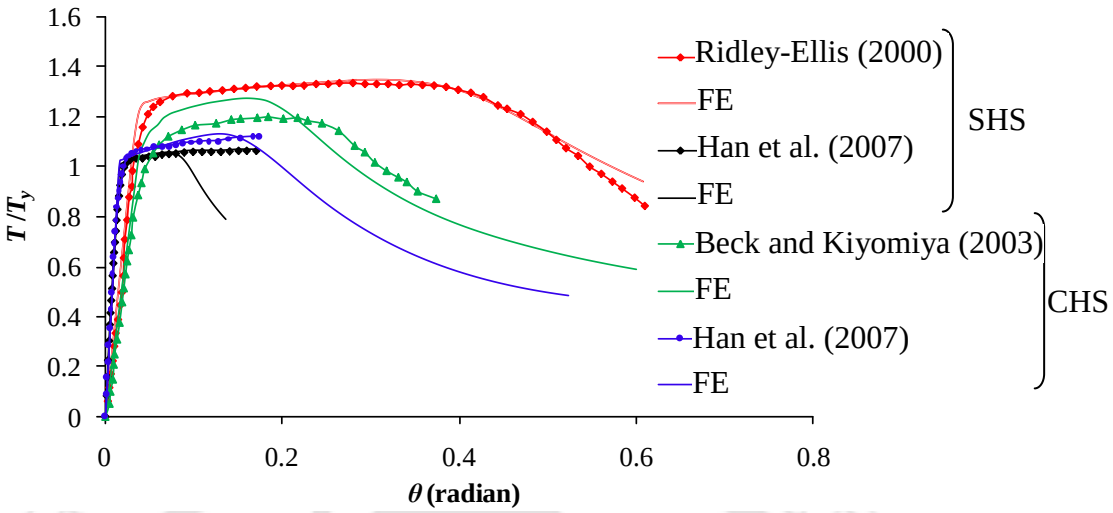

Figure 3.8: Comparison of results from literature and present FE modelling approach

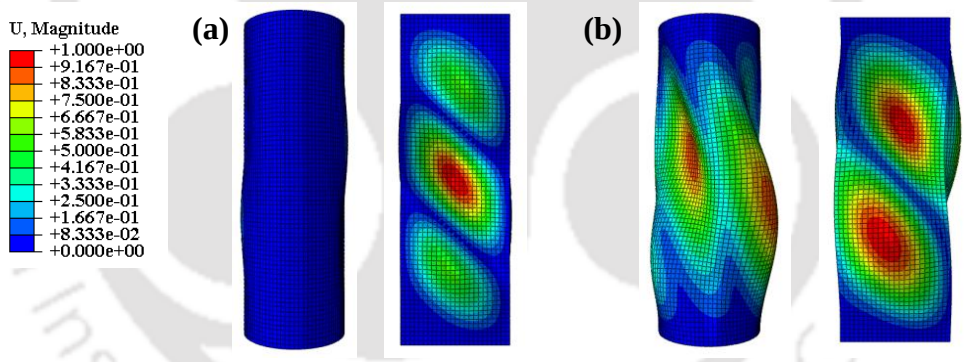

Figure 3.9: First eigen buckling mode for (a) slender (t = 2.7 mm) and (b) stocky (t = 17 mm) section

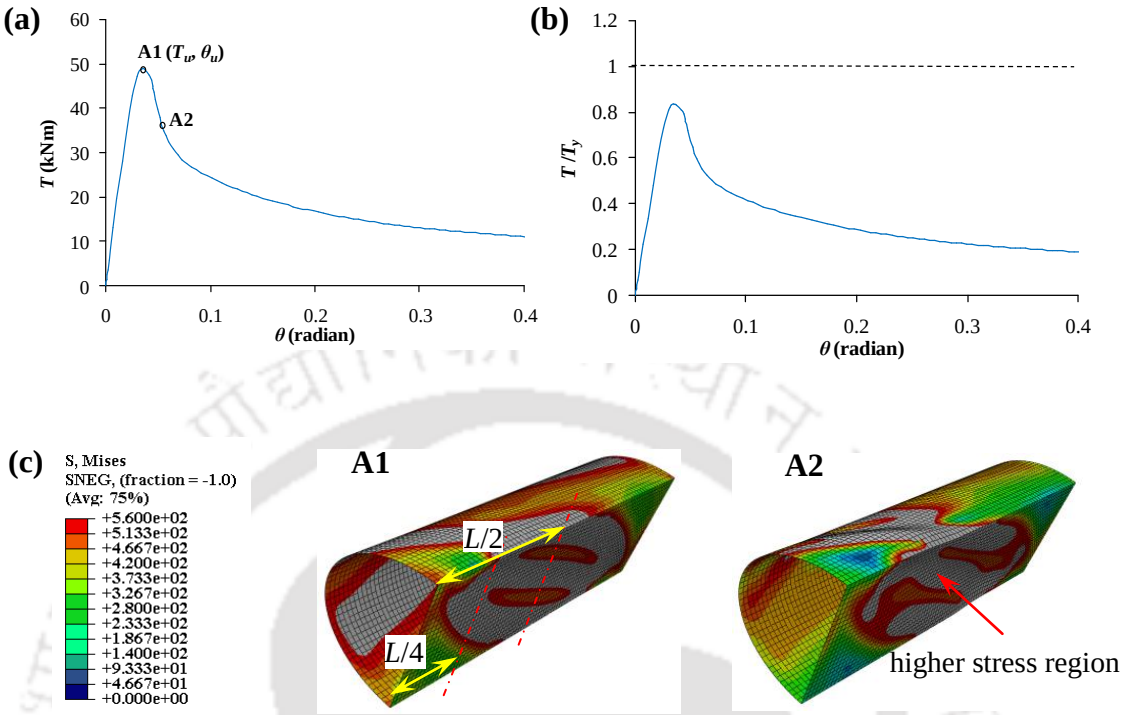

Figure 3.10: (a) Typical T vs θ curve, (b) T/T_y vs θ curve and (c) Von Mises stress contour at θ_u (A1) and 1.5 θ_u (A2) for slender section (h/b = 1.5, t = 2.7 mm)

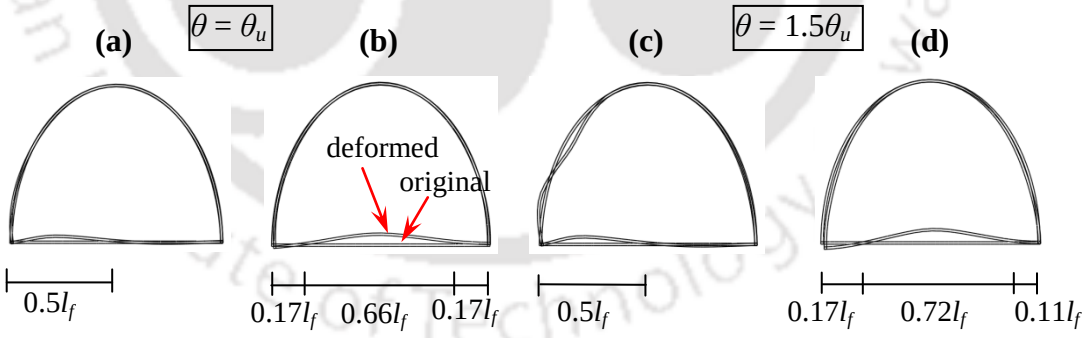

Figure 3.11: Comparison of deformed and undeformed transverse cross section profile at (a) $L/4$, (b) $L/2$ ($\theta = \theta_u$); (c) $L/4$, (d) $L/2$ (θ = 1.5 θ_u)

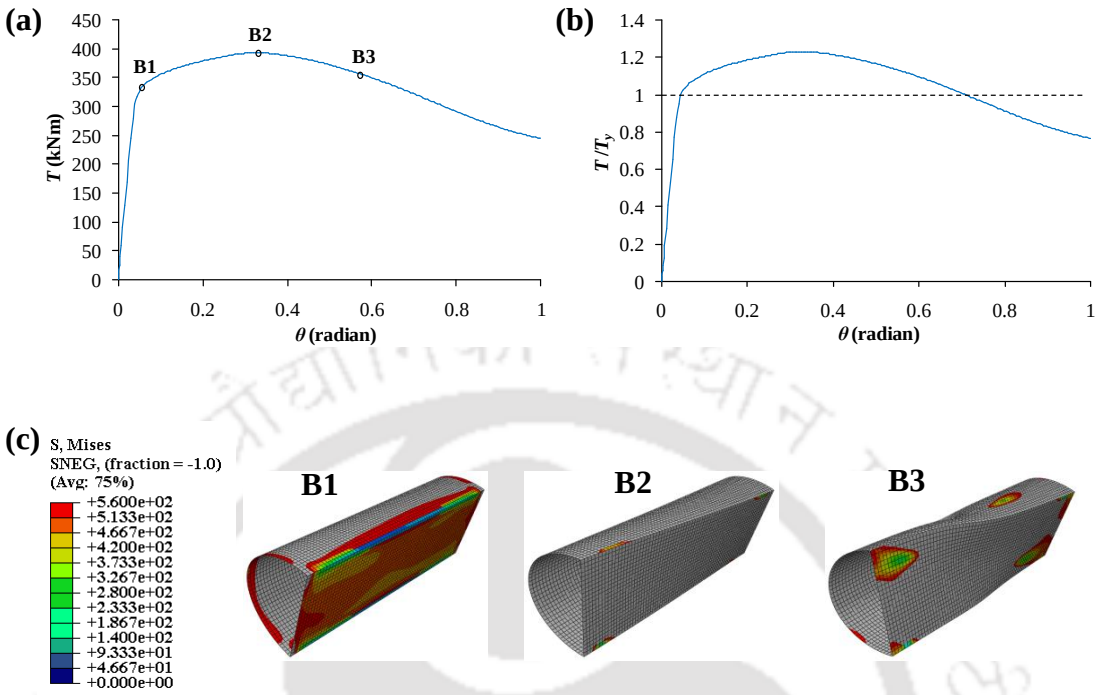

Figure 3.12: (a) Typical T vs θ curve (b) T/T_y vs θ curve and (c) Von Mises stress contour at θ = 0.15 θ_u (B1), θ_u (B2) and 1.5 θ_u (B3) of a stocky section (h/b = 1.5, t = 17 mm)

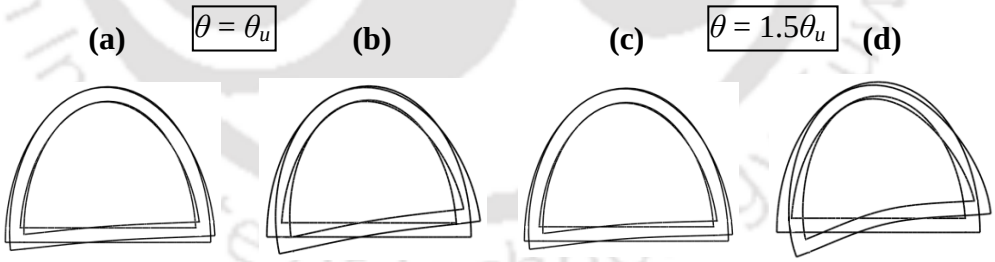

Figure 3.13: Comparison of deformed and undeformed transverse cross-section profile at (a) $L/4$ at θ_u (b) $L/2$ at θ_u (c) $L/4$ length at 1.5 θ_u and (d) $L/2$ at 1.5 θ_u

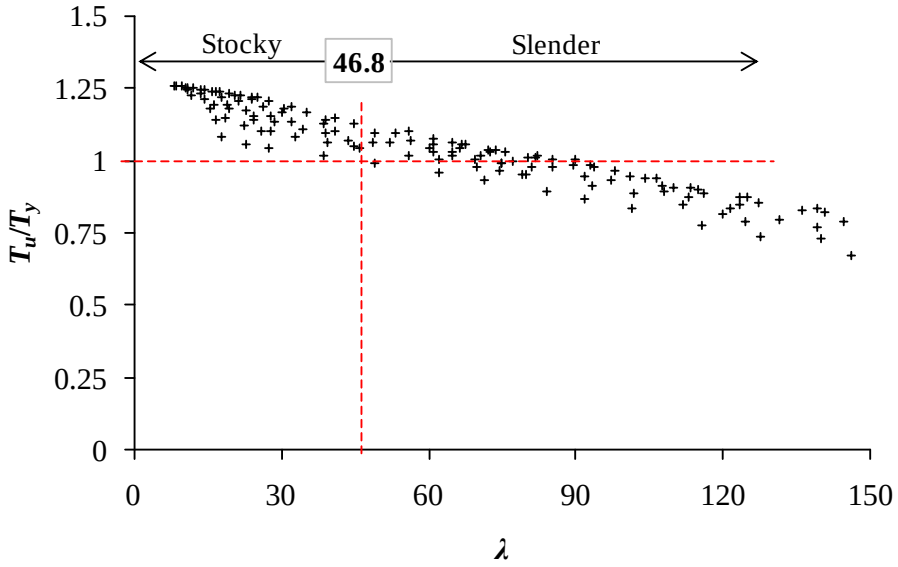

Figure 3.14: T_u/T_y vs cross-section slenderness (λ)

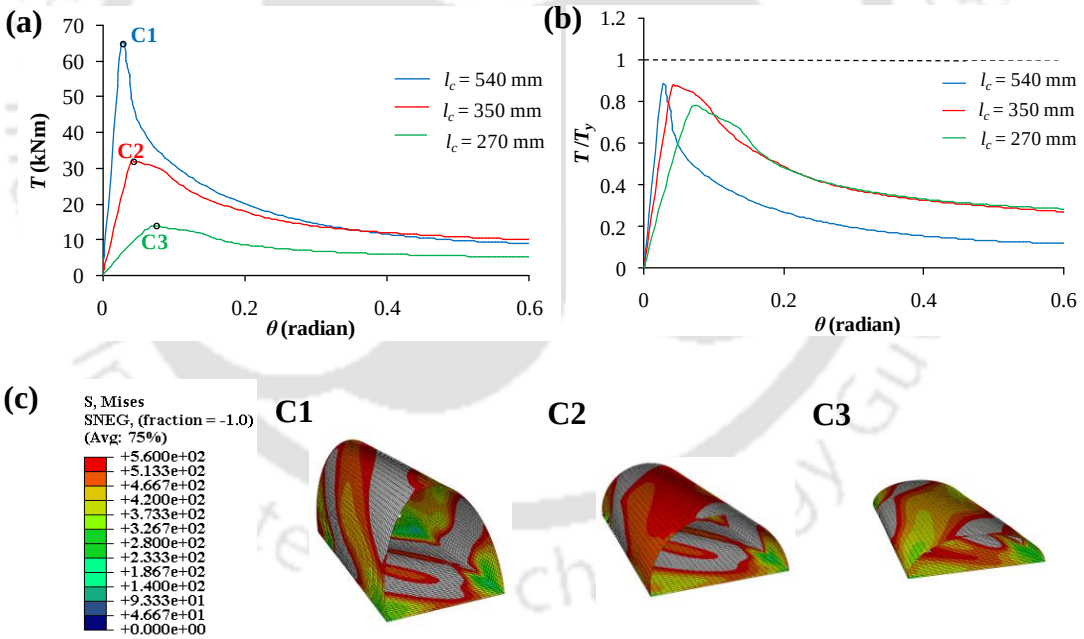

Figure 3.15: (a) Typical T vs θ curve (b) T/T_y vs θ and (c) Von mises stress contour at T_u (C1-C3) for a slender section (t =3 mm)

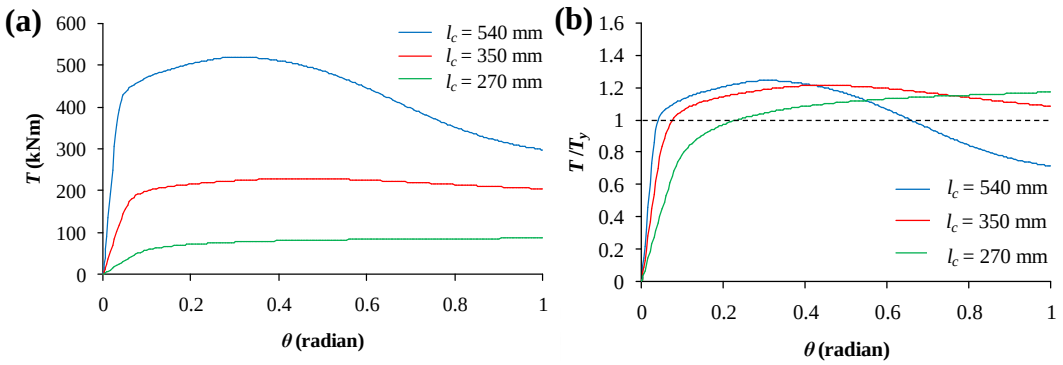

Figure 3.16: (a) Typical T vs θ curve and (b) T/T_y vs θ for a stocky section (t = 20 mm)

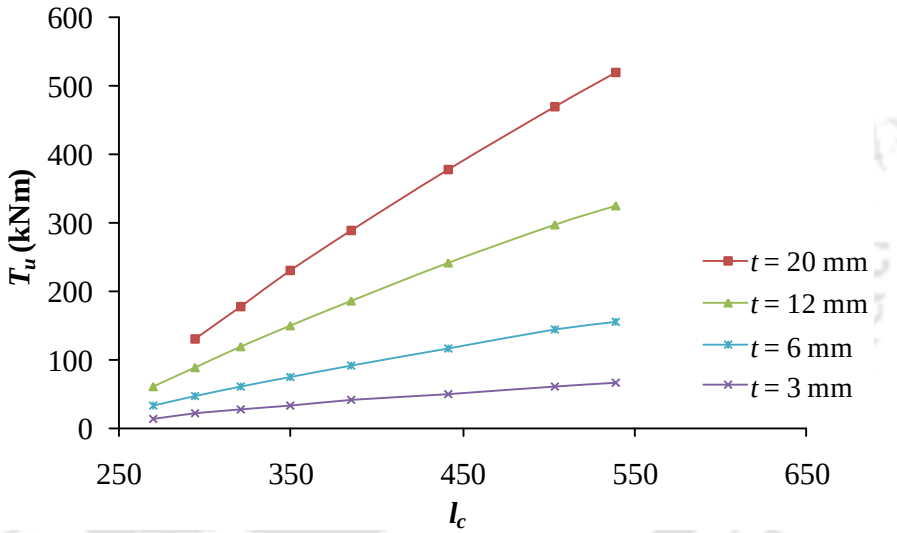

Figure 3.17: T_u vs curve length (l_c)

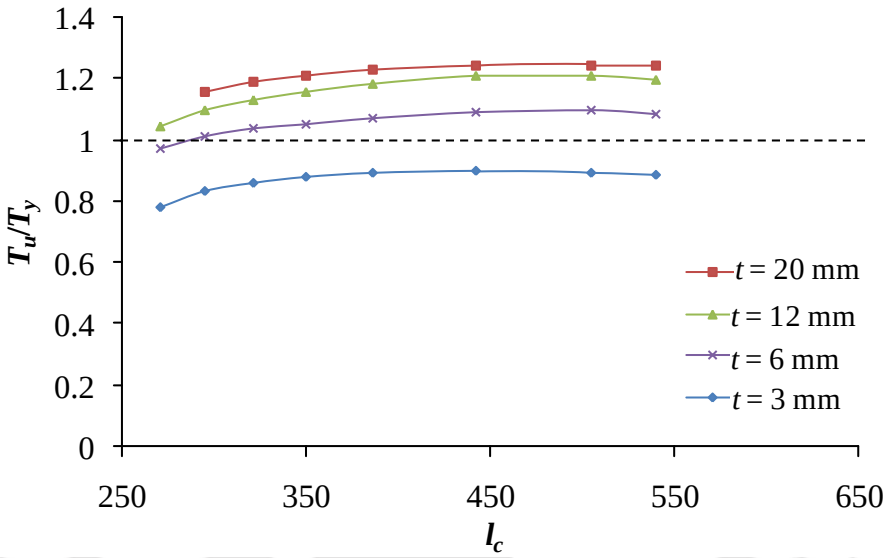

Figure 3.18: T_u/T_y vs curve length (l_c)

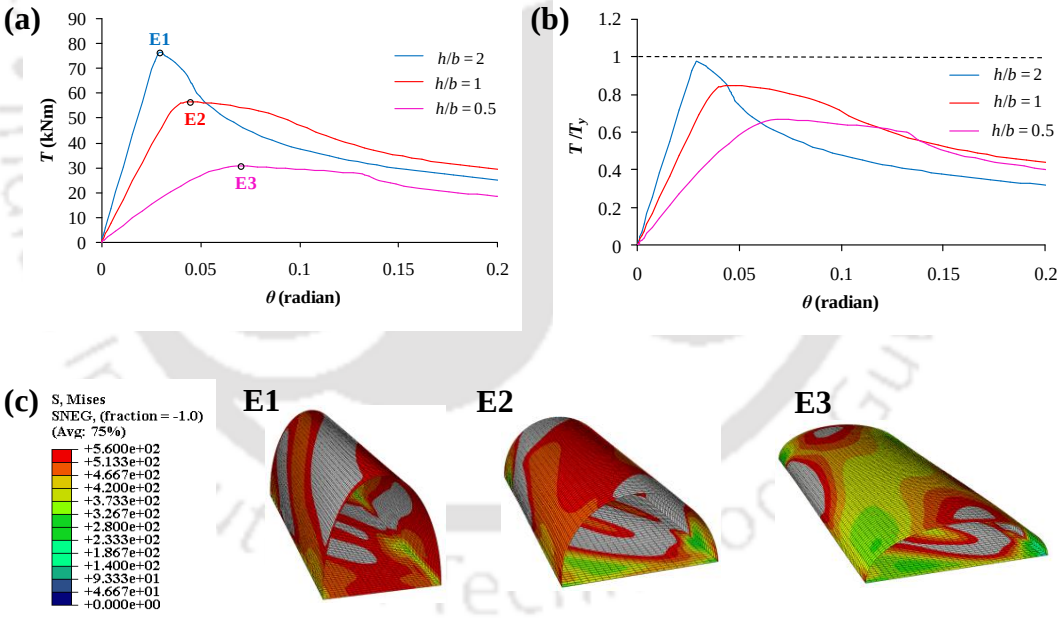

Figure 3.19: (a) T vs θ response (b) T/T_y vs θ and (c) Von mises stress contour of deformed shape at T_u for a slender section (t = 3.5 mm)

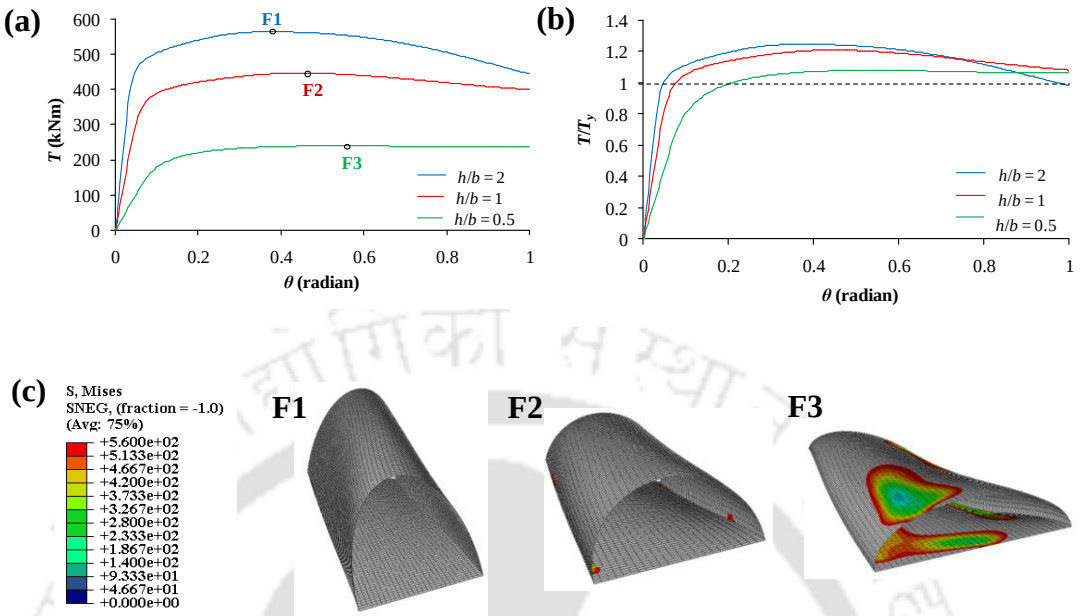

Figure 3.20: (a) T vs θ response (b) T/T_y vs θ and (c) Von mises stress contour of deformed shape at T_u for stocky section (t = 25 mm)

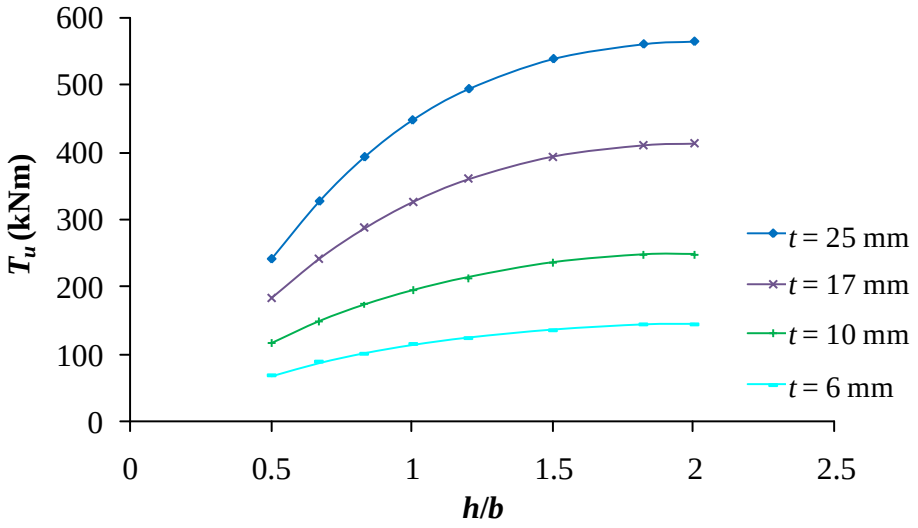

Figure 3.21: Variation of T_u with h/b

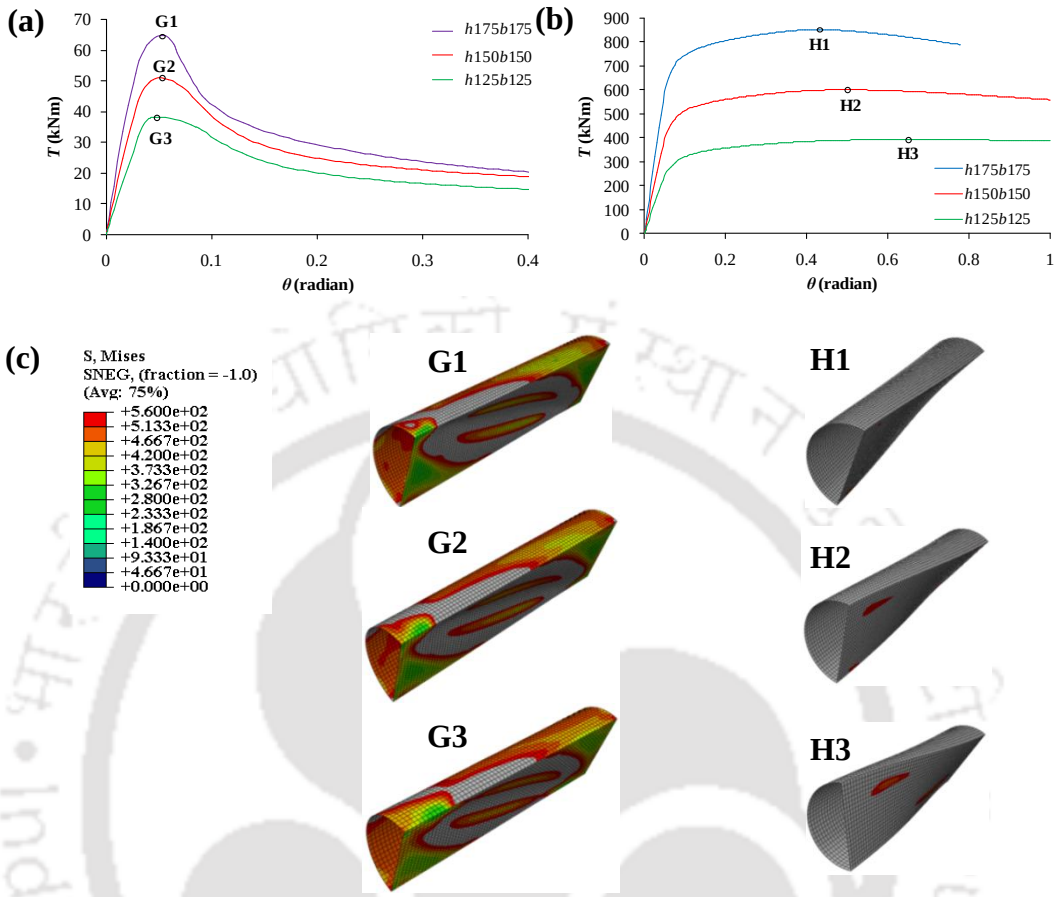

Figure 3.22: T vs θ curve for (a) a slender section (t = 3 mm) and (b) a stocky section (t = 30 mm); (c)Von mises stress contour at T_u for slender (**G1-G3**) and stocky sections (**H1-H3**) (h/b = 1)

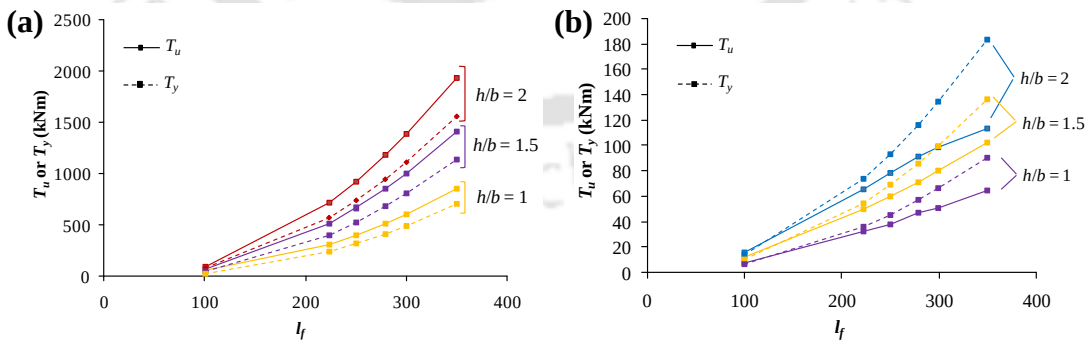

Figure 3.23: T_u vs l_f: (a) stocky section (t = 30 mm) and (b) slender section (t = 3 mm)

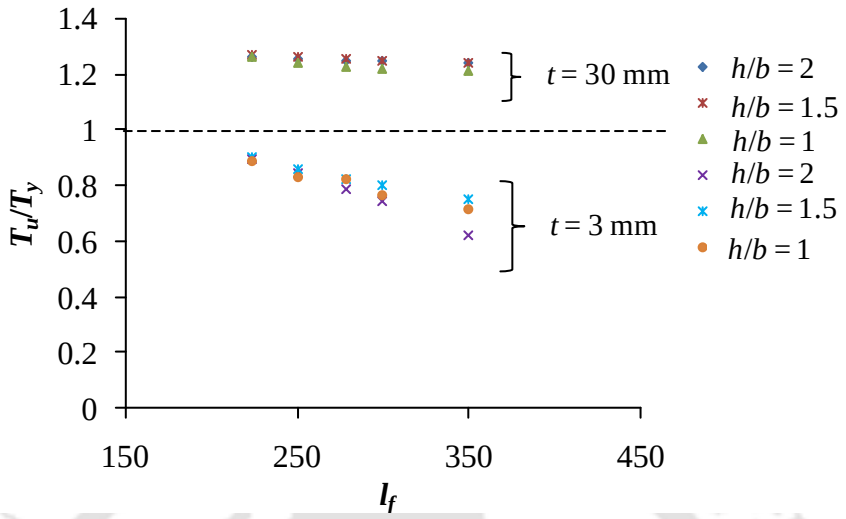

Figure 3.24: T_u/T_y vs l_f for slender (t = 3 mm) and stocky section (t = 30 mm)

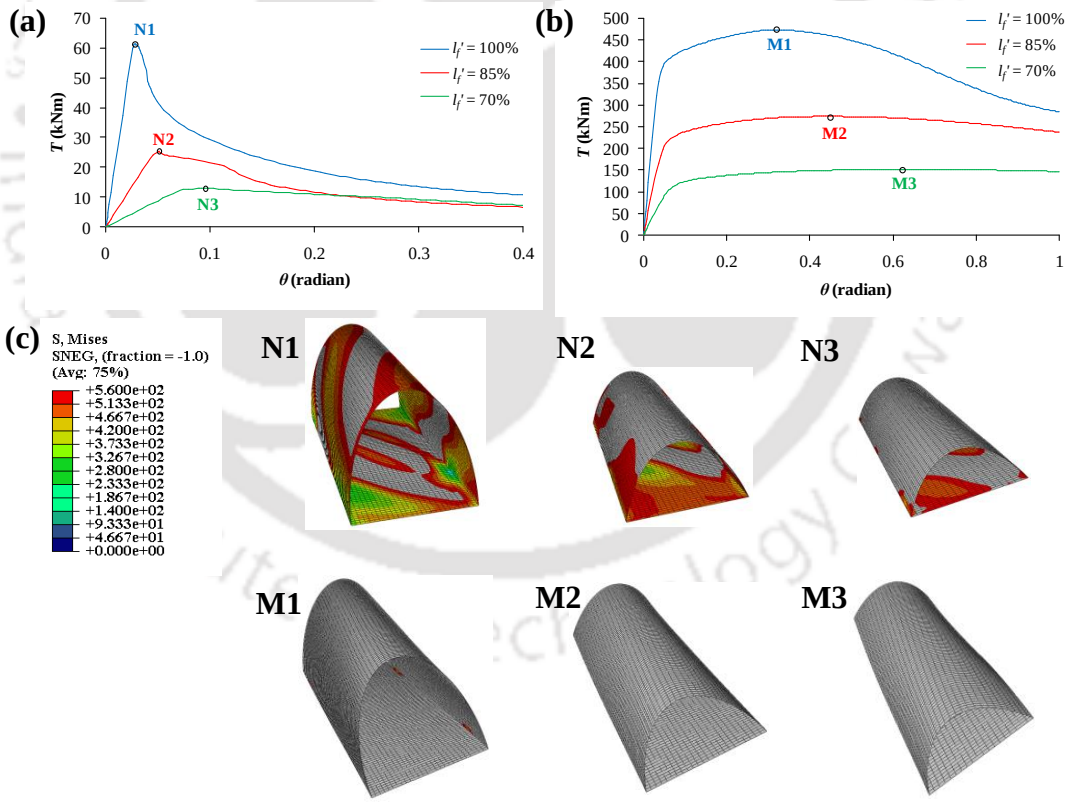

Figure 3.25: T vs θ curve for (a) slender section (h/b = 2, t = 3 mm)and (b) stocky section (h/b = 2, t = 20 mm); (c) Von Mises stress plot at T_u

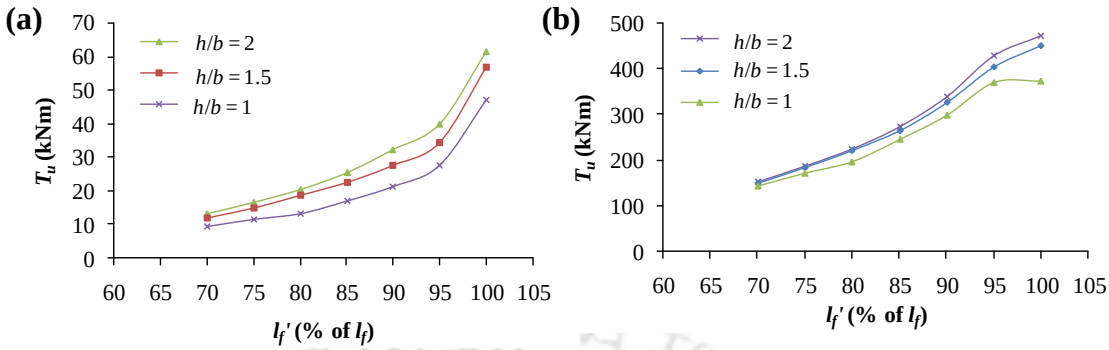

Figure 3.26: T_u vs l_f' for different aspect ratio for (a) slender section (t = 3mm) and (b) stocky section (t = 20 mm)

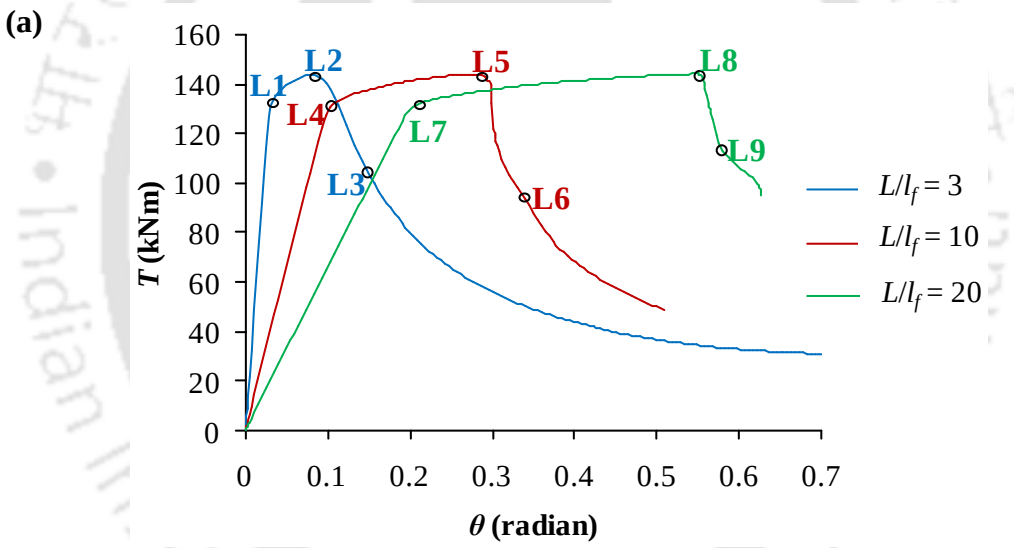

(b)

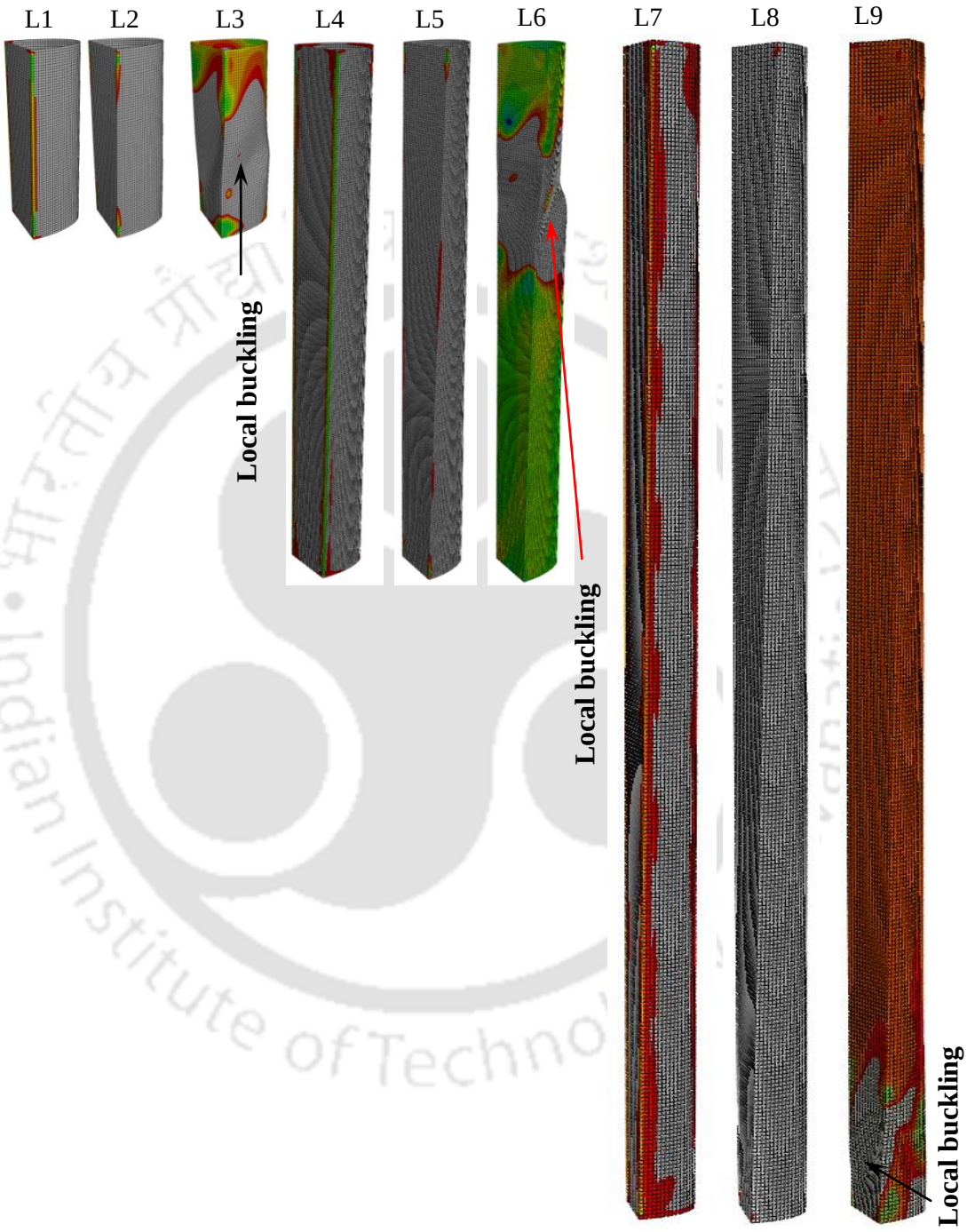

Figure 3.27: (a) T vs θ curve and (b) Von mises stress plot on deformed shape of section at various stages of T-θ curve (h/b = 2, t = 6mm)

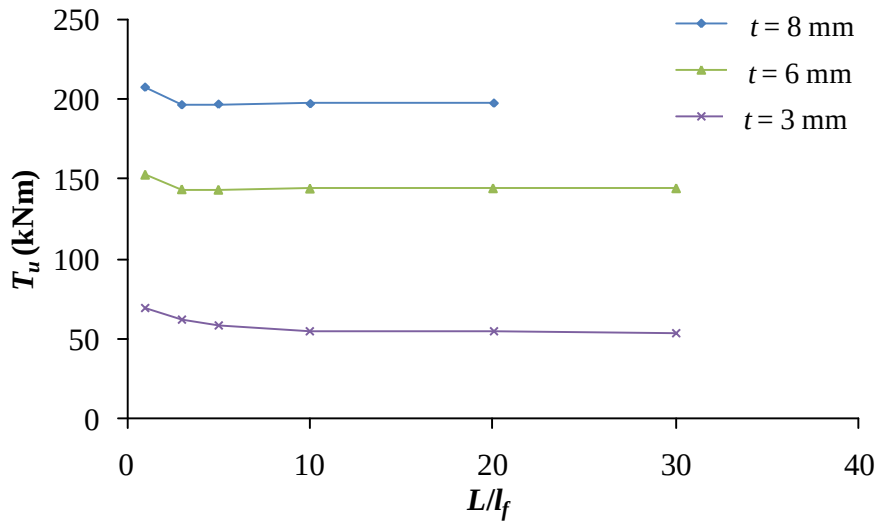

Figure 3.28: T_u vs L/l_f

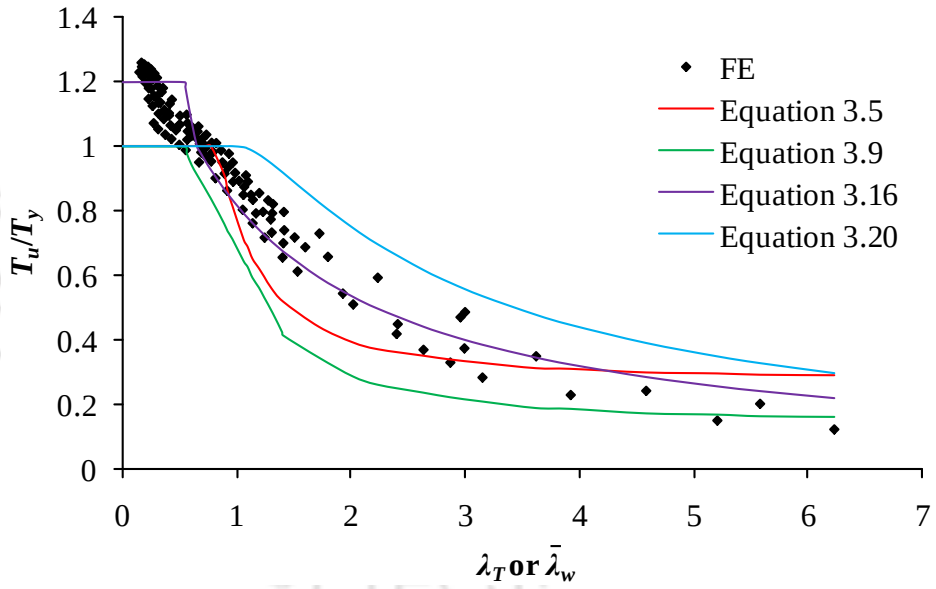

Figure 3.29: Comparison of FE results with design strengths

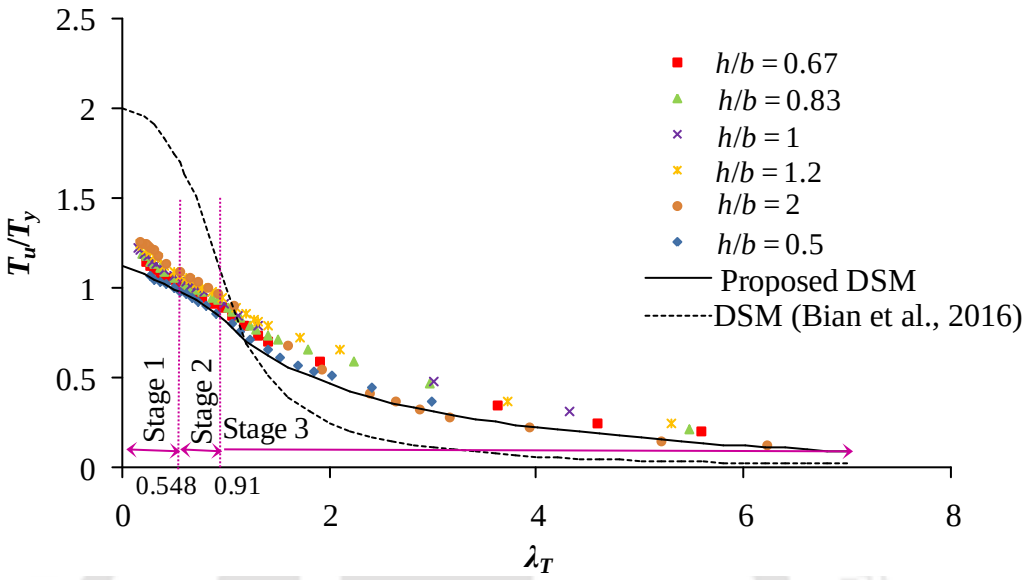

Figure 3.30: Comparison of FE and DSM strength

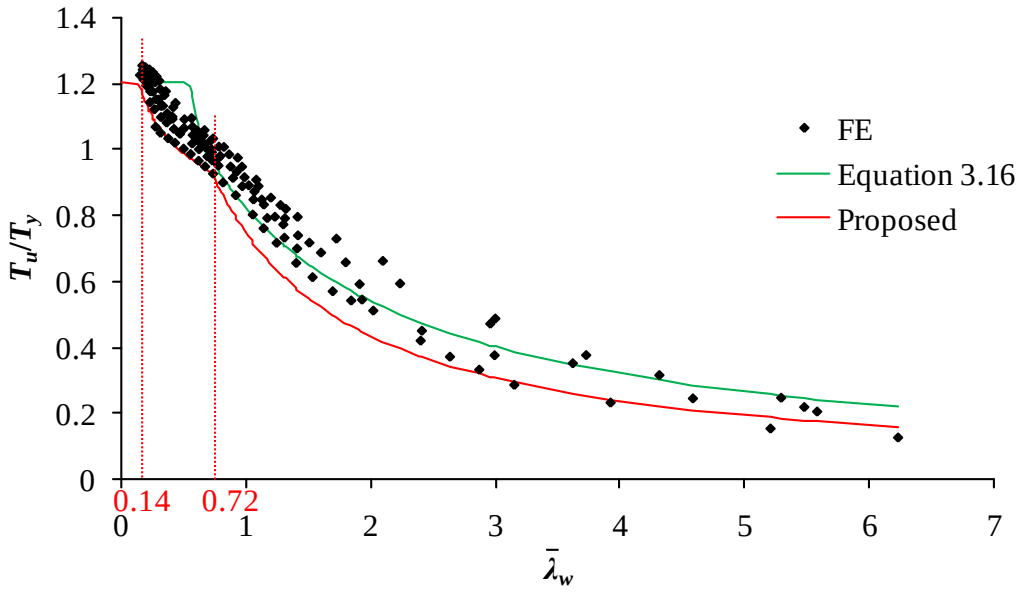

Figure 3.31: Existing and modified Eurocode design curves

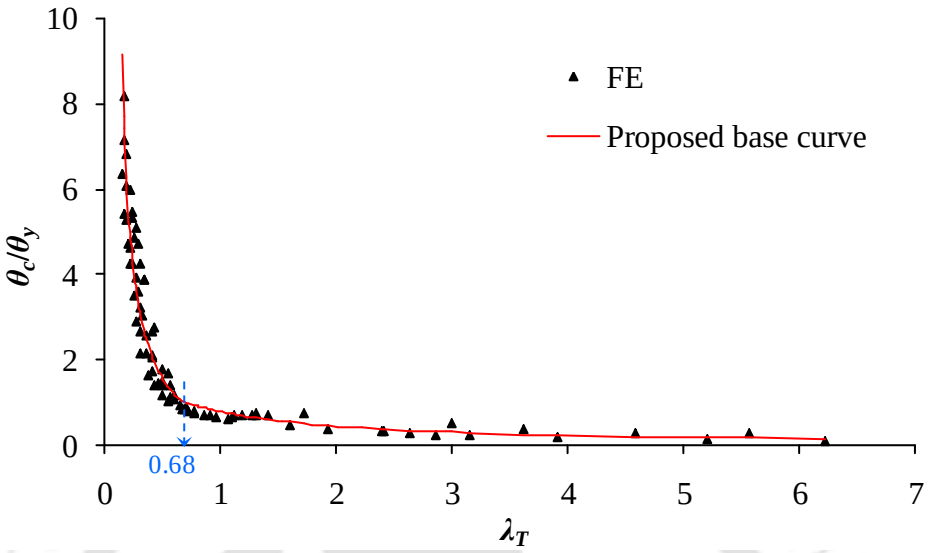

Figure 3.32: Rotation capacity (θ_c/θ_y) vs torsional slenderness (λ_T)

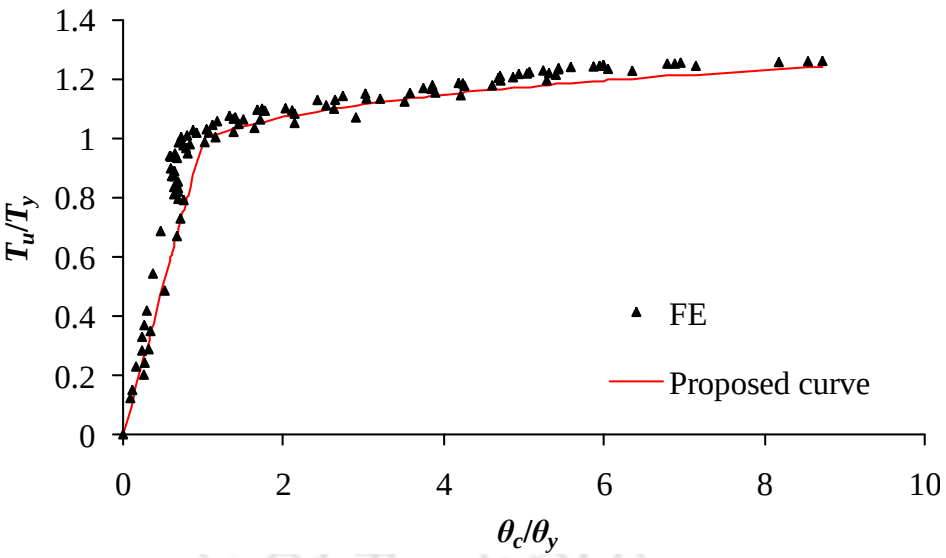

Figure 3.33: T_u/T_y vs θ_c/θ_y

CHAPTER 4

LEAN DUPLEX STAINLESS STEEL SEMI-ELLIPTICAL HOLLOW SECTION MEMBERS WITH SINGLE CIRCULAR PERFORATION SUBJECTED TO TORSION

4.1 Introduction

As outlined in Chapter 1, perforations are introduced in a structural member for various reasons such as electrical and plumbing services, ease of maintenance, aesthetics, connections etc. (Hagen et al., 2009; Lawson et al., 2015; Moen & Schafer, 2010; Yu & Davis, 1973). However, introduction of perforation has been reported to reduce ultimate capacity of the member and also influences its failure behavior (e.g. Ridley-Ellis, 2000; Shanmugam, 1997). Studies on shear capacity of perforated members have been reported in the literature (e.g. Cooper & Roychowdhury, 1990; Hagen et al., 2009; Narayanan & Der-Avanessian, 1985; Pellegrino et al., 2009; Ridley-Ellis, 2000; Sonu & Singh, 2017a; Wanniarachchi et al., 2017). However, most of these studies mentioned above were conducted for open sections or carbon steel members. Very limited studies have been reported for

perforated stainless steel members in shear failure (or torsional failure) (e.g. Lawson et al., 2015). Lawson et al. (2015) investigated stainless steel sections with circular perforation loaded in shear. However, the study was conducted on open sections (C section) and considering a limited range of cross-section slenderness. Thus, to the best of author's literature review, no studies have yet been reported on stainless steel closed hollow section (or tubular) member subjected to torsion.

Hence, an attempt has been made to study the torsional behavior of perforated cold-formed LDSS SEHS members under torsion with single central circular perforation using finite element (FE) modelling. The finite element modelling procedure for the parametric study was validated using similar indirect approach mentioned in Chapter 3. Initially, experimental torsion tests on perforated SHS members have been presented for completeness of FE modelling validation process, while focus of the present study remains only on the finite element study of LDSS SEHS members under torsion. For the finite element parametric study, a single circular perforation was introduced either on flat or curve element of SEHS members located at mid-length. The diameter of the circular perforation was varied from 10% to 90% of the flat length of SEHS. A wide range of cross-section slenderness was also considered to have an overview of the behavior and failure pattern for different classes of cross-section. The results from the parametric study were further used to develop design equations for perforated members under torsion. Proposed design equations for unperforated members were extended for perforated cases using a perforation reduction factor (R_f). A 3 – dimensional surface curve considering both perforation size and section slenderness was then proposed for perforation reduction factor. These proposed design equations were then assessed by reliability analysis.

4.2 Experimental investigation

For the purpose of validating indirectly the finite element modelling approach, torsional experiments were conducted on perforated SHS members of carbon steel (YSt 310 variety available in India) and comparing against developed FE models. Member testing was carried out on perforated YSt 310 steel SHS member (SHS 60 × 60 × 3.2) subjected to torsion. The test set up is similar to that mentioned in Section 3.2.2 and the test set up of a perforated SHS member is shown in Figure 4.1. Two similar test specimens were prepared in the laboratory from a 5 m long YSt 310 cold-formed steel tube. The specimens were cut in a length of 600 mm using a rotary hacksaw. Two central circular perforations of diameter (d_p) 25 mm each on two opposite faces at mid length were cut out by a Laser cutting machine. With all the inserts and fixtures at the ends of the specimen, a clear length of ~ 455 mm was available. The experiment was carried out in a servo hydraulic torsion testing machine having a load cell of capacity 10 kNm. One end of the machine is fixed while the other end has a rotating actuator with a stroke of ± 50 degrees. The specimen was twisted at a rate of ~ 9.68×10^{-4} radian/sec. Two similar specimens were tested and torque (T) – twist (θ) responses are shown in Figure 4.2 (- 1 and – 2 represents samples 1 and 2 respectively). A very close match in the response can be seen. These present test results along with results from the literature (Ridley-Ellis, 2000) were then used for validating FE modelling procedure used for parametric study.

4.3 Numerical modelling

Finite element (FE) modelling steps detailed in Section 3.3 were adopted for developing FE models of the parametric study, considering additional parameters related to perforation. Hence, in this section, only the additional parameters related to perforation in FE modelling have been focused. Either the flat element or curve

element was perforated with single central circular perforation at mid-length of SEHS member (see Figure 4.3 with designated symbols). The perforation diameter (or size) on flat/curve element ($d_{p,f}$/ $d_{p,c}$) was varied from 10% to 90% of l_f. A schematic representation of boundary conditions is given in Figure 4.4. This is similar to the boundary condition described in Section 3.3.2. The FE models were discretised with the general purpose shell element S4R (available in Abaqus, 2009). Number of elements on flat and curve elements were approximately equal to one-tenth of flat length and one-ninth of curve length respectively. Finer local mesh was adopted around the perforation to capture stress localization/gradient accurately and also for proper stress distribution. Aspect ratio of all elements was maintained ~ 1. Typical fan type meshing around the perforation is shown in Figure 4.5. Number of elements at the edge of perforation of all sizes ranges from ~ 24 – 148.

4.3.1 Validation

An indirect scheme of validation for FE modelling procedure has been employed because of two main reasons: (a) unavailability of torsion test data for stainless steel closed members in the literature and (b) unavailability of LDSS SEHS in Indian market due to which there was no scope of conducting torsion tests on LDSS SEHS members, as mentioned earlier. Hence, the validation of the current FE modelling procedure has been carried out against a total of 6 experimental torsion test results of perforated carbon steel closed hollow section members (3 different tests and three repeats) from the present experimental investigation and the literature (Ridley-Ellis, 2000), as shown in Figure 4.6. Overall experimental and FE $T - \theta$ response and failure pattern were compared. Figures 4.6a and 4.6b show the comparisons of FE with experimental results from present experimental investigation (Section 4.2) and literature (Ridley-Ellis, 2000) respectively. Initial stiffness of the curve, ultimate torque (T_{up}) and corresponding twist (θ_u) of FE models were found to agree well with the experimental curves. Moreover, failure patterns were found to be in good agreement. A comparison of deformation

patterns is shown in Figure 4.6c for the tested specimen, a 3D scan image of the tested specimen (using a non contact 3D Laser scanner) and FE model. Both experiment and FE model were found to exhibit similar failure pattern with localised buckling near the perforation. This confirms the validity of the FE modelling procedure for cold formed members under torsion. Hence, the developed FE models can be safely considered to be valid, and fairly correct for the parameters associated with numerical modelling.

4.4 Results and Discussion

In this study, parametric study was carried out on perforated LDSS SEHS members subjected to torsion. The members were perforated with single central circular perforation at mid-length of the member. The perforation was made either on flat element or curve element of the member. The perforation diameter on flat ($d_{p,f}$) and curve ($d_{p,c}$) was varied as a function of l_f from 10% l_f – 90% l_f to investigate the influence of perforation size on member ultimate capacity and behavior. Thickness was varied from 1 – 30 mm to cover a wide range of cross section slenderness. Details of all FE results generated from the parametric study for members with perforation on flat and curve element are provided in Tables 4.1 and 4.2 respectively. Behavior of perforated LDSS slender and stocky members under torsion is discussed below.

4.4.1 Perforation on flat element

Figure 4.7a shows $T - \theta$ curve of perforated slender SEHS members (h/b = 0.67) under torsion with different sizes of perforation. Corresponding T - θ curves for unperforated member were also included as a basis for comparison. It can be seen from Figure 4.7a that perforation reduces the torsional capacity of a member except when the perforation is very small (~ 34% reduction for $d_{p,f}/l_f$ = 0.9). Two different failure modes were observed for slender sections. Members with smaller (~ $d_{p,f}/l_f$ =

0.1) and medium (~ $d_{p,f}/l_f$ = 0.5) sized perforation were seen to fail due to local buckling at the periphery of perforation in the flat element (Mode I) whereas large (~ $d_{p,f}/l_f$ = 0.9) sized perforations lead to Vierendeel failure mechanism (Mode II). Failure was found to occur at mid-length of all members. A significant change in the stress distribution pattern at ultimate torque was seen with introduction of perforation. Stress localisation was observed at the periphery of perforation. On the other hand, stress relaxation was found at remaining regions. When the diameter of the perforation is very large ($d_{p,f}/l_f$ = 0.9), stiffness of the member was observed to be significantly reduced. Furthermore, while torsional capacity deteriorates with increase in perforation diameter, an improvement in θ_u and ductility was found. Figure 4.7b shows $T - \theta$ curves for perforated stocky SEHS members with different sizes of perforation. Perforated stocky SEHS members were also seen to fail in two different modes (Modes II and III). Members with medium and large size perforation were found to fail by Vierendeel mechanism (Mode II). On the other hand, members with smaller sized perforation were yielded before failure with no signs of local buckling anywhere (Mode III). Otherwise, observations similar to that of slender sections were seen such as insignificant difference in behavior of unperforated and perforated member for small diameter of perforation, decrease in T_{up} and increase in θ_u with increase in perforation size.

Typical $T - \theta$ curves for perforated SEHS member of h/b = 1.82 are also shown in Figure 4.8. Similar observations as in SEHS members with lower h/b ratio were found for both slender and stocky sections. The failure modes of slender SEHS members are pictorially shown in Figure 4.9 with superimposed Von Mises stress distribution on deformed shapes at ultimate torque (grey color represents the regions that has reached yield stress). Variation of T_{up} normalized with torsional capacity of unperforated member (T_u) with perforation size is shown in Figure 4.10. It can be seen from the figure that the rate of reduction in T_{up} with $d_{p,f}$ is more for higher $d_{p,f}$ and also varies for different cross section slenderness. Hence, it can be said that the torsional capacity of a perforated member is influenced by both cross

section slenderness and perforation diameter.

4.4.2 Perforation on curve element

In this section, the torsional behavior and associated failure modes of perforated LDSS SEHS members with perforation on curve element only are presented. Figure 4.11 shows $T - \theta$ response of perforated SEHS member (h/b = 0.67) with different diameters of perforation on curve element. Small perforation shows identical member response with that of unperforated ones (also observed in previous Section 4.4.1). Introducing perforation leads to reduction in member capacity (as much as ~ 61% for $d_{p,c}/l_f$ = 0.9) as well as difference in failure modes of slender SEHS members. Two types of failure modes were observed depending on the size of perforation. Members with smaller sized perforation ($d_{p,c}/l_f$ = 0.1) were seen to fail by initiation of local buckling in the flat element (Mode IV). This is similar to the failure mode of corresponding unperforated member where flat element of the cross section was found to be the critical element. On the other hand, a member with medium and large sized perforation ($d_{p,c}/l_f \geq 0.5$) was found to fail by local buckling in both flat and curve elements (Mode V). Local buckling was observed in the periphery of perforation in the curve element while local buckling was found to be initiated near mid-length and extended towards the fixed member end in the flat element. A major reduction in initial stiffness of member was also seen with increase in $d_{p,c}/l_f$. While T_{up} reduces, θ_u and ductility were found to be increased with increasing size of perforation. However, in case of stocky sections, similarities in behavior and failure modes were observed for perforation on either flat or curve element. But, it can be concluded that adding a perforation on curve element was found to be more deteriorating than introducing the same size of perforation on flat element. Figure 4.12 shows $T - \theta$ curves for perforated SEHS (h/b = 1.82) members with perforation in curve element only. Similar failure modes (Modes IV and V) were also observed for SEHS members with higher h/b ratio. The above mentioned failure modes are represented in Figure 4.13. Variation

of T_{up}/T_u with $d_{p,c}/l_f$ is shown in Figure 4.14 for members with perforation on curve element only. Variation in rate of reduction of torsional capacity with increase in perforation size was found for sections with different cross section slenderness (also observed in members with perforation in flat element).

4.5 Proposed design rules

The FE results generated from the parametric study for a wide range of cross section slenderness and perforation diameter were used to propose design rules for perforated members. Torsional capacity of perforated member has been treated as a function of corresponding unperforated member by using a reduction factor in literature (e.g. Keerthan & Mahendran, 2013; Pham, 2017). A similar approach has also been adopted in this study to propose design rules. Design equations were extended from unperforated to perforated members through a perforation reduction factor (R_f). The proposed design equations are presented in the subsequent sections.

4.5.1 Perforated member

Torsional capacity of perforated members is expressed as a function of corresponding unperforated members by using a perforation reduction factor (R_f) in this study. The reduction in torsional capacity was found to be influenced by both cross section slenderness and perforation diameter from the parametric study. Hence, the reduction factor is expressed as a function of both these parameters. Then, the torsional capacity of a perforated member (T_{up}) can be calculated by using Equation 4.1.

$$T_{up,(DSM\ or\ EN\text{-}modified\ or\ DBM)} = (R_{f,f}\ \text{or}\ R_{f,c})\ T_{u,(DSM\ or\ EN\text{-}modified\ or\ DBM)} \quad (4.1)$$

where $R_{f,f}$ and $R_{f,c}$ are reduction factors for members with perforation on flat and curve element respectively. The reduction factors were fitted based on lower bound

FE data of T_{up}/T_u as function of λ ($\bar{\lambda}_w$ or λ_T) and ($d_{p,f}$ or $d_{p,c}$)/l_f. The proposed general equation of reduction factors is given in Equation 4.2.

$$R_f = A\lambda^2 + B\lambda + C \tag{4.2}$$

The coefficients A, B and C corresponding to $R_{f,f}$ and $R_{f,c}$ are given below in Equations 4.3 and 4.4 respectively.

(a) *For members with perforation on flat element only*

$$A = \begin{cases} -0.388\left(\frac{d_{p,f}}{l_f}\right)^2 + 0.646\left(\frac{d_{p,f}}{l_f}\right) & \lambda \le 1 \\ 0.047\left(\frac{d_{p,f}}{l_f}\right)^2 - 0.053\left(\frac{d_{p,f}}{l_f}\right) & \lambda > 1 \end{cases}$$

$$B = \begin{cases} 0.349\left(\frac{d_{p,f}}{l_f}\right)^2 - 0.756\left(\frac{d_{p,f}}{l_f}\right) & \lambda \le 1 \\ -0.23\left(\frac{d_{p,f}}{l_f}\right)^2 + 0.315\left(\frac{d_{p,f}}{l_f}\right) & \lambda > 1 \end{cases} \tag{4.3}$$

$$C = \begin{cases} -0.204\left(\frac{d_{p,f}}{l_f}\right)^2 - 0.076\left(\frac{d_{p,f}}{l_f}\right) + 1.002 & \lambda \le 1 \\ -0.498\left(\frac{d_{p,f}}{l_f}\right) + 1.003 & \lambda > 1 \end{cases}$$

(b) *For members with perforation on curve element only*

$$A = \begin{cases} -0.703\left(\frac{d_{p,c}}{l_f}\right)^2 + 1.229\left(\frac{d_{p,c}}{l_f}\right) & \lambda \le 0.75 \\ -0.159\left(\frac{d_{p,c}}{l_f}\right)^2 + 0.165\left(\frac{d_{p,c}}{l_f}\right) & \lambda > 0.75 \end{cases} \tag{4.4}$$

$$B = \begin{cases} 0.66\left(\frac{d_{p,c}}{l_f}\right)^2 - 1.462\left(\frac{d_{p,c}}{l_f}\right) & \lambda \le 0.75 \\ 1.033\left(\frac{d_{p,c}}{l_f}\right)^2 - 1.026\left(\frac{d_{p,c}}{l_f}\right) & \lambda > 0.75 \end{cases}$$

$$C = \begin{cases} -0.45\left(\frac{d_{p,c}}{l_f}\right)^2 + 0.005\left(\frac{d_{p,c}}{l_f}\right) + 1.00 & \lambda \le 0.75 \\ -1.033\left(\frac{d_{p,c}}{l_f}\right)^2 + 0.274\left(\frac{d_{p,c}}{l_f}\right) + 1.00 & \lambda > 0.75 \end{cases}$$

The resulted surface curves of $R_{f,f}$ and $R_{f,c}$ are plotted and shown in Figures 4.15a and 4.15b. Using these values, design curves for perforated members with perforation on flat element only are plotted in Figures 4.16a, 4.16b and 4.16c for DSM, EN and DBM respectively for three different values of perforation diameter *viz*. $d_{p,f}/l_f$ = 0.1, 0.5, 0.9. Similar plots for members with perforation in curve element only are also provided in Figures 4.17a, 4.17b and 4.17c for DSM, EN and DBM respectively.

4.6 Reliability analysis

To assess effectiveness of the proposed design equations in this study, a reliability analysis was carried out (adopting procedure mentioned in Section 3.6). Comparison of torsional strength from FE parametric study and proposed design equations was carried out for perforated members. Tables 4.3 and 4.4 give the comparison results of FE and proposed design strength for perforated members with perforation on flat and curve elements respectively. DSM was found to give the least scattered prediction out of all proposed design predictions. From Figures 4.16c and 4.17c, DBM was seen to provide accurate results for stocky sections while a comparatively larger scatter was observed for slender sections, which is

reflected in a slightly higher COV compared to DSM and EN. Reliability of all design equations was found to be greater than 2.5. Hence, these equations can be safely adopted for design of perforated LDSS SEHS members under torsion.

4.7 Conclusion

A systematic finite element based parametric study was conducted on perforated LDSS semi-elliptical hollow tubular members under torsion. Effect of including perforation in flat and curve elements of SEHS members of various aspect ratios was studied with variations in perforation size. Based on the parametric study, the following observations have been made:

1. Introducing perforation on curve element was found to be more deteriorating to its torsional capacity than perforation on flat element.
2. SEHS members with higher aspect ratio were found to have higher torsional capacity compared to that of lower aspect ratio. Although torsional capacity varies with aspect ratio, failure modes of corresponding SEHS members were observed to be similar.
3. Different modes of failure were observed for members with varying perforation size. Also, failure modes were found to vary depending on the element of the SEHS section on which perforation was introduced in case of slender sections. On the other hand, similar failure modes were observed in case of stocky sections.
4. Torsional capacity of member was found to reduce with increasing perforation size and more pronounced for higher perforation size. Also, cross section slenderness was found to affect the rate of reduction in the torsional capacity.

Design equations for perforated LDSS SEHS members subjected to torsion were proposed based on FE results obtained from the present parametric study. Design

equations of unperforated members were further extended to perforated members by using a reduction factor, as a function of corresponding unperforated member. Perforation reduction factors were developed based on a non linear best fit on lower bound FE data. The proposed equations were assessed and verified for its reliability. The proposed equations were found to be reliable and hence may be adopted for design of perforated LDSS SEHS members subjected to torsion. It may be noted that, subject to availability of torsion test results in future, these design equations could be improved further.

Table 4.1: Cross-section details and ultimate torque values of generated FE models for parametric study with perforation on flat element of SEHS member

Cross-section	h (mm)	b (mm)	h/b	t (mm)	$T_{up,FE}$ (kNm) $d_{p,f}/l_f$		
					0.1	0.5	0.9
*h*82.3-*b*164.6-*t*1	82.3	164.6	0.5	1	2.78	2.52	2.20
*h*82.3-*b*164.6-*t*2	82.3	164.6	0.5	2	12.27	11.62	9.47
*h*82.3-*b*164.6-*t*2.5	82.3	164.6	0.5	2.5	-	17.33	12.56
*h*82.3-*b*164.6-*t*3	82.3	164.6	0.5	3	23.41	23.01	16.43
*h*82.3-*b*164.6-*t*4	82.3	164.6	0.5	4	37.3	34.78	25.0
*h*82.3-*b*164.6-*t*5	82.3	164.6	0.5	5	52.29	46.12	-
*h*82.3-*b*164.6-*t*6	82.3	164.6	0.5	6	66.21	57.33	43.25
*h*82.3-*b*164.6-*t*8	82.3	164.6	0.5	8	91.7	80.4	59.3
*h*82.3-*b*164.6-*t*10	82.3	164.6	0.5	10	114.8	100.9	74.17
*h*82.3-*b*164.6-*t*14.2	82.3	164.6	0.5	14.2	-	138.0	103.2
*h*82.3-*b*164.6-*t*17	82.3	164.6	0.5	17	181.6	159.6	-
*h*82.3-*b*164.6-*t*20	82.3	164.6	0.5	20	204.2	180.5	-
*h*82.3-*b*164.6-*t*25	82.3	164.6	0.5	25	-	215.5	-
*h*103.9-*b*155.1-*t*1	103.9	155.1	0.67	1	-	4.01	3.46
*h*103.9-*b*155.1-*t*1.4	103.9	155.1	0.67	1.4	9.12	8.6	7.01
*h*103.9-*b*155.1-*t*2	103.9	155.1	0.67	2	17.5	16.7	13.1
*h*103.9-*b*155.1-*t*2.5	103.9	155.1	0.67	2.5	24.2	23.7	18.1
*h*103.9-*b*155.1-*t*3	103.9	155.1	0.67	3	31.8	31.0	22.5
*h*103.9-*b*155.1-*t*3.5	103.9	155.1	0.67	3.5	40.2	38.3	28.7
*h*103.9-*b*155.1-*t*4	103.9	155.1	0.67	4	49.6	45.6	33.4
*h*103.9-*b*155.1-*t*4.5	103.9	155.1	0.67	4.5	59.5	52.7	39.5
*h*103.9-*b*155.1-*t*5	103.9	155.1	0.67	5	68.1	59.8	45.6
*h*103.9-*b*155.1-*t*5.5	103.9	155.1	0.67	5.5	77.3	67.0	51.4
*h*103.9-*b*155.1-*t*6	103.9	155.1	0.67	6	85.2	74.3	57.2
*h*103.9-*b*155.1-*t*7	103.9	155.1	0.67	7	101.4	89.5	68.3
*h*103.9-*b*155.1-*t*8	103.9	155.1	0.67	8	117.3	104.0	78.9
*h*103.9-*b*155.1-*t*9	103.9	155.1	0.67	9	132.5	117.6	89.2
*h*103.9-*b*155.1-*t*10	103.9	155.1	0.67	10	147.6	130.6	99.2
*h*103.9-*b*155.1-*t*12.5	103.9	155.1	0.67	12.5	182.5	161.3	123.4
*h*103.9-*b*155.1-*t*14.2	103.9	155.1	0.67	14.2	205.0	181.0	139.1
*h*103.9-*b*155.1-*t*17	103.9	155.1	0.67	17	239.7	211.4	163.7
*h*103.9-*b*155.1-*t*20	103.9	155.1	0.67	20	273.9	241.3	188.7
*h*103.9-*b*155.1-*t*25	103.9	155.1	0.67	25	323	286.1	-
*h*103.9-*b*155.1-*t*30	103.9	155.1	0.67	30	365.5	329.3	-
*h*122.1-*b*147.1-*t*1	122.1	147.1	0.83	1	5.58	5.45	4.64
*h*122.1-*b*147.1-*t*1.4	122.1	147.1	0.83	1.4	11.72	11.02	9.06
*h*122.1-*b*147.1-*t*2	122.1	147.1	0.83	2	21.56	20.83	15.94

*h*122.1-*b*147.1-*t*2.5	122.1	147.1	0.83	2.5	29.76	28.91	21.16
*h*122.1-*b*147.1-*t*3	122.1	147.1	0.83	3	38.78	37.24	28.37
*h*122.1-*b*147.1-*t*3.5	122.1	147.1	0.83	3.5	48.48	45.54	33.74
*h*122.1-*b*147.1-*t*4	122.1	147.1	0.83	4	59.28	53.72	40.67
*h*122.1-*b*147.1-*t*4.5	122.1	147.1	0.83	4.5	70.53	61.88	47.71
*h*122.1-*b*147.1-*t*5	122.1	147.1	0.83	5	80.63	70.09	54.66
*h*122.1-*b*147.1-*t*5.5	122.1	147.1	0.83	5.5	90.31	78.4	61.43
*h*122.1-*b*147.1-*t*6	122.1	147.1	0.83	6	99.64	87.08	67.9
*h*122.1-*b*147.1-*t*7	122.1	147.1	0.83	7	118.2	104.8	80.7
*h*122.1-*b*147.1-*t*8	122.1	147.1	0.83	8	136.2	121.6	93.6
*h*122.1-*b*147.1-*t*9	122.1	147.1	0.83	9	154.3	137.6	106.4
*h*122.1-*b*147.1-*t*10	122.1	147.1	0.83	10	171.8	153.1	118.9
*h*122.1-*b*147.1-*t*12.5	122.1	147.1	0.83	12.5	214.0	190.3	149.2
*h*122.1-*b*147.1-*t*14.2	122.1	147.1	0.83	14.2	241.4	214.2	168.5
*h*122.1-*b*147.1-*t*17	122.1	147.1	0.83	17	284.0	251.4	198.7
*h*122.1-*b*147.1-*t*20	122.1	147.1	0.83	20	327.0	288.7	229.1
*h*122.1-*b*147.1-*t*25	122.1	147.1	0.83	25	388.7	344.0	275.5
*h*122.1-*b*147.1-*t*30	122.1	147.1	0.83	30	440.6	393.5	-
*h*203-*b*111.5-*t*1	203	111.5	1.82	1	7.46	7.13	5.14
*h*203-*b*111.5-*t*1.4	203	111.5	1.82	1.4	15.30	12.35	11.10
*h*203-*b*111.5-*t*2	203	111.5	1.82	2	33.08	30.60	24.37
*h*203-*b*111.5-*t*2.5	203	111.5	1.82	2.5	46.38	39.97	31.14
*h*203-*b*111.5-*t*3	203	111.5	1.82	3	59.42	54.40	42.54
*h*203-*b*111.5-*t*3.5	203	111.5	1.82	3.5	73.99	63.09	49.94
*h*203-*b*111.5-*t*4	203	111.5	1.82	4	87.65	74.63	58.24
*h*203-*b*111.5-*t*4.5	203	111.5	1.82	4.5	100.8	85.88	66.20
*h*203-*b*111.5-*t*5	203	111.5	1.82	5	114.1	97.18	74.56
*h*203-*b*111.5-*t*5.5	203	111.5	1.82	5.5	127.1	108.6	82.88
*h*203-*b*111.5-*t*6	203	111.5	1.82	6	140.9	119.6	91.30
*h*203-*b*111.5-*t*7	203	111.5	1.82	7	167.5	141.2	108.7
*h*203-*b*111.5-*t*8	203	111.5	1.82	8	193.5	162.6	126.3
*h*203-*b*111.5-*t*9	203	111.5	1.82	9	219.2	184.2	144.0
*h*203-*b*111.5-*t*10	203	111.5	1.82	10	244.6	205.9	162.6
*h*203-*b*111.5-*t*12.5	203	111.5	1.82	12.5	306.6	259.9	238.9
*h*203-*b*111.5-*t*14.2	203	111.5	1.82	14.2	346.1	295.9	238.9
*h*203-*b*111.5-*t*17	203	111.5	1.82	17	407.1	352.6	288.8
*h*203-*b*111.5-*t*20	203	111.5	1.82	20	467.6	409.8	339.7
*h*203-*b*111.5-*t*25	203	111.5	1.82	25	558.3	496.9	417.7
*h*203-*b*111.5-*t*30	203	111.5	1.82	30	638.3	576.8	488.1

Table 4.2: Cross-section details and ultimate torque values of generated FE models for parametric study with perforation on curve element of SEHS member

Cross-section	h (mm)	b (mm)	h/b	t (mm)	$T_{up,FE}$ (kNm) $d_{p,c}/l_f$		
					0.1	0.5	0.9
*h*82.3-*b*164.6-*t*1	82.3	164.6	0.5	1	2.82	1.75	1.39
*h*82.3-*b*164.6-*t*1.4	82.3	164.6	0.5	1.4	5.94	3.49	2.28
*h*82.3-*b*164.6-*t*2	82.3	164.6	0.5	2	12.12	8.0	4.72
*h*82.3-*b*164.6-*t*3	82.3	164.6	0.5	3	23.5	16.35	7.94
*h*82.3-*b*164.6-*t*4	82.3	164.6	0.5	4	37.7	25.8	12.8
*h*82.3-*b*164.6-*t*5	82.3	164.6	0.5	5	52.6	36.2	18.1
*h*82.3-*b*164.6-*t*6	82.3	164.6	0.5	6	66.8	46.4	22.4
*h*82.3-*b*164.6-*t*8	82.3	164.6	0.5	8	92.0	67.1	33.7
*h*82.3-*b*164.6-*t*10	82.3	164.6	0.5	10	115.4	86.7	44.3
*h*82.3-*b*164.6-*t*14.2	82.3	164.6	0.5	14.2	157.9	123.7	67.0
*h*82.3-*b*164.6-*t*20	82.3	164.6	0.5	20	205.2	169.7	-
*h*103.9-*b*155.1-*t*1	103.9	155.1	0.67	1	4.15	2.48	-
*h*103.9-*b*155.1-*t*1.4	103.9	155.1	0.67	1.4	8.50	4.85	3.10
*h*103.9-*b*155.1-*t*2	103.9	155.1	0.67	2	16.49	9.63	6.62
*h*103.9-*b*155.1-*t*3	103.9	155.1	0.67	3	31.75	21.47	12.61
*h*103.9-*b*155.1-*t*4	103.9	155.1	0.67	4	50.27	33.72	18.53
*h*103.9-*b*155.1-*t*5	103.9	155.1	0.67	5	69.26	47.0	26.01
*h*103.9-*b*155.1-*t*5.5	103.9	155.1	0.67	5.5	77.9	53.9	29.6
*h*103.9-*b*155.1-*t*6	103.9	155.1	0.67	6	86.2	60.8	33.4
*h*103.9-*b*155.1-*t*7	103.9	155.1	0.67	7	102.5	74.4	40.6
*h*103.9-*b*155.1-*t*8	103.9	155.1	0.67	8	118.2	87.5	47.8
*h*103.9-*b*155.1-*t*9	103.9	155.1	0.67	9	133.4	100.2	54.8
*h*103.9-*b*155.1-*t*10	103.9	155.1	0.67	10	148.1	-	-
*h*103.9-*b*155.1-*t*12.5	103.9	155.1	0.67	12.5	183.1	112.5	78.7
*h*103.9-*b*155.1-*t*14.2	103.9	155.1	0.67	14.2	205.6	160.5	89.9
*h*103.9-*b*155.1-*t*17	103.9	155.1	0.67	17	240.3	-	108.6
*h*103.9-*b*155.1-*t*20	103.9	155.1	0.67	20	274.2	219.3	-
*h*103.9-*b*155.1-*t*25	103.9	155.1	0.67	25	324.1	267.6	-
*h*122.1-*b*147.1-*t*1	122.1	147.1	0.83	1	5.34	3.12	1.70
*h*122.1-*b*147.1-*t*1.4	122.1	147.1	0.83	1.4	10.69	6.02	3.83
*h*122.1-*b*147.1-*t*2	122.1	147.1	0.83	2	20	11.77	8.23
*h*122.1-*b*147.1-*t*3	122.1	147.1	0.83	3	38.4	25.56	16.44
*h*122.1-*b*147.1-*t*4	122.1	147.1	0.83	4	60.26	40.09	23.78
*h*122.1-*b*147.1-*t*5	122.1	147.1	0.83	5	81.55	55.53	33.39
*h*122.1-*b*147.1-*t*5.5	122.1	147.1	0.83	5.5	90.87	63.51	38.02
*h*122.1-*b*147.1-*t*6	122.1	147.1	0.83	6	100.7	71.53	42.76
*h*122.1-*b*147.1-*t*7	122.1	147.1	0.83	7	119.2	87.11	51.83

*h*122.1-*b*147.1-*t*8	122.1	147.1	0.83	8	137.4	102.3	60.63
*h*122.1-*b*147.1-*t*9	122.1	147.1	0.83	9	155.1	117.0	69.29
*h*122.1-*b*147.1-*t*10	122.1	147.1	0.83	10	172.6	131.5	77.74
*h*122.1-*b*147.1-*t*12.5	122.1	147.1	0.83	12.5	214.7	166.2	98.17
*h*122.1-*b*147.1-*t*14.2	122.1	147.1	0.83	14.2	242.0	188.6	111.4
*h*122.1-*b*147.1-*t*17	122.1	147.1	0.83	17	284.7	223.6	133.8
*h*122.1-*b*147.1-*t*20	122.1	147.1	0.83	20	327	258.8	156
*h*122.1-*b*147.1-*t*25	122.1	147.1	0.83	25	389.4	314.3	-
*h*203-*b*111.5-*t*1	203	111.5	1.82	1	8.19	4.96	-
*h*203-*b*111.5-*t*1.4	203	111.5	1.82	1.4	15.3	9.53	6.1
*h*203-*b*111.5-*t*2	203	111.5	1.82	2	32.26	19.18	13.21
*h*203-*b*111.5-*t*2.5	203	111.5	1.82	2.5	44.88	28.44	19.91
*h*203-*b*111.5-*t*3	203	111.5	1.82	3	58.66	38.61	26.97
*h*203-*b*111.5-*t*3.5	203	111.5	1.82	3.5	73.64	49.76	34.73
*h*203-*b*111.5-*t*4	203	111.5	1.82	4	87.55	62.19	42.7
*h*203-*b*111.5-*t*4.5	203	111.5	1.82	4.5	100.7	73.13	51.08
*h*203-*b*111.5-*t*5	203	111.5	1.82	5	113.1	82.72	58.73
*h*203-*b*111.5-*t*5.5	203	111.5	1.82	5.5	126.2	92.63	65.87
*h*203-*b*111.5-*t*6	203	111.5	1.82	6	139.1	102.6	72.8
*h*203-*b*111.5-*t*7	203	111.5	1.82	7	165.1	122.7	86.4
*h*203-*b*111.5-*t*8	203	111.5	1.82	8	191.0	142.9	99.78
*h*203-*b*111.5-*t*9	203	111.5	1.82	9	216.9	16.3	112.9
*h*203-*b*111.5-*t*10	203	111.5	1.82	10	242.4	183.8	125.8
*h*203-*b*111.5-*t*12.5	203	111.5	1.82	12.5	304.4	234.3	157.5
*h*203-*b*111.5-*t*14.2	203	111.5	1.82	14.2	344.1	267.5	178.6
*h*203-*b*111.5-*t*17	203	111.5	1.82	17	-	319.7	212.3
*h*203-*b*111.5-*t*20	203	111.5	1.82	20	466.3	372.7	247.0
*h*203-*b*111.5-*t*25	203	111.5	1.82	25	557.6	454.9	302.6

Table 4.3: Comparison of FE and proposed design strength for members with perforation on flat element only

	$T_{up,FE}/T_{up,DSM}$			$T_{up,FE}/T_{up,EN}$			$T_{up,FE}/T_{up,DBM}$		
$d_{p,f}/l_f$	0.1	0.5	0.9	0.1	0.5	0.9	0.1	0.5	0.9
Mean	1.13	1.16	1.16	1.16	1.19	1.20	1.11	1.15	1.16
COV	0.08	0.09	0.09	0.10	0.11	0.11	0.12	0.13	0.13
Resistance factor (φ)	0.90	0.90	0.90	0.91	0.91	0.91	0.90	0.90	0.90
Reliability analysis (β)	3.20	3.29	3.29	3.15	3.20	3.26	2.91	2.98	3.03

Table 4.4: Comparison of FE and proposed design strength for members with perforation on curve element only

	$T_{up,FE}/T_{up,DSM}$			$T_{up,FE}/T_{up,EN}$			$T_{up,FE}/T_{up,DBM}$		
$d_{p,c}/l_f$	0.1	0.5	0.9	0.1	0.5	0.9	0.1	0.5	0.9
Mean	1.18	1.16	1.28	1.2	1.18	1.32	1.16	1.15	1.27
COV	0.10	0.11	0.15	0.12	0.13	0.17	0.15	0.16	0.18
Resistance factor (φ)	0.90	0.90	0.90	0.91	0.91	0.91	0.90	0.90	0.90
Reliability analysis (β)	3.25	3.15	3.24	3.19	3.08	3.15	2.92	2.81	2.99

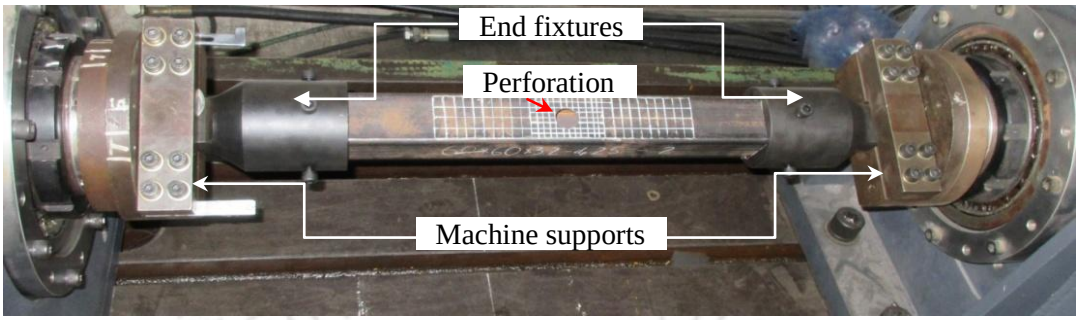

Figure 4.1: Arrangement of perforated SHS sample on torsion testing machine

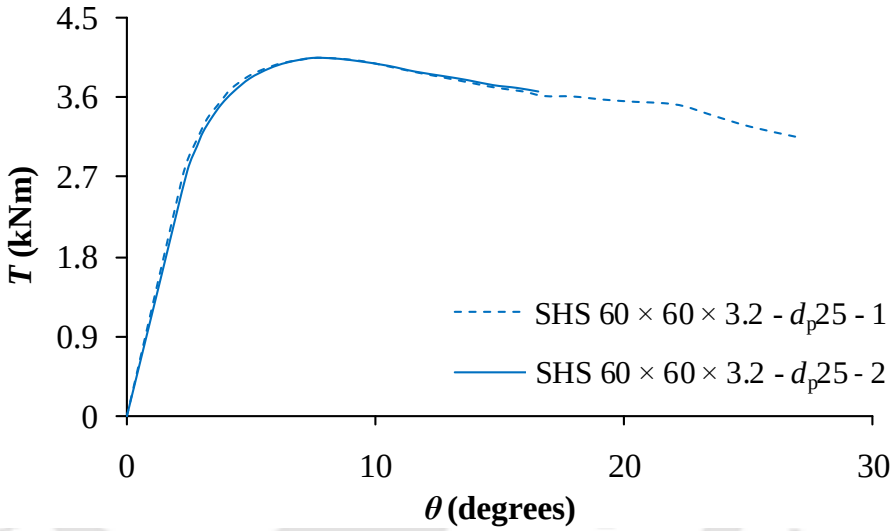

Figure 4.2: Experimental $T - \theta$ curve from present experimental investigation

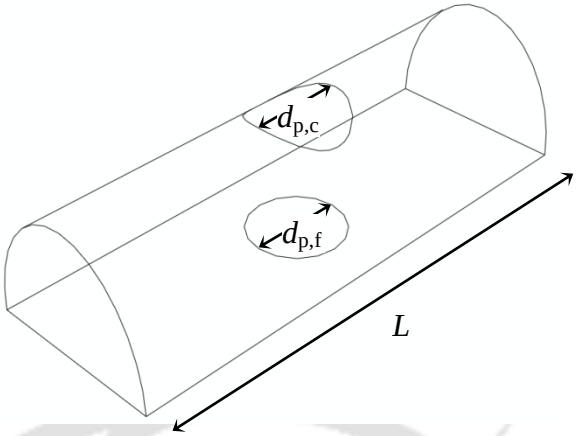

Figure 4.3: Member geometry of perforated SEHS member with designated symbols

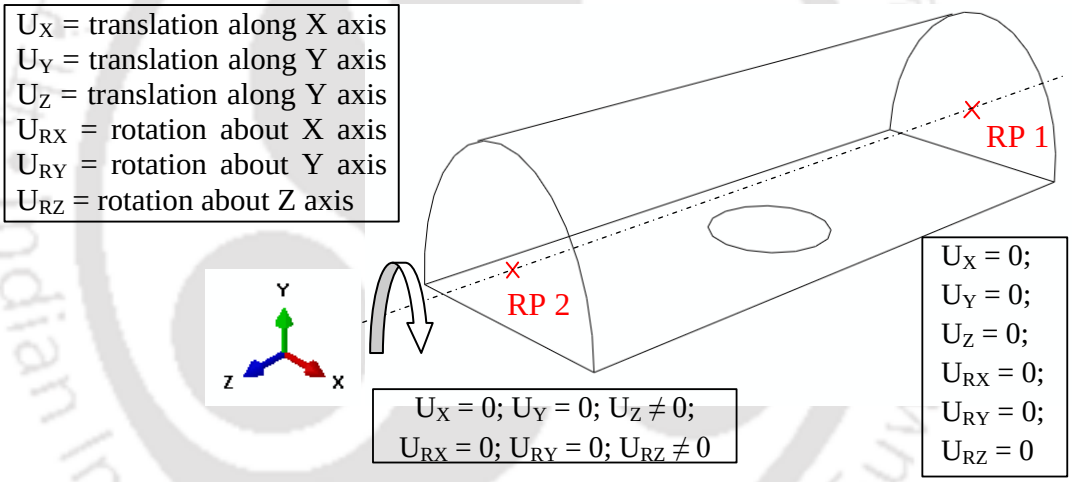

Figure 4.4: Boundary condition used for FE models

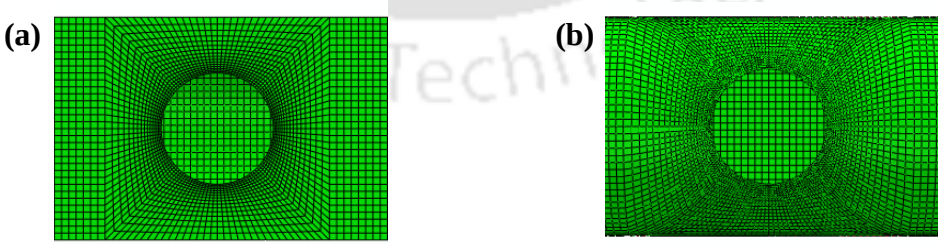

Figure 4.5: Fan type meshing around perforation on (a) flat and (b) curve elements

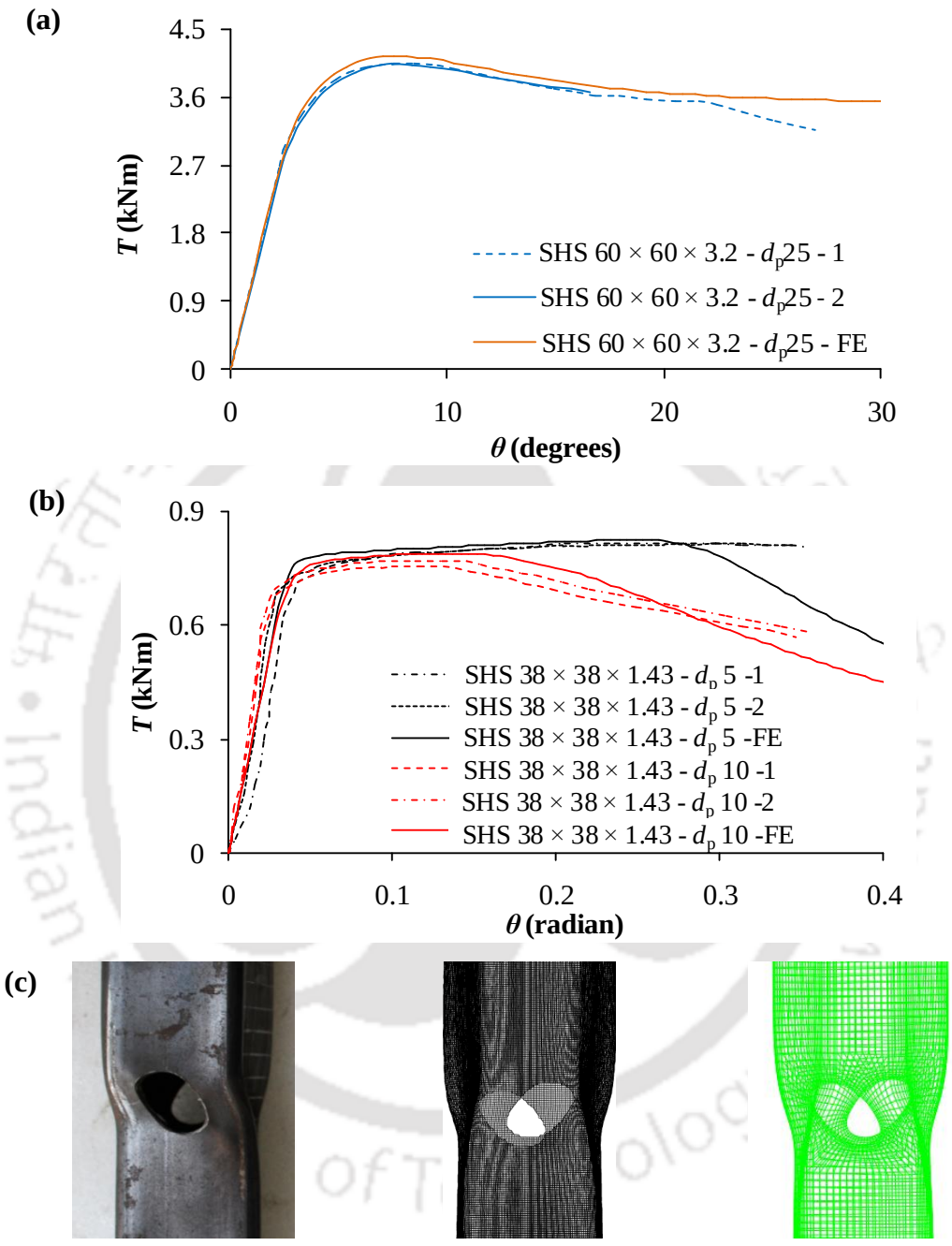

Figure 4.6: Comparison of experimental and FE T - θ curves from (a) present experimental investigation, (b) Ridley-Ellis (2000) and (c) comparison of deformed shapes of tested specimen, 3D scan image of the tested specimen and FE model (in order from left to right)

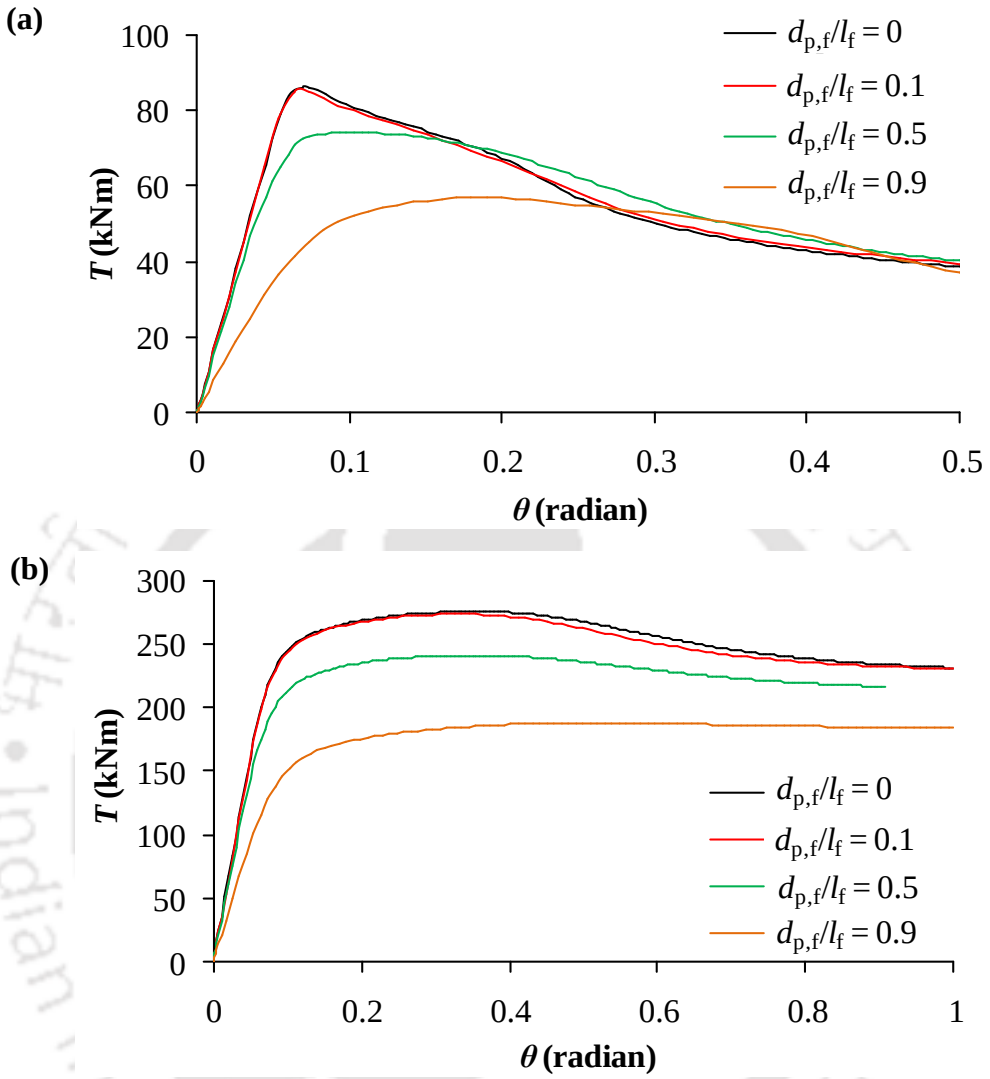

Figure 4.7: Typical $T - \theta$ curves for (a) slender (t = 6 mm) and (b) stocky (t = 20 mm) SEHS member with perforation on flat element (h/b = 0.67)

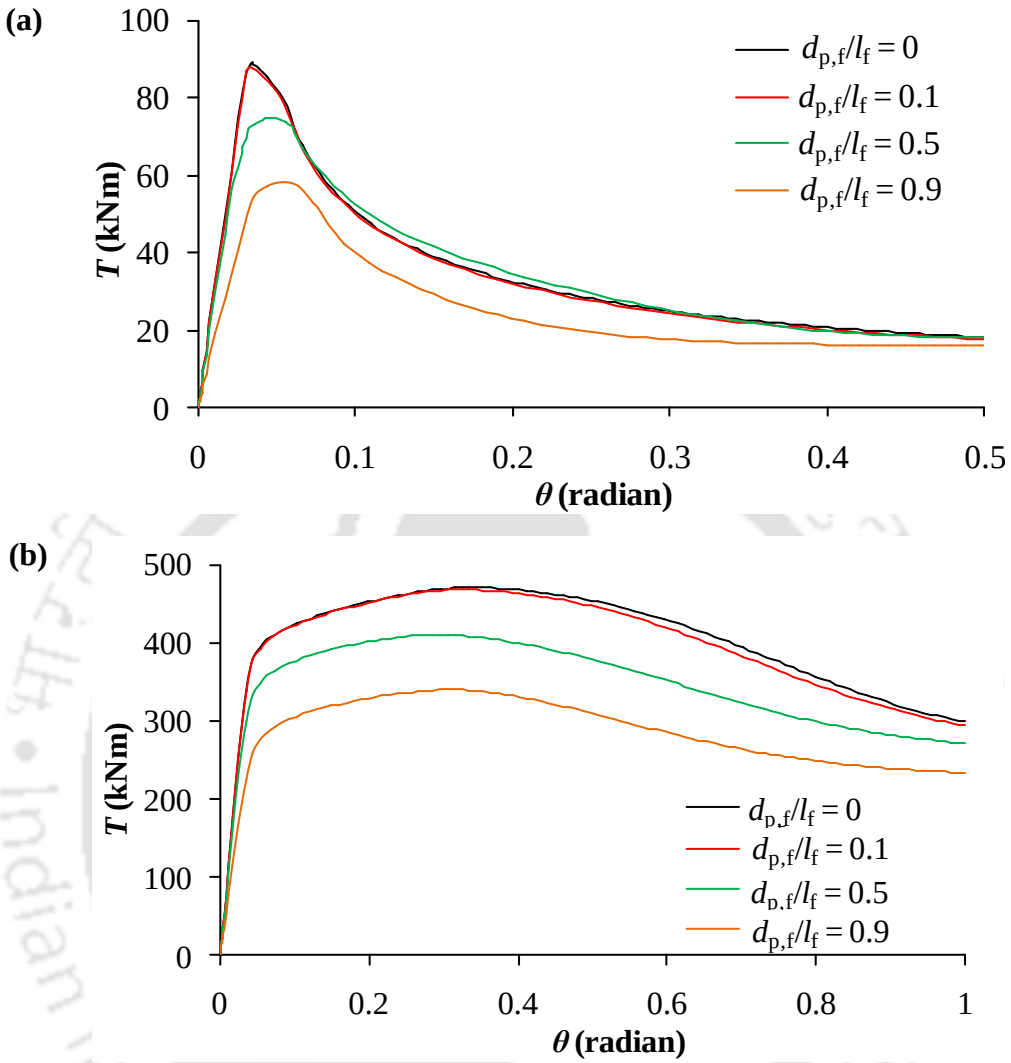

Figure 4.8: Typical $T - \theta$ curves for (a) slender (t = 4 mm) and (b) stocky (t = 20 mm) SEHS member with perforation on flat element (h/b = 1.82)

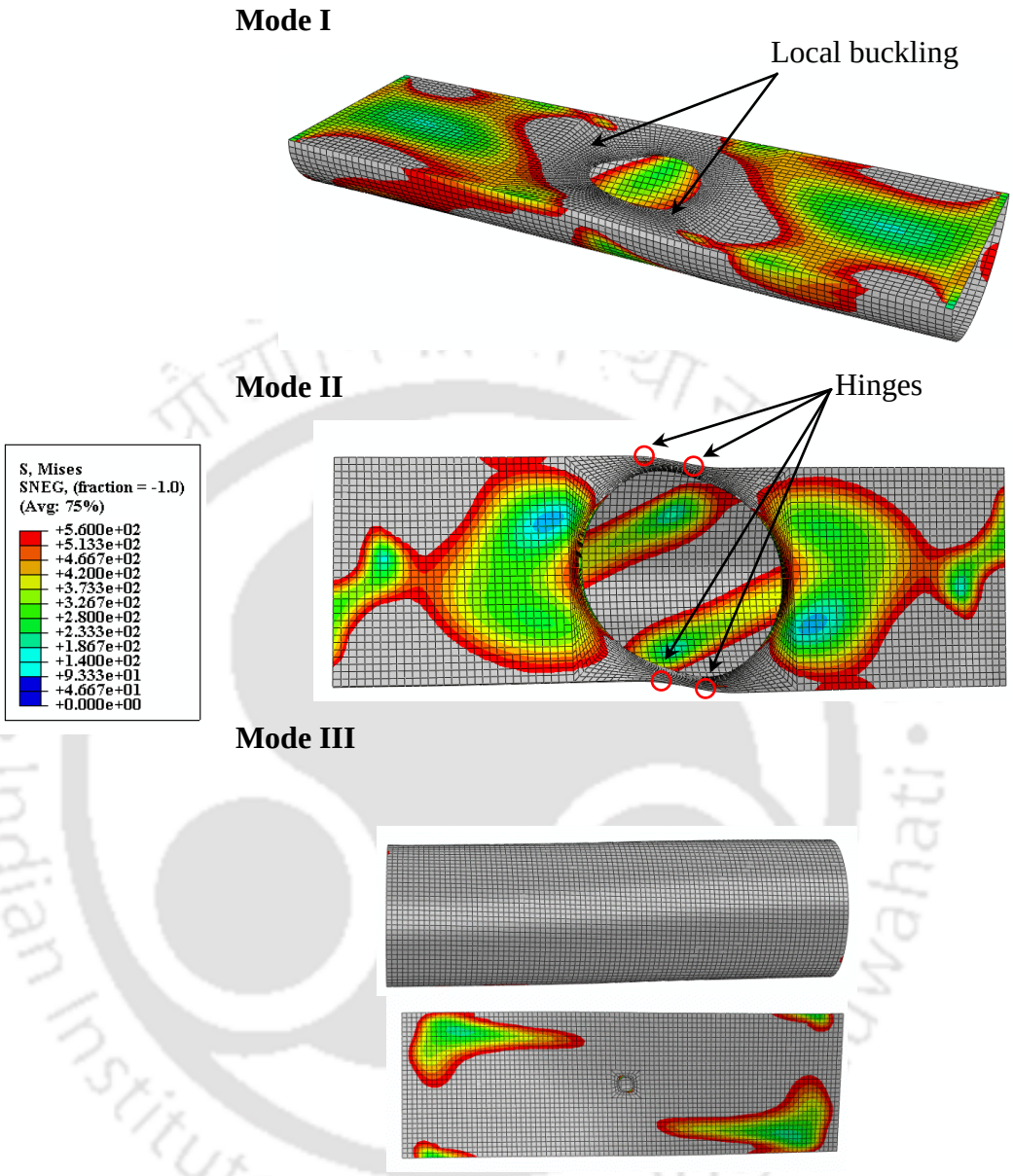

Figure 4.9: Various failure modes observed in perforated LDSS SEHS members under torsion with different sizes of perforation on flat element only

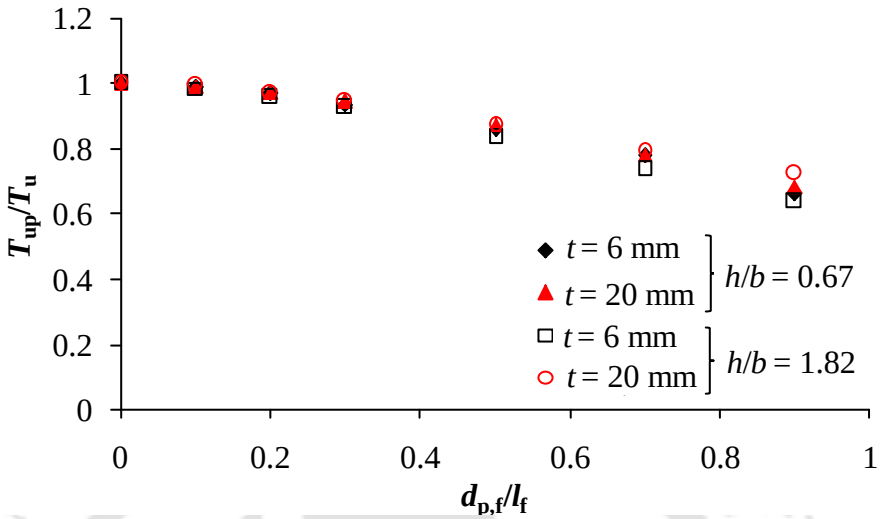

Figure 4.10: Variation of T_{up}/T_u with perforation diameter for perforation on flat element

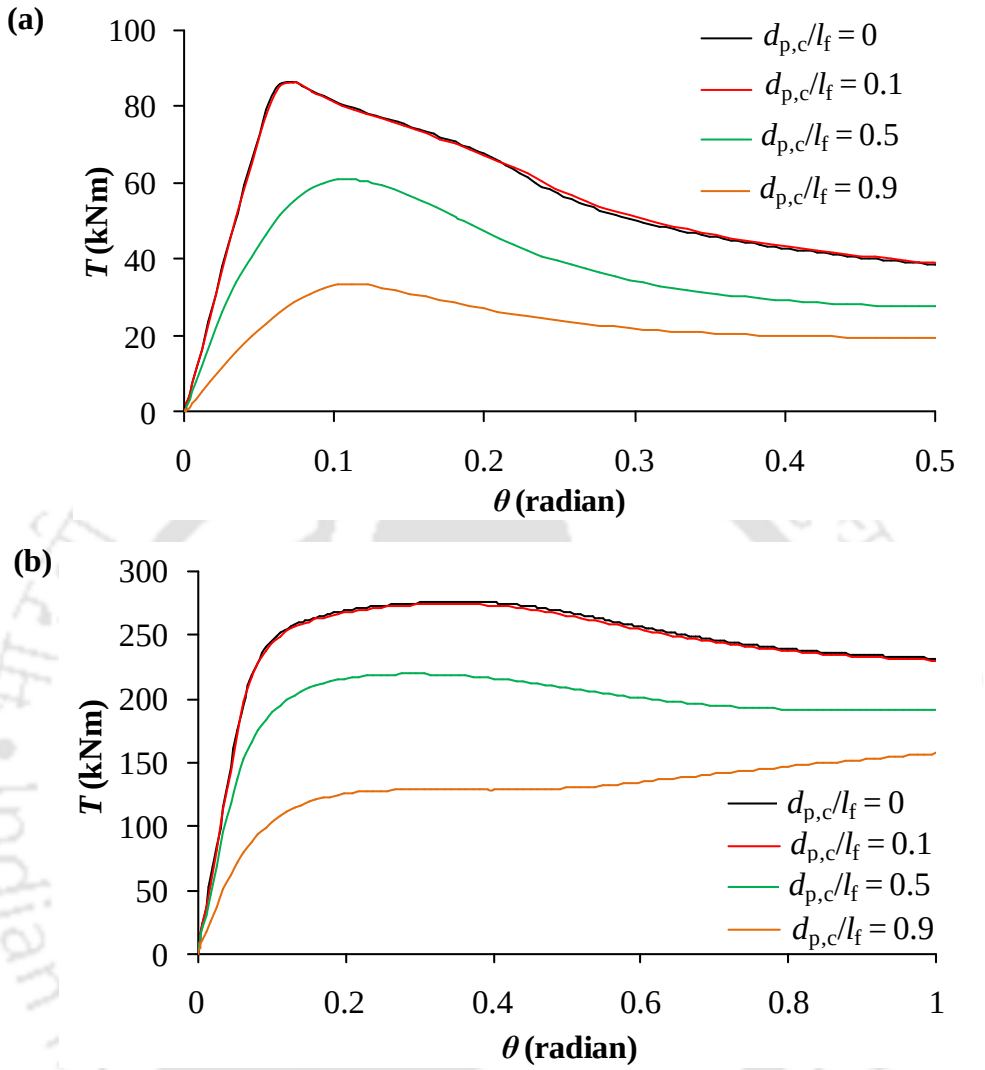

Figure 4.11: Typical $T - \theta$ curves for (a) slender (t = 6 mm) and (b) stocky (t = 20 mm) SEHS member with perforation on curve element (h/b = 0.67)

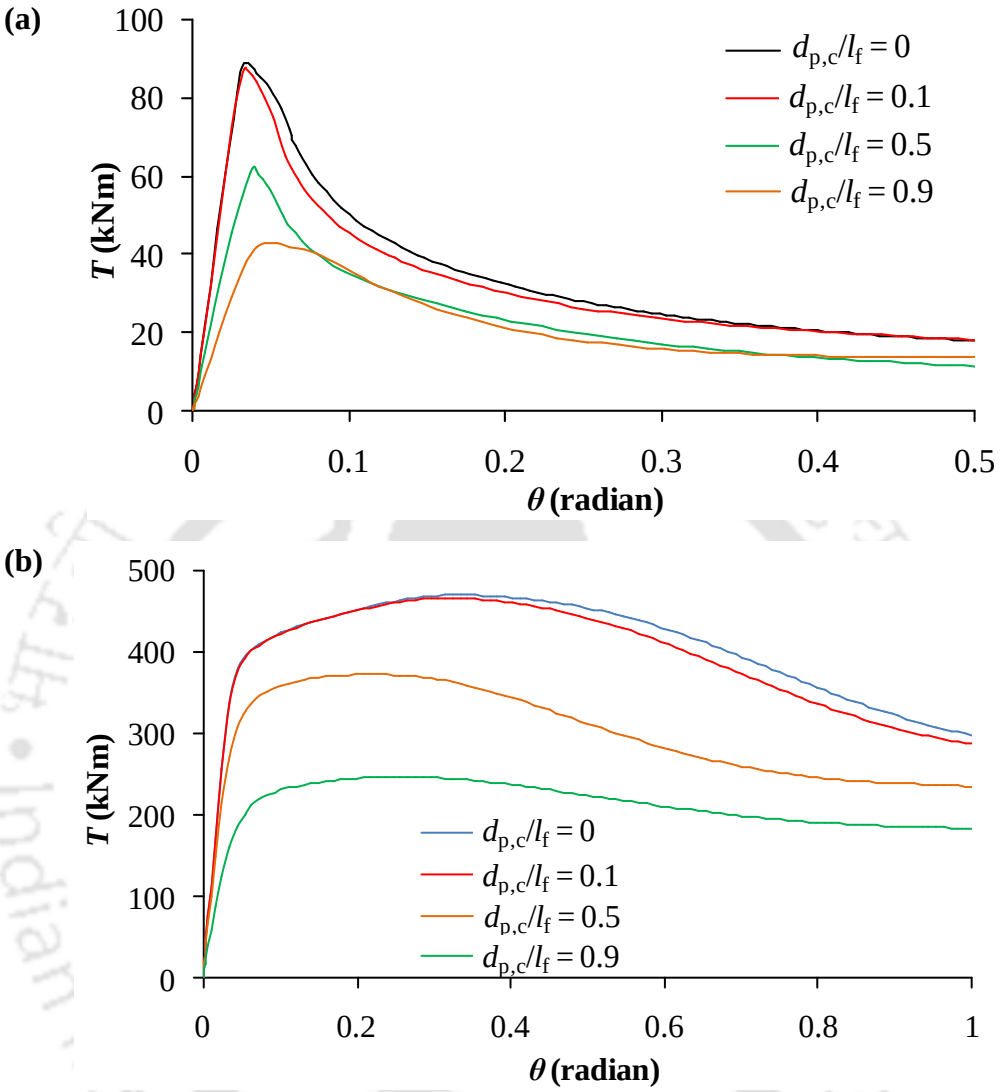

Figure 4.12: Typical $T - \theta$ curves for (a) slender (t = 4 mm) and (b) stocky (t = 20 mm) SEHS member with perforation on curve element (h/b = 1.82)

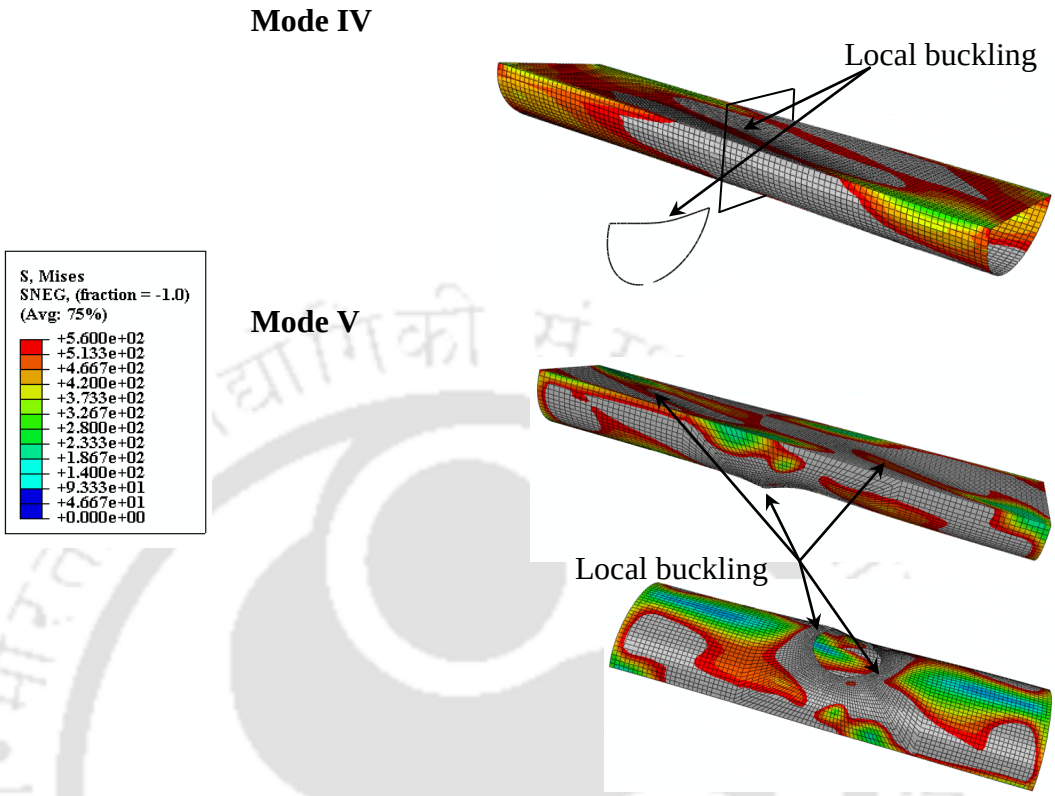

Figure 4.13: Various failure modes observed in perforated LDSS SEHS members under torsion with different sizes of perforation on curve element only

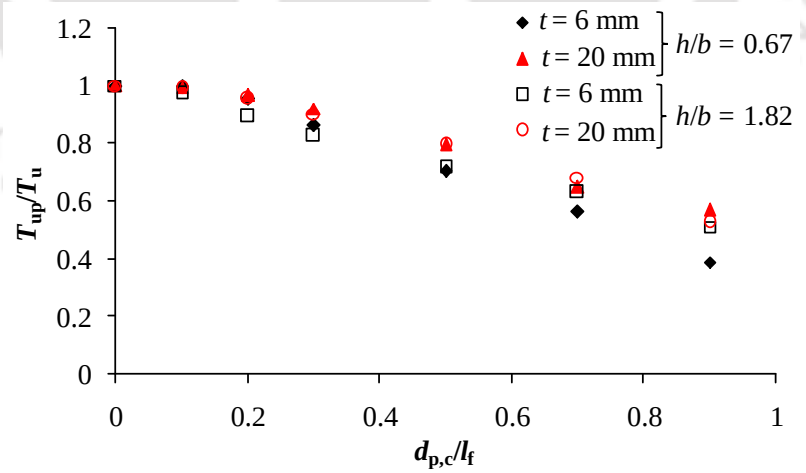

Figure 4.14: Variation of T_{up}/T_u with perforation diameter for perforation on curve element

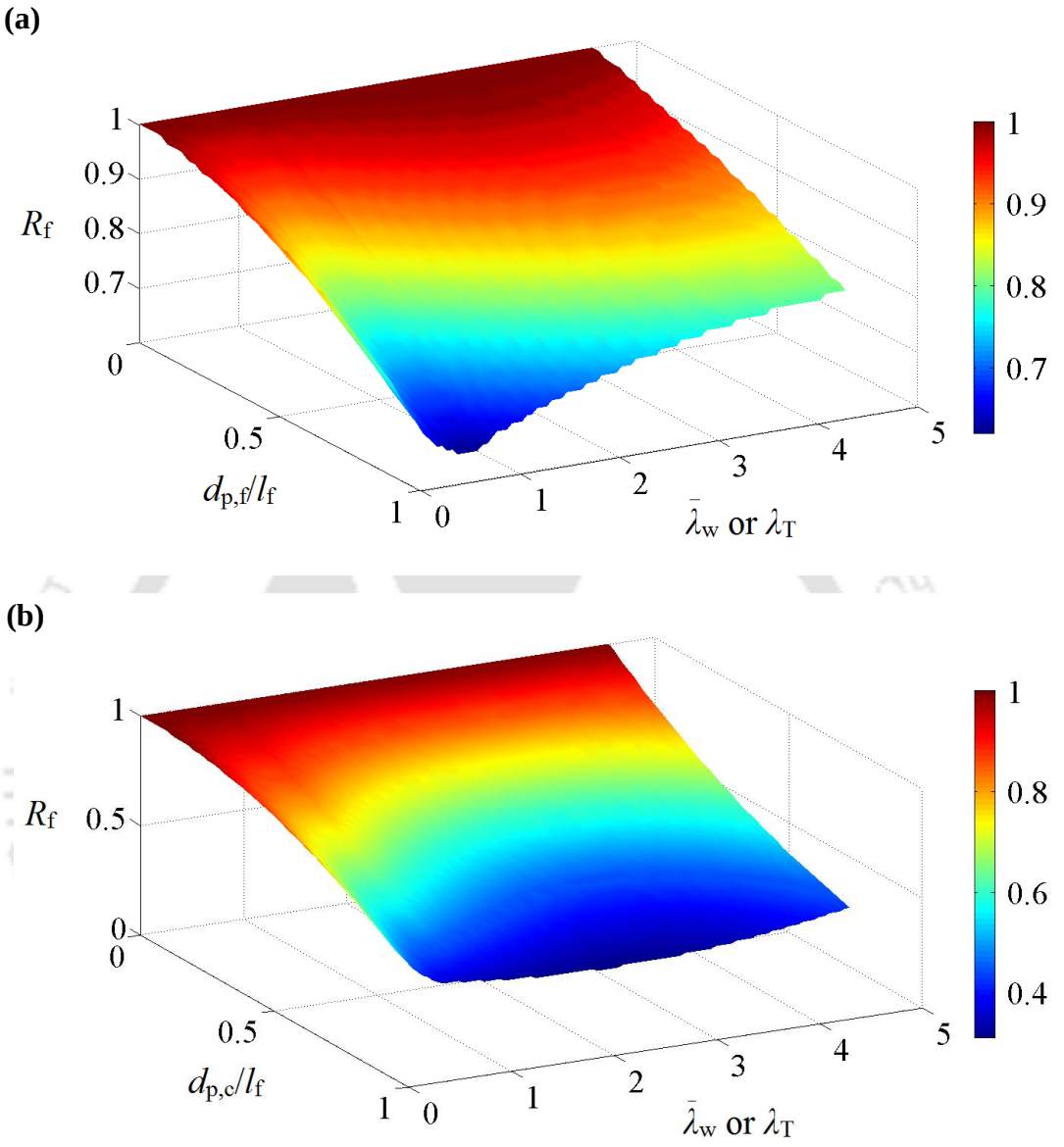

Figure 4.15: Surface plot of R_f for perforation on (a) flat element and (b) curve element

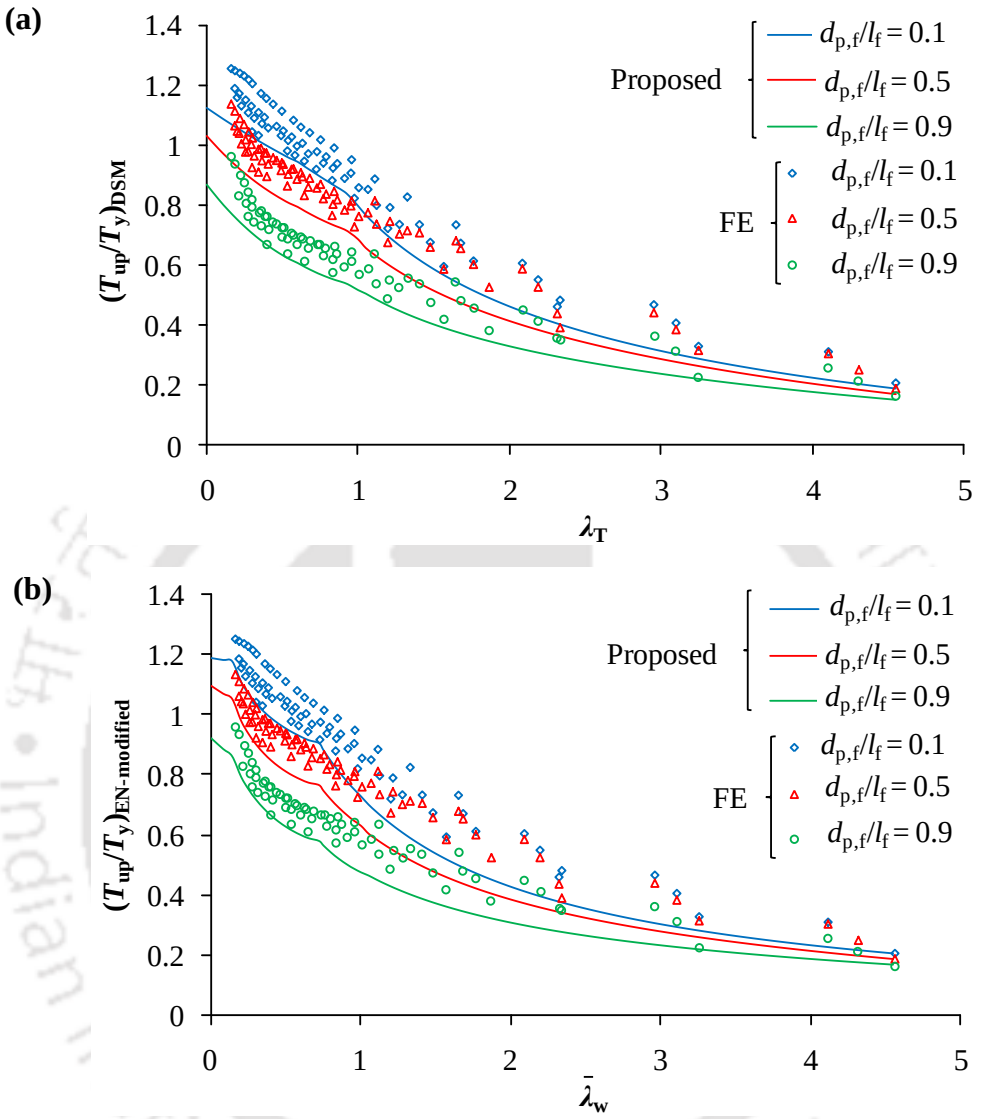

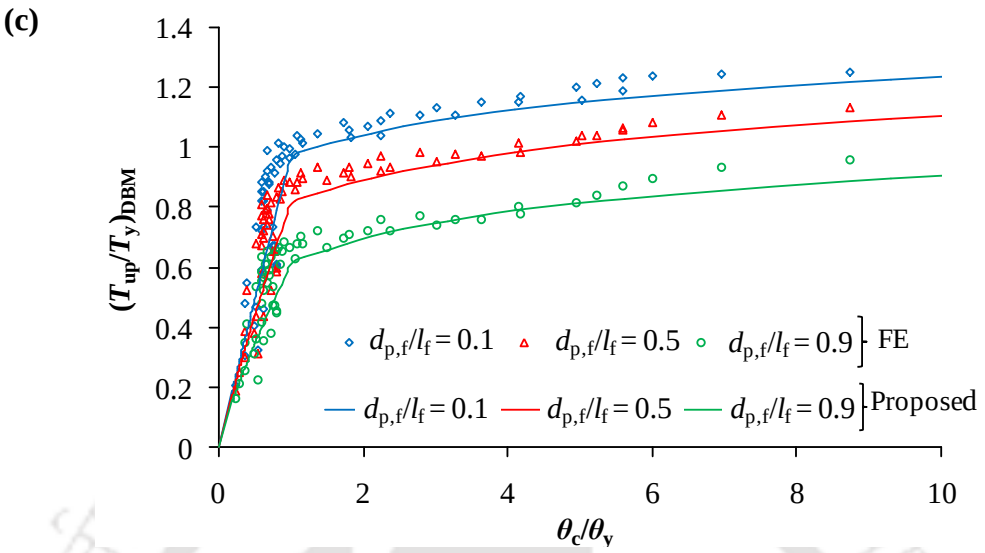

Figure 4.16: Proposed design curves for perforated SEHS members with perforation on flat element in (a) DSM, (b) EN and (c) DBM format

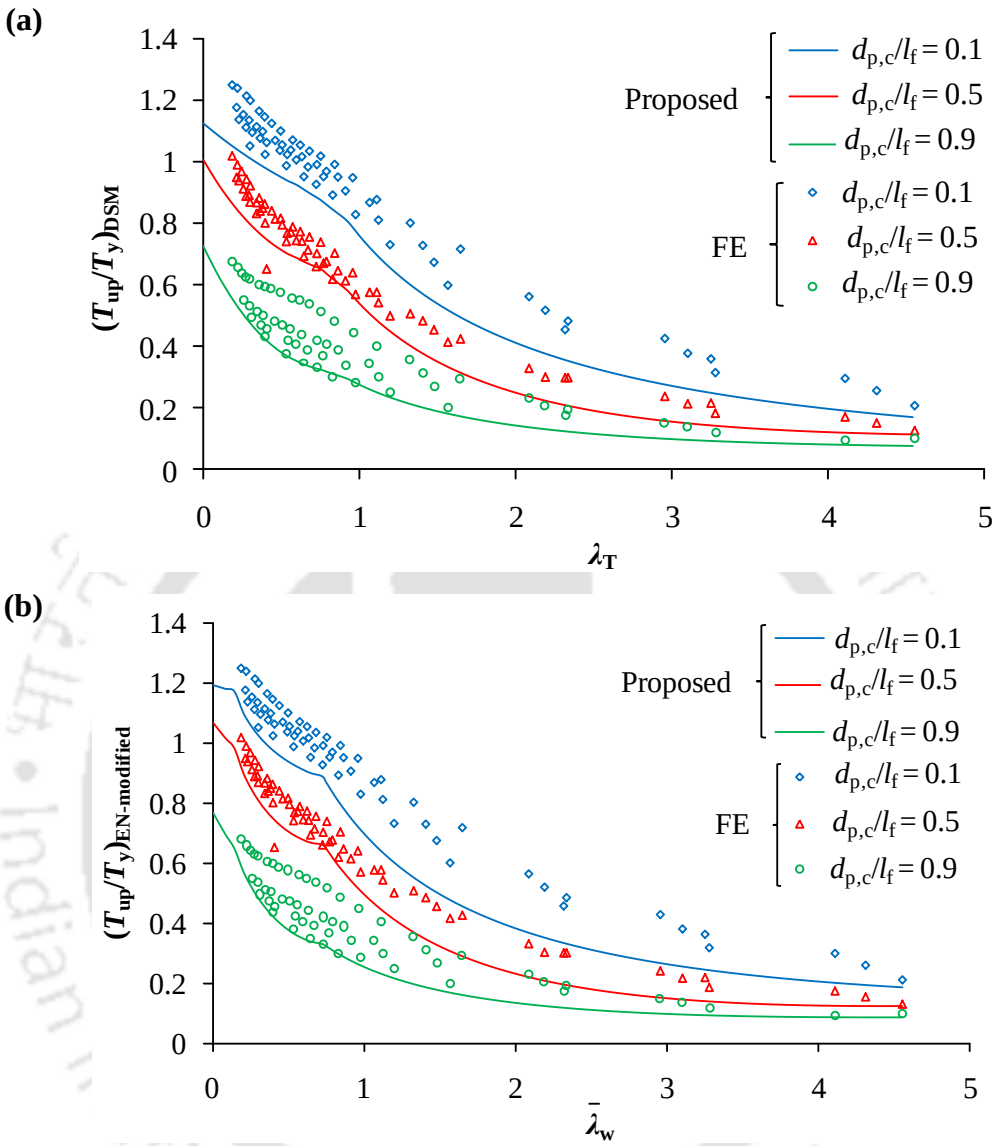

(c)

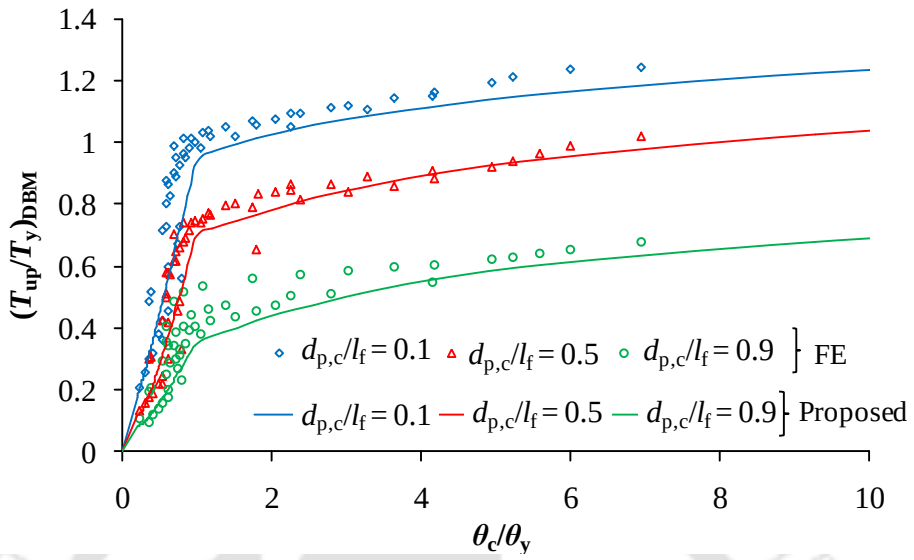

Figure 4.17: Proposed design curves for perforated SEHS members with perforation on curve element in (a) DSM, (b) EN and (c) DBM format

CHAPTER 5

LEAN DUPLEX STAINLESS STEEL SEMI-ELLIPTICAL HOLLOW MEMBERS WITH STIFFENED PERFORATION SUBJECTED TO TORSION

5.1 Introduction

Perforations (or cutouts or openings) are often introduced in thin-walled steel structures for various reasons such as maintenance, accessibility purposes, electrical fittings, plumbing services etc. (Hagen et al., 2009; Mahendran & Keerthan, 2013; Narayanan & Chow, 1985; Shakerley & Brown, 1996) as mentioned earlier. When such perforations are present in steel members, it can lead to reduction in the member capacity, depending on several factors *viz*. size, position, number of perforation etc. (Moen & Schafer, 2008; Narayanan & Chow, 1985; Shakerley & Brown, 1996; Wanniarachchi et al., 2017), as reviewed in Chapter 2. In cases where perforations are unavoidable, one of the cost effective ways adopted to improve the reduced member capacity is using stiffeners around the perforation. In the literature, attempts have been made by various researchers to

study the stiffening effects on structural steel member capacity (e.g. Alsalah et al., 2017; Bennett et al., 1982; Dimopoulos & Gantes, 2013; Jiao et al., 2018; Toda, 1983; Zhu et al., 2016). Bennett et al. (1982) carried out experimental and analytical study on perforated stainless steel cylinders with or without reinforcements under axial compression by adopting the Area Replacement Method (ARM) for reinforcing cut outs. Alsalah et al. (2017) considered a variety of stiffener configurations (such as vertical, combination of vertical and horizontal, frame ring stiffeners) and checked the effectiveness of each stiffener configuration in improving the compressive capacity of perforated cylindrical shells. Out of all stiffener configurations considered, frame ring stiffener arrangement was found to provide full recovery of compressive capacity. Jiao et al. (2018) investigated experimentally and numerically the effects of ring stiffener on compressive capacity of cylindrical shells. Ring stiffener was found to significantly improve the global buckling load of the perforated cylindrical shells. Mahendran & Keerthan (2013) conducted experiments on cold formed LiteSteel beams with stiffened web perforations subjected to shear failure. Recommendations for design of stiffeners capable of improving capacity were made for perforations of size up to 70% of web depth. Dimopoulos & Gantes (2013) provided a comparative study of different stiffener arrangements consisting of simple and complex arrangements. Simple arrangements such as ring stiffener or a ring combined with two straight stiffeners were found comparatively effective as the complex ones, and hence such simple stiffeners were recommended. However, to the best of authors' knowledge, no study has yet been reported on torsional behaviour of members with stiffened perforation.

Hence, in order to study the stiffening effect on torsional capacity of perforated steel members, a systematic parametric study has been conducted on stiffened perforated lean duplex stainless steel semi-elliptical hollow section members subjected to torsion. The parametric study has been carried out on LDSS hollow section members with single circular perforation on either flat or curve element of

SEHS member, at mid-length. Various arrangements/patterns of stiffeners *viz*., horizontal, vertical, square frame and ring were adopted for stiffening perforation sizes ranging from 30% to 70% of flat element length. The effect of stiffener dimensions on member torsional capacity was evaluated. Also, efficiency of the stiffeners for compensating the reduced torsional capacity was studied. Based on the results obtained, recommendations were made for optimum stiffener dimensions to achieve partial or full recovery of reduced torsional capacity due to perforation.

5.2 Numerical modelling

Parametric study on stiffened perforated LDSS SEHS members was carried out using Finite element (FE) software Abaqus (Abaqus, 2009). An established standard and widely adopted procedure for modelling thin-walled hollow members has been adopted (e.g. Hassanein, 2011; Theofanous & Gardner, 2009; Umbarkar et al., 2013). The modelling parameters and steps involved with the FE models are detailed in the following subsections.

5.2.1 Geometry

The SEHS member considered for parametric study has geometrical dimensions h and b equal to 203 mm and 223 mm respectively. Thickness of slender SEHS member (t) adopted was 4 mm. Single circular perforation was introduced either on flat or curve element of SEHS at mid length of member. Diameter of perforation on flat element ($d_{p,f}$) and curve element ($d_{p,c}$) was varied from 30% to 70% of l_f. Perforation size smaller than 30% l_f was not considered, since it was not found to lead to significant reduction in torsional capacity (see Chapter 4). To allow sufficient space for providing the stiffeners, maximum perforation size was also limited to 70% l_f in the parametric study. Stiffeners were arranged in different configurations as shown in Figures 5.1 and 5.2 for perforation on flat element and

curve element respectively. Four different types of simple stiffener arrangements/patterns were adopted at the periphery of the perforation located on the flat element *viz.* horizontal, vertical, square frame and ring as shown in Figures 5.1a, 5.1b, 5.1c and 5.1d respectively. Also, two simple stiffener arrangements were made for perforation located on curve element i.e. horizontal and ring stiffeners as shown in Figures 5.2a and 5.2b respectively. A clearance of 10 mm from the edge of perforation was provided as suggested by Lawson & Hicks (2011) to reserve enough space for adjusting fillet weld, while no such clearance was provided in the case of ring stiffener. In case of ring stiffener, inner diameter and outer diameter of the stiffener were made to fit the perforation edges on flat element and curve element respectively. Thickness of stiffener (t_s) was presented as a percentage of t, while width (b_s) and anchorage length (l_v) of stiffener were derived as a percentage of perforation size ($d_{p,f}$ or $d_{p,c}$) in this parametric study. Length (L) of all members was taken equal to three times that of the flat length (l_f) to meet the requirements of a stub column (Galambos, 1998).

5.2.2 Boundary conditions, FE mesh and analysis

Fixed boundary condition was adopted for the SEHS members in the parametric study. All translational and rotational degrees of freedom were fixed at one end of member. At the other end, only the longitudinal translation was released while a unit twist was applied about the longitudinal axis (z axis). All degrees of freedom were tied to reference points RP1 and RP2 at each member end through kinematic coupling available in Abaqus, 2009 (see Figure 5.3). The boundary conditions were then applied through these reference points. The stiffeners were connected to the SEHS members by using surface based tie constraint available in Abaqus, 2009. Such boundary conditions for studying torsional behaviour of members and tie constraints for connecting stiffeners to members have also been reported in literature (e.g. Aisyah Mohd Zaifuddin et al., 2017; Jiao et al., 2018; Shen et al., 2018).

The FE models were discretised with general purpose shell element S4R (available in Abaqus, 2009) with reduced integration having four nodes with six degrees of freedom (3 translations and 3 rotations) at each node. Based on mesh convergence study, an optimum mesh size of ~ l_f/25 was adopted for the SEHS member as well as the stiffener. Finer local mesh (fan type mesh) was adopted around the perforation to capture stress localization/gradient accurately and also for proper stress distribution. Aspect ratio of all elements was maintained ~ 1. Number of elements at the edge of perforation was approximately 5/8th of perforation diameter. Initially, eigen buckling analysis was carried out to obtain buckling mode shapes. First eigen mode was then used for incorporating imperfections in the FE models. Non linear analysis was then carried out using *STEP Static, General available in Abaqus, 2009.

5.2.3 Validation

The above mentioned FE modelling procedure adopted for the parametric study is similar to that of unstiffened perforated members under torsion as shown in Chapter 4. The only additional parameter in the present study is the addition of stiffeners in the perforated members. Validity of the adopted modelling procedure and associated parameters for torsional behaviour of unstiffened perforated members has been checked and presented in Chapter 4. The same procedure has been followed in this chapter for modelling stiffened perforated members under torsion.

5.3 Results and Discussion

A parametric study has been carried out to investigate the stiffening effect on torsional capacity of perforated LDSS SEHS members. Four different simple arrangements of stiffener were made to reinforce/stiffen perforation on flat element of the LDSS SEHS members *viz*. horizontal, vertical, square frame and ring

stiffeners (see Figure 5.1). For members with perforation on curve element, two arrangements of stiffeners i.e. horizontal and ring stiffeners were adopted as shown in Figure 5.2. The main aim of the parametric study is, then to seek optimum dimensions of stiffeners required for restoring torsional capacity to that of unperforated members. The study was conducted for three different sizes of perforations consisting of $d_{p,(f\ or\ c)}/l_f$ = 0.3, 0.5 and 0.7, referred to as small, medium and large perforation size respectively in this chapter. The optimum size of stiffener can be characterised by its width (b_s) and thickness (t_s); and additionally anchorage length (l_v) for horizontal and vertical stiffeners. These stiffener parameters are defined as factors of perforation size ($d_{p,f}$ or $d_{p,c}$) or thickness of member (t). The following sections present the results and discussion of the parametric study.

5.3.1. Anchorage length (l_v)

To determine the optimum anchorage length of horizontal and vertical stiffeners, l_v was varied from 0 to 1.0 $d_{p,(f\ or\ c)}$ for a fixed width (b_s) and thickness (t_s) of stiffener. Due to flat length limitation, it was not possible for l_v to extend further than 0.25$d_{p,f}$ in case of members with $d_{p,f}/l_f$ = 0.7 and vertical stiffeners. Figures 5.4a and 5.4b show the variation of ultimate torsional capacity for stiffened perforated members ($T_{up\text{-}s}$) with perforation on flat element for different values of l_v; for vertical and horizontal stiffener respectively. An improvement (maximum of ~ 2%) in torque capacity ($T_{up\text{-}s}$) can be seen when anchorage length (l_v) is increased from 0.25$d_{p,f}$ to 0.50$d_{p,f}$; however, beyond l_v value of 0.50$d_{p,f,}$ no apparent increase in torsional capacity could be seen. This is found to be true for all sizes of perforation considered. On the other hand, in some cases, $T_{up\text{-}s}$ was found to drop slightly when l_v = 1.0$d_{p,f}$. It can be said that although anchorage length is necessary, a longer anchorage length may also be undesirable to member torsional capacity. Hence, an optimum anchorage length of 0.50$d_{p,f}$ has been adopted for both vertical and horizontal stiffeners; except for vertical stiffeners on flat element with $d_{p,f}$ = 0.7, in

which case a lower value of $l_v = 0.25d_{p,f}$ was adopted (limited by width of flat element).

Figure 5.4c shows the variation of $T_{up\text{-}s}$ with l_v for perforated members stiffened by horizontal stiffeners on curve element. Similar observations as mentioned in the previous paragraph were made for horizontal stiffeners with perforation on curve element. Hence, an optimum anchorage length of $0.50d_{p,c}$ has been adopted for horizontal stiffeners on curve element. The adopted value of l_v also accounts for minimum requirement (0.25 times diameter of circular perforation) specified by Lawson & Hicks (2011).

5.3.2 Width of stiffener (b_s)

The width of stiffener can also have an effect on the torque capacity of perforated members. Two important considerations that can decide the width of the stiffeners are: 1) the stiffener should be wide enough to provide stiffening effect to the perforation as well as fit the fillet weld for connection, and 2) longer outstand width (and hence slender section) may be avoided as it may not enhance member capacity (Lawson & Hicks, 2011). To determine the optimum width of stiffener (b_s), b_s was varied from $0.10d_{p,f}$ to $0.75d_{p,f}$ for members with perforation on flat element and its effect on $T_{up\text{-}s}$ was checked. Figures 5.5a-5.5d represents the variation of $T_{up\text{-}s}$ with b_s for all arrangements of stiffener on flat element (keeping t_s constant and l_v as per Section 5.3.1 (e.g. $l_v = 0.5d_{p,f}$ for horizontal stiffeners)). In the case of small size perforation ($d_{p,f}/l_f = 0.3$), minor improvement (maximum of ~ 3%) in $T_{up\text{-}s}$ was visible as b_s increases from $0.10d_{p,f}$ to $0.25d_{p,f}$, while further increase in b_s was seen to have no significant effect. For larger size perforation ($d_{p,f}/l_f \geq 0.3$), variation in b_s has insignificant effect on $T_{up\text{-}s}$ for all types of stiffener considered.

For the case of members with perforation on curve element, stiffener width (b_s) was varied from $0.25d_{p,c}$ to $0.75d_{p,c}$. Variation of $T_{up\text{-}s}$ with $b_s/d_{p,c}$ for horizontal and ring

stiffeners on curve element are shown in Figures 5.6e and 5.6f respectively. No significant change in $T_{up\text{-}s}$ was observed with variation of b_s, except for minor increase in $T_{up\text{-}s}$ for smaller size perforation, as $b_s/d_{p,c}$ changes from 0.25 to 0.5. Based on the results obtained and to maintain a low slenderness value of outstand stiffener width, a value of b_s equal to 0.25 times the perforation diameter (> 0.1 times perforation diameter as suggested by Lawson & Hicks (2011) for horizontal stiffener) was adopted for further parametric study.

5.3.3 Thickness of stiffener (t_s)

5.3.3.1 Perforation on flat element

In this section, the effect of stiffener thickness on $T_{up\text{-}s}$ on member with perforation on flat element was studied by varying t_s as multiple of t. For all the stiffener arrangements, t_s was varied from 1t - 10t. The following subsections present the FE results obtained for the different types of stiffeners adopted in the study.

5.3.3.1.1 Horizontal stiffener

A comparison of T - θ curves for members with no perforation, unstiffened perforation and stiffened (with horizontal stiffeners) perforation are shown in Figures 5.6a and 5.6b for $d_{p,f}/l_f$ = 0.3 and 0.7 respectively. It can be seen from the figures that horizontal stiffeners are capable of partially restoring the reduced torsional capacity of member due to introduction of perforation. In the case of members with smaller perforation size ($d_{p,f}/l_f$ = 0.3), although torsional capacity is improved by the presence of horizontal stiffeners, variation in t_s was found to have negligible effect. Relatively higher improvement in torsional strength was observed in the case of members with larger perforation size ($d_{p,f}/l_f$ = 0.7). Moreover, initial stiffness of $T - \theta$ curve was seen to increase as t_s increases. The interception of local buckling zone by the horizontal stiffeners on two opposite sides of perforation provides a restriction on local buckling zone which helps in improving torsional capacity of the member.

Figure 5.7 shows the deformed shapes of members at $T_{up\text{-}s}$ with Von-Mises stress contour on it. In the case of members with $d_{p,f}/l_f$ = 0.3, although local buckling at the periphery of perforation cannot be avoided, the horizontal stiffeners were found to confine the zone of local buckling. Members with stiffened perforation were found to have similar failure modes with that of unstiffened ones (see Chapter 4). For smaller perforations, the stress distribution at failure (peak torque) remains nearly unchanged with increase in t_s, which may be associated with insignificant influence of t_s on torsional capacity. For larger perforation size, at $T_{up\text{-}s}$, horizontal stiffeners were seen to deform along with the member at the buckled zone when t_s/t = 1 (see Figure 5.7b). But as t_s increases, relatively lesser stiffener deformation can be seen accompanied by widening of yielded zone at the periphery of perforation, which may be the reason for improvement in $T_{up\text{-}s}$ with t_s.

Figure 5.8 shows the variation in $T_{up\text{-}s}/T_u$ with t_s/t for members with perforation stiffened by horizontal stiffeners on two opposite sides of perforation (h/b = 1.82). An immediate increase in $T_{up\text{-}s}$ was observed with introduction of stiffeners having thickness same as that of member (i.e. t_s/t = 1). The horizontal stiffeners were able to restore ~ 42% and 48% of the reduced member torsional capacity for small ($d_{p,f}/l_f$ = 0.3) and large ($d_{p,f}/l_f$ = 0.7) perforation sizes respectively. This recovery in $T_{up\text{-}s}$ for smaller size perforation was seen at a relatively lower value of t_s (i.e. t_s/t = 2), and further increase in t_s was found to have insignificant effect on member torsional capacity. On the other hand, in case of larger perforation size, gradual recovery of $T_{up\text{-}s}$ was observed with increase in t_s and ~ 48% recovery was observed at t_s/t =10. However, it may be noted that, t_s/t > 10 would result in impractically large value of stiffener thickness.

5.3.3.1.2 Vertical stiffener

To study the effect of thickness of vertical stiffeners placed on two opposite sides of perforation, t_s/t was varied from 1 - 10. Figures 5.9a and 5.9b show $T - \theta$ curves for members with $d_{p,f}/l_f$ = 0.3 and 0.7 respectively, for unstiffened and stiffened

perforations and corresponding unperforated members. It was observed that the torsional capacity can be improved with the introduction of vertical stiffeners having thickness same as that of member near the perforation when the perforation size is smaller (see Figure 5.9a), while it is not advantageous for larger size perforations (see Figure 5.9b). However, further improvement in $T_{up\text{-}s}$ was not visible with increasing t_s in both cases. Figures 5.10a and 5.10b show the deformed shapes of stiffened perforated member with vertical stiffeners on flat element at peak torque for $d_{p,f}/l_f$ = 0.3 and $d_{p,f}/l_f$ = 0.7 respectively. From the deformed shape at $T_{up\text{-}s}$, it was observed that local buckling in flat element of stiffened perforated member has been largely restricted due to the presence of vertical stiffeners around the perforation compared to unstiffened perforated member, in case of small perforation size (i.e. $d_{p,f}/l_f$ = 0.3) as shown in Figure 5.10a. In the case of members with larger size perforation (i.e. $d_{p,f}/l_f$ = 0.7), it can be seen that the vertical stiffeners are located farther away from the region where local buckling occurs (in unstiffened perforated member) and hence the local buckled zone remains unaffected (or are not intercepted) by the stiffener. This explains the insignificant effect of vertical stiffeners on large size perforations.

Figure 5.11 provides variation of $T_{up\text{-}s}$ with thickness with vertical stiffener thickness for h/b = 1.82. An immediate increase in $T_{up\text{-}s}$ was observed for all sizes of perforation when stiffened with vertical stiffeners having same thickness as that of member (i.e. t_s/t = 1). But, increasing t_s further was not found to provide enhanced recovery of $T_{up\text{-}s}$. A recovery of ~ 64% of reduced torsional capacity of perforation size $d_{p,f}/l_f$ = 0.3 was obtained by vertical stiffeners of t_s/t = 1. On the other hand, the recovery was as small as 4% in case of larger perforation size ($d_{p,f}/l_f$ = 0.7) even at higher vertical stiffener thickness (t_s/t = 10).

5.3.3.1.3 Square frame stiffener

A square frame stiffener reinforces the perforation from all sides and is expected to have the combined stiffening effect of both horizontal and vertical stiffeners.

Figure 5.12 shows $T - \theta$ curves for perforated members stiffened by square frame stiffener of varying thickness. It can be seen from the figures that the square frame stiffener is capable of restoring full member torsional capacity. For smaller size perforation (i.e. $d_{p,f}/l_f = 0.3$), the square frame stiffener provides excellent recovery even at a lower value of t_s and attains full member capacity as t_s increases. On the other hand, a gradual recovery of torsional capacity was observed with increase in t_s for larger size perforation (i.e. $d_{p,f}/l_f = 0.7$). Moreover, the reduced initial stiffness of member was also found to be recovered with increase in t_s. Deformed shapes at $T_{up\text{-}s}$ for members with stiffened perforation of sizes $d_{p,f}/l_f = 0.3$ and 0.7 are provided in Figures 5.13a and 5.13b respectively. Stiffened perforated ($d_{p,f}/l_f = 0.3$) members fail by local buckling at locations away from the perforation or outside the boundary of the square frame stiffener. Although failure mechanism for all stiffened perforated members are similar, wider distribution of higher stress level across the member was seen to be more for higher value of t_s (see Figure 5.13b). This may be associated with the increase in $T_{up\text{-}s}$ with increase in t_s for square frame stiffener.

Variation of $T_{up\text{-}s}$ with t_s/t of square frame stiffened perforated member is provided in Figure 5.14 for SEHS members with $h/b = 1.82$. A square frame stiffener having $t_s/t = 1$ provides as much as ~ 64% recovery for $d_{p,f}/l_f = 0.3$. As t_s/t increases to a value equal to 4, recovery was found to increase to ~ 89%, and it reaches ~ 113% for further increase of t_s/t to a value of 10. In case of $d_{p,f}/l_f = 0.7$, a near linear increase in $T_{up\text{-}s}$ was observed with increase in t_s. While a square frame thickness of $t_s/t = 4$ recovers ~ 42% of the reduced torsional capacity, the recovery amounts to ~ 101% as t_s/t increases to a value of 10 (see Figure 5.14).

5.3.3.1.4 Ring stiffener

Figures 5.15a and 5.15b represent $T - \theta$ curves for stiffened perforated members with ring stiffener for $d_{p,f}/l_f = 0.3$ and 0.7 respectively. Like square frame stiffeners, ring stiffeners also reinforce the perforation from all sides and hence similarities in

their behavior were observed. While full recovery was achieved with lesser value of t_s in smaller size perforation members, it was found to be achieved at a comparatively higher value of t_s in case of members with larger perforation size. Similar modes of member failure observed for square frame stiffeners (see Section 5.3.3.1.3) were also seen in ring stiffener. For $d_{p,f}/l_f$ = 0.3, presence of the ring stiffener was found to change the stress distribution pattern at failure (at peak torque), wherein a major portion of the stiffened perforated member has reached member yield capacity (see Figure 5.16a) unlike unstiffened perforated members. This may be related to the improvement in $T_{up\text{-}s}$ by ring stiffeners.

Variation of $T_{up\text{-}s}$ with t_s/t of ring stiffened perforated members is presented in Figure 5.17. For members with $d_{p,f}/l_f$ = 0.3, full torsional capacity was seen to be regained at a lower value of t_s. A recovery of ~ 87% was made with a ring stiffener of t_s/t = 2 and further increase in t_s/t to a value equal to 4 could regain ~113% of the reduced torsional strength. This rate of recovery is higher compared to the case of square frame stiffener and full torsional capacity was recovered at a relatively lower stiffener thickness. Also, for the case of members with $d_{p,f}/l_f$ = 0.7, although full recovery was made at similar values of t_s/t (i.e. t_s/t = 10), the rate of recovery was seen to be comparatively higher when ring stiffeners were used in place of square frame stiffeners. For example, $T_{up\text{-}s}$ was observed to have regained by ~ 53% for ring stiffener of t_s/t = 4 while ~ 42% recovery was made for square frame stiffener.

5.3.3.2 Perforation on curve element

This section presents and discusses the variation of $T_{up\text{-}s}$ with varying stiffener thickness (t_s) for members with perforation on curve element. For horizontal stiffener, t_s was varied from 1t - 10t, while it was varied from 1t - 6t in case of ring stiffener.

5.3.3.2.1 Horizontal stiffener

T - θ curves for SEHS members with stiffened perforation on curve element by horizontal stiffeners having various thickness are shown in Figures 5.18a and 5.18b for $d_{p,c}/l_f$ = 0.3 and 0.7 respectively. Although $T_{up\text{-}s}$ cannot be regained fully to reach T_u, improvement in $T_{up\text{-}s}$ was observed by the introduction of horizontal stiffeners on two opposite sides of the perforation. Moreover, initial stiffness of the member was seen to be enhanced. But, stiffener thickness was found to have little influence on $T_{up\text{-}s}$. The deformed shapes of stiffened perforated SEHS members at $T_{up\text{-}s}$ are shown in Figure 5.19. The members were found to fail by local buckling in both flat and curve elements; near member mid length and at periphery of perforation. This is similar to the failure of corresponding member with unstiffened perforation (see Chapter 4). Although the mechanism of failure remains unchanged with introduction of horizontal stiffeners, the stress distribution was observed to be altered which may be the reason of improvement in $T_{up\text{-}s}$.

Figure 5.20 shows the variation of $T_{up\text{-}s}/T_u$ with t_s/t of horizontal stiffeners on curve element of SEHS members with h/b = 1.82. Increase in $T_{up\text{-}s}$ by providing horizontal stiffeners was observed for all sizes of perforation on curve element. Increasing t_s improves $T_{up\text{-}s}$ further up to a value of t_s/t = 4, after which little or negligible difference in $T_{up\text{-}s}$ was observed. While ~ 42% improvement was found for members with $d_{p,c}/l_f$ = 0.3, it was only ~ 20% for $d_{p,c}/l_f$ = 0.7. Hence, horizontal stiffeners are found to be more effective for smaller size perforation on curve element of SEHS members. However, T_u was not achieved by the horizontal stiffeners even with a higher value of t_s/t = 10.

5.3.3.2.2 Ring stiffener

Figures 5.21a and 5.21b provide comparison of T – θ curves for stiffened perforated SEHS members with varying stiffener thickness for $d_{p,c}/l_f$ = 0.3 and 0.7 respectively. Significant recovery of reduced torsional capacity due to perforation on curve element was observed when the perforated members were reinforced with

ring stiffener. With increasing thickness of ring stiffener, $T_{up\text{-}s}$ was found to increase further and achieved T_u for t_s/t = 6. The mode of member failure for ring stiffened perforation was found to be similar to that of corresponding unstiffened ones (see Section 5.3.3.2.1) at lower values of t_s/t (t_s/t < 4). However, as t_s/t increases, at $T_{up\text{-}s}$, local buckling was observed only on flat element and no signs of local buckling on curve element (see Figures 5.22a and 5.22b). Moreover, the stress distribution pattern was seen to vary as t_s increase; accompanied by widespread distribution of higher stress.

Variation of $T_{up\text{-}s}$ with t_s/t for perforated SEHS members (h/b = 1.82) with ring stiffener on curve element is shown in Figure 5.23. A gradual increase in $T_{up\text{-}s}$ was observed with increase in t_s/t for all sizes of perforations considered. The improvement in $T_{up\text{-}s}$ was seen to be relatively faster at lower values of t_s/t (i.e. t_s/t < 4) and the rate gradually slows down as t_s/t increases. For members with $d_{p,c}/l_f$ = 0.3, the reduced torsional capacity was found to be recovered by ~ 94% for t_s/t = 6 (~ 99% of T_u). In case of $d_{p,c}/l_f$ = 0.7, ~ 97% of T_u was achieved with ring stiffener of t_s/t = 6 with a recovery rate of ~ 93% of reduced torsional capacity. Hence, it can be inferred that a ring stiffener provided for perforation on curve element of perforated SEHS member is effective in restoring its reduced torsional capacity due to perforation.

5.4 Conclusion

This study presented a parametric study on slender cross-section LDSS SEHS members with stiffened perforation using FE software Abaqus. Several stiffener arrangements were considered for stiffening perforation on flat or curve element of SEHS members. The optimum dimensions (e.g. width, thickness etc.) of stiffener for partial or full recovery of reduced torsional capacity were determined. Based on the parametric study, recommendations were made for optimum stiffener

dimensions. The following conclusions have been drawn from the FE study:

1. Increase in torsional capacity of perforated member was observed when the perforation was stiffened with various types of stiffeners such as horizontal, vertical, square frame and ring, having same thickness as that of member.
2. Stiffener width was observed to have insignificant or very little effect on torsional capacity of perforated member.
3. An optimum anchorage length equal to half the perforation diameter was recommended if horizontal and vertical stiffeners are to be provided, since further increase in anchorage length was seen to have negligible effect on member torsional capacity.
4. Horizontal stiffeners provided on either side of perforation on flat element of SEHS member were found to be able to recover slightly higher than 40% of the reduced torsional capacity. This recovery was achieved at a lower stiffener thickness (t_s/t = 2) for small perforation size ($d_{p,f}/l_f$ = 0.3) and further increase in thickness was not found advantageous. In case of large size perforation ($d_{p,f}/l_f$ = 0.7), this recovery was seen at a higher stiffener thickness (t_s/t = 10). On the other hand, horizontal stiffeners on curve element were found to be more effective for small size perforation with ~ 42% recovery. Only ~ 20% recovery in reduced torsional strength was observed for large size perforation even with thicker stiffeners (t_s/t = 10). However, full recovery of capacity was not achieved by the use of horizontal stiffeners.
5. Vertical stiffeners on either side of small size perforation on flat element were observed to provide more than 60% recovery of reduced torsional capacity with thinner/slender stiffener (t_s/t = 1). But, further increase in thickness beyond t_s/t = 1 did not enhance the recovery. For large size perforation, the recovery was as small as 4% even for thicker/stockier stiffener. Hence vertical stiffeners are not recommended for large size perforation.

6. A square frame stiffener provided around perforation on flat element was found to fully recover the reduced torsional perforated member capacity with thicker stiffener (t_s/t = 10). Even at a lower value of stiffener thickness (i.e. t_s/t = 4), more than 60% and 40% recovery was observed for small and large size perforations respectively. Hence, thicker square frame stiffener is recommended for all size of perforation to achieve full recovery of capacity.
7. Full torsional strength recovery was also observed in case of ring stiffener on flat element. This was seen to achieve at t_s/t = 4 and t_s/t = 10 for small and large perforation sizes respectively. For the same thickness of stiffeners, recovery rate was found to be higher with ring stiffener as compared to square frame stiffener. For ring stiffener on curve element of member, at t_s/t = 6, ~94% and 93% recovery was found for small and large perforations respectively. With this recovery, torsional capacity amounts approximately to that of corresponding unperforated member.

In general, ring and square frame stiffeners with stiffener thickness greater than six times that of member thickness and stiffener width equal to one-fourth of perforation diameter has been seen to provide good stiffening effects for slender SEHS members, considered in this study.

Table 5.1: Details of vertical stiffener adopted around perforation and corresponding values of $T_{up\text{-}s}$

Sl. No.	$d_{p,f}/l_f$	$d_{p,c}/l_f$	t_s/t	$l_v/(d_{p,f}$ or $d_{p,c})$	$b_s/(d_{p,f}$ or $d_{p,c})$	$T_{up\text{-}s}$ (kNm)
1	0.3	-	1	0	0.25	83.8
2	0.3	-	1	0.25	0.25	85.2
3	0.3	-	1	0.50	0.25	86.3
4	0.3	-	1	0.75	0.25	86.2
5	0.5	-	1	0	0.25	75.4
6	0.5	-	1	0.25	0.25	76.8
7	0.5	-	1	0.50	0.25	77.6
8	0.7	-	1	0	0.25	66.7
9	0.7	-	1	0.25	0.25	67.1
10	0.3	-	1	0.5	0.10	85.5
11	0.3	-	1	0.5	0.25	86.3
12	0.3	-	1	0.5	0.50	86.3
13	0.3	-	1	0.5	0.75	86.3
14	0.5	-	1	0.5	0.10	77.5
15	0.5	-	1	0.5	0.25	77.6
16	0.5	-	1	0.5	0.50	77.7
17	0.5	-	1	0.5	0.75	77.5
18	0.7	-	1	0.25	0.10	67.1
19	0.7	-	1	0.25	0.25	67.1
20	0.7	-	1	0.25	0.50	67.1
21	0.7	-	1	0.25	0.75	67.1
22	0.3	-	1	0.5	0.25	86.3
23	0.3	-	1.5	0.5	0.25	86.4
24	0.3	-	2	0.5	0.25	86.4
25	0.3	-	4	0.5	0.25	86.4
26	0.3	-	6	0.5	0.25	86.4
27	0.3	-	10	0.5	0.25	86.4
28	0.5	-	1	0.5	0.25	77.6
29	0.5	-	1.5	0.5	0.25	77.7
30	0.5	-	2	0.5	0.25	77.7
31	0.5	-	4	0.5	0.25	77.8
32	0.5	-	6	0.5	0.25	77.6
33	0.5	-	10	0.5	0.25	77.5
34	0.7	-	1	0.25	0.25	67.1
35	0.7	-	1.5	0.25	0.25	67.1
36	0.7	-	2	0.25	0.25	67.2
37	0.7	-	4	0.25	0.25	67.3
38	0.7	-	6	0.25	0.25	67.4

39	0.7	-	10	0.25	0.25	67.4

Table 5.2: Details of horizontal stiffener adopted around perforation and corresponding values of $T_{up\text{-}s}$

Sl. No	$d_{p,f}/l_f$	$d_{p,c}/l_f$	t_s/t	$l_v/(d_{p,f}$ or $d_{p,c})$	$b_s/(d_{p,f}$ or $d_{p,c})$	$T_{up\text{-}s}$ (kNm)
1	0.3	-	1	0	0.25	82.4
2	0.3	-	1	0.25	0.25	83.0
3	0.3	-	1	0.50	0.25	84.7
4	0.3	-	1	0.75	0.25	85.3
5	0.3	-	1	1	0.25	84.0
6	0.5	-	1	0	0.25	76.1
7	0.5	-	1	0.25	0.25	78.0
8	0.5	-	1	0.50	0.25	78.1
9	0.5	-	1	0.75	0.25	78.0
10	0.5	-	1	1	0.25	78.2
11	0.7	-	1	0	0.25	69.1
12	0.7	-	1	0.25	0.25	69.3
13	0.7	-	1	0.50	0.25	69.6
14	0.7	-	1	0.75	0.25	69.9
15	0.7	-	1	1	0.25	70.2
16	-	0.3	1	0	0.25	72.5
17	-	0.3	1	0.25	0.25	73.6
18	-	0.3	1	0.50	0.25	75.3
19	-	0.3	1	0.75	0.25	75.3
20	-	0.3	1	1	0.25	74.5
21	-	0.5	1	0	0.25	63.9
22	-	0.5	1	0.25	0.25	65.0
23	-	0.5	1	0.50	0.25	66.6
24	-	0.5	1	0.75	0.25	66.7
25	-	0.5	1	1	0.25	66.7
26	-	0.7	1	0	0.25	55.9
27	-	0.7	1	0.25	0.25	58.5
28	-	0.7	1	0.50	0.25	59.6
29	-	0.7	1	0.75	0.25	59.6
30	-	0.7	1	1	0.25	59.6
31	0.3	-	1	0.5	0.10	83.7
32	0.3	-	1	0.5	0.25	84.7
33	0.3	-	1	0.5	0.50	85.1
34	0.3	-	1	0.5	0.75	85.2
35	0.5	-	1	0.5	0.10	78.0

36	0.5	-	1	0.5	0.25	78.1
37	0.5	-	1	0.5	0.50	78.2
38	0.5	-	1	0.5	0.75	78.2
39	0.7	-	1	0.5	0.10	69.2
40	0.7	-	1	0.5	0.25	69.6
41	0.7	-	1	0.5	0.50	69.7
42	0.7	-	1	0.5	0.75	69.7
43	-	0.3	1	0.5	0.25	75.3
44	-	0.3	1	0.5	0.50	77.2
45	-	0.3	1	0.5	0.75	77.6
46	-	0.5	1	0.5	0.25	66.6
47	-	0.5	1	0.5	0.50	68.1
48	-	0.5	1	0.5	0.75	68.4
49	-	0.7	1	0.5	0.25	59.6
50	-	0.7	1	0.5	0.50	60.2
51	-	0.7	1	0.5	0.75	60.1
52	0.3	-	1	0.5	0.25	84.7
53	0.3	-	1.5	0.5	0.25	84.9
54	0.3	-	2	0.5	0.25	85.2
55	0.3	-	4	0.5	0.25	85.0
56	0.3	-	6	0.5	0.25	84.9
57	0.3	-	10	0.5	0.25	84.6
58	0.5	-	1	0.5	0.25	78.1
59	0.5	-	1.5	0.5	0.25	78.4
60	0.5	-	2	0.5	0.25	79.0
61	0.5	-	4	0.5	0.25	8.0
62	0.5	-	6	0.5	0.25	80.8
63	0.5	-	10	0.5	0.25	82.5
64	0.7	-	1	0.5	0.25	69.6
65	0.7	-	1.5	0.5	0.25	70.2
66	0.7	-	2	0.5	0.25	70.9
67	0.7	-	4	0.5	0.25	74.4
68	0.7	-	6	0.5	0.25	77.1
69	0.7	-	10	0.5	0.25	78.9
70	-	0.3	1	0.5	0.25	75.3
71	-	0.3	1.5	0.5	0.25	76.6
72	-	0.3	2	0.5	0.25	77.4
73	-	0.3	4	0.5	0.25	78.8
74	-	0.3	6	0.5	0.25	79.5
75	-	0.3	10	0.5	0.25	80.1
76	-	0.5	1	0.5	0.25	66.6
77	-	0.5	1.5	0.5	0.25	67.6

78	-	0.5	2	0.5	0.25	68.4
79	-	0.5	4	0.5	0.25	70.2
80	-	0.5	6	0.5	0.25	70.6
81	-	0.5	10	0.5	0.25	70.5
82	-	0.7	1	0.5	0.25	59.6
83	-	0.7	1.5	0.5	0.25	59.8
84	-	0.7	2	0.5	0.25	59.4
85	-	0.7	4	0.5	0.25	60.8
86	-	0.7	6	0.5	0.25	61.1
87	-	0.7	10	0.5	0.25	61.4

Table 5.3: Details of square frame stiffener adopted around perforation and corresponding values of $T_{up\text{-}s}$

Sl. No.	$d_{p,f}/l_f$	$d_{p,c}/l_f$	t_s/t	$l_v/(d_{p,f}$ or $d_{p,c})$	$b_s/(d_{p,f}$ or $d_{p,c})$	$T_{up\text{-}s}$ (kNm)
1	0.3	-	1	-	0.10	84.0
2	0.3	-	1	-	0.25	86.4
3	0.3	-	1	-	0.50	86.5
4	0.3	-	1	-	0.75	86.6
5	0.5	-	1	-	0.10	77.9
6	0.5	-	1	-	0.25	78.3
7	0.5	-	1	-	0.50	78.3
8	0.5	-	1	-	0.75	78.4
9	0.7	-	1	-	0.10	69.0
10	0.7	-	1	-	0.25	69.3
11	0.7	-	1	-	0.50	69.5
12	0.7	-	1	-	0.75	69.8
13	0.3	-	1	-	0.25	86.4
14	0.3	-	1.5	-	0.25	86.6
15	0.3	-	2	-	0.25	87.0
16	0.3	-	4	-	0.25	88.1
17	0.3	-	6	-	0.25	87.7
18	0.3	-	10	-	0.25	89.7
19	0.5	-	1	-	0.25	78.3
20	0.5	-	1.5	-	0.25	78.6
21	0.5	-	2	-	0.25	79.2
22	0.5	-	4	-	0.25	83.2
23	0.5	-	6	-	0.25	87.0
24	0.5	-	10	-	0.25	89.7
25	0.7	-	1	-	0.25	69.3
26	0.7	-	1.5	-	0.25	70.1

27	0.7	-	2	-	0.25	70.8
28	0.7	-	4	-	0.25	75.9
29	0.7	-	6	-	0.25	81.7
30	0.7	-	10	-	0.25	89.0

Table 5.4: Details of ring stiffener adopted around perforation and corresponding values of $T_{up\text{-}s}$

Sl. No.	$d_{p,f}/l_f$	$d_{p,c}/l_f$	t_s/t	$l_v/(d_{p,f}$ or $d_{p,c})$	$b_s/(d_{p,f}$ or $d_{p,c})$	$T_{up\text{-}s}$ (kNm)
1	0.3	-	1	-	0.10	86.6
2	0.3	-	1	-	0.25	86.9
3	0.3	-	1	-	0.50	87.5
4	0.3	-	1	-	0.75	87.6
5	0.5	-	1	-	0.10	78.3
6	0.5	-	1	-	0.25	79.7
7	0.5	-	1	-	0.50	80.1
8	0.5	-	1	-	0.75	80.2
9	0.7	-	1	-	0.10	70.2
10	0.7	-	1	-	0.25	71.3
11	0.7	-	1	-	0.50	71.6
12	0.7	-	1	-	0.75	71.7
13	-	0.3	1	-	0.25	76.3
14	-	0.3	1	-	0.50	78.6
15	-	0.3	1	-	0.75	79.6
16	-	0.5	1	-	0.25	67.5
17	-	0.5	1	-	0.50	68.4
18	-	0.5	1	-	0.75	68.8
19	-	0.7	1	-	0.25	58.1
20	-	0.7	1	-	0.50	58.1
21	-	0.7	1	-	0.75	58.3
22	0.3	-	1	-	0.25	85.9
23	0.3	-	1.5	-	0.25	87.8
24	0.3	-	2	-	0.25	87.9
25	0.3	-	4	-	0.25	89.7
26	0.3	-	6	-	0.25	88.4
27	0.3	-	10	-	0.25	88.9
28	0.5	-	1	-	0.25	79.7
29	0.5	-	1.5	-	0.25	80.4
30	0.5	-	2	-	0.25	81.2
31	0.5	-	4	-	0.25	85.1
32	0.5	-	6	-	0.25	88.5

33	0.5	-	10	-	0.25	89.6
34	0.7	-	1	-	0.25	71.3
35	0.7	-	1.5	-	0.25	72.2
36	0.7	-	2	-	0.25	73.2
37	0.7	-	4	-	0.25	78.3
38	0.7	-	6	-	0.25	83.8
39	0.7	-	10	-	0.25	89.2
40	-	0.3	1	-	0.25	76.3
41	-	0.3	1.5	-	0.25	79.5
42	-	0.3	2	-	0.25	82.4
43	-	0.3	4	-	0.25	87.5
44	-	0.3	6	-	0.25	87.7
45	-	0.5	1	-	0.25	67.5
46	-	0.5	1.5	-	0.25	70.9
47	-	0.5	2	-	0.25	74.6
48	-	0.5	4	-	0.25	86.8
49	-	0.5	6	-	0.25	87.9
50	-	0.7	1	-	0.25	58.1
51	-	0.7	1.5	-	0.25	61.6
52	-	0.7	2	-	0.25	66.1
53	-	0.7	4	-	0.25	83.2
54	-	0.7	6	-	0.25	86.3

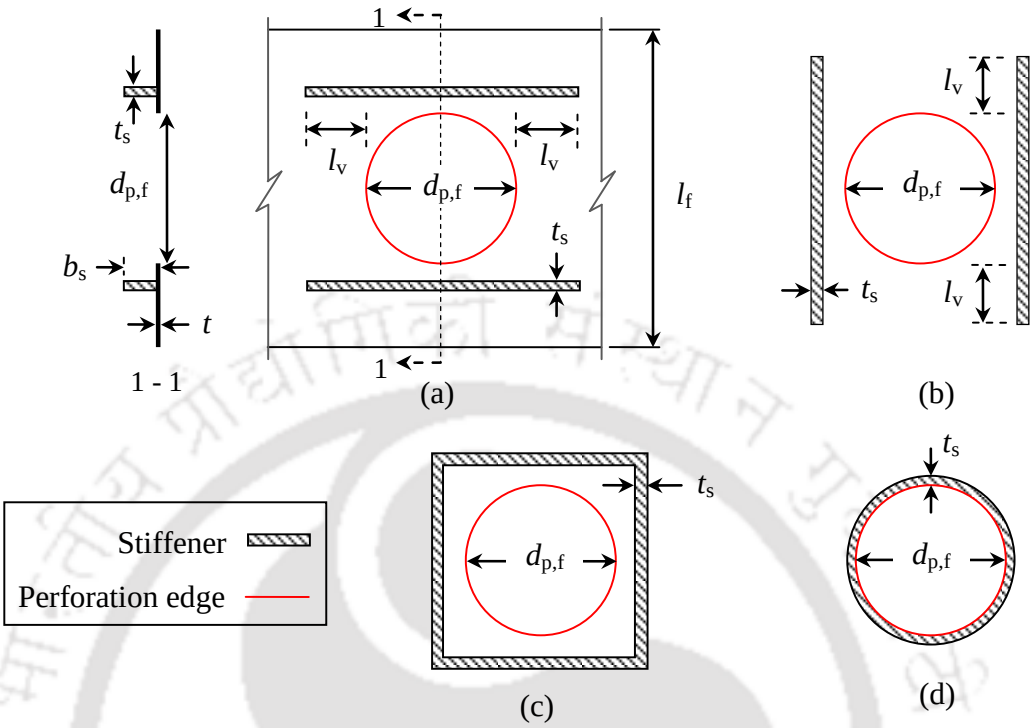

Figure 5.1: Stiffener arrangements for reinforcing/stiffening perforation on flat element (a) Horizontal stiffener, (b) Vertical stiffener, (c) Square frame stiffener and (d) Ring stiffener

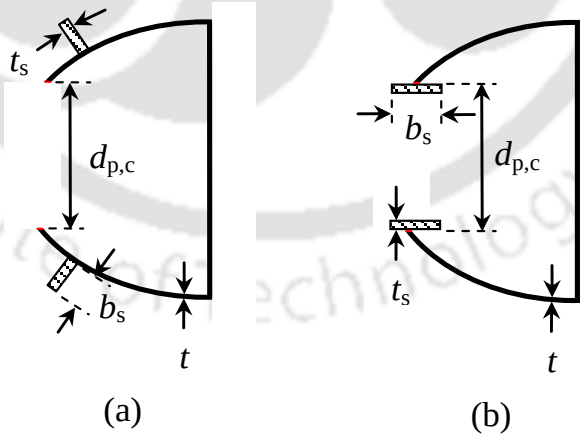

Figure 5.2: Stiffener arrangements for reinforcing perforation on curve element (a) Horizontal stiffener and (b) Ring stiffener

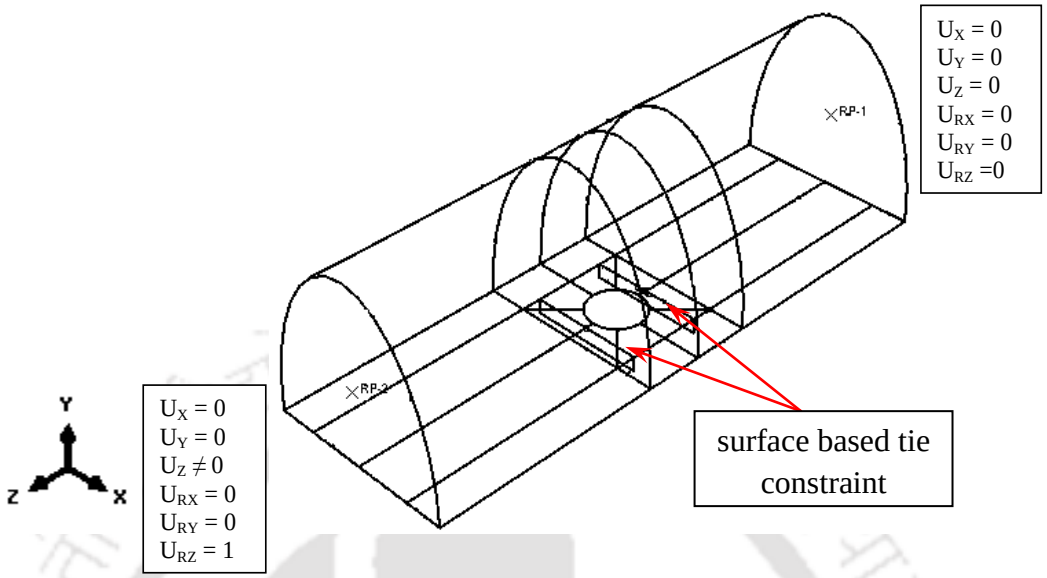

Figure 5.3: Boundary conditions and tie constraints

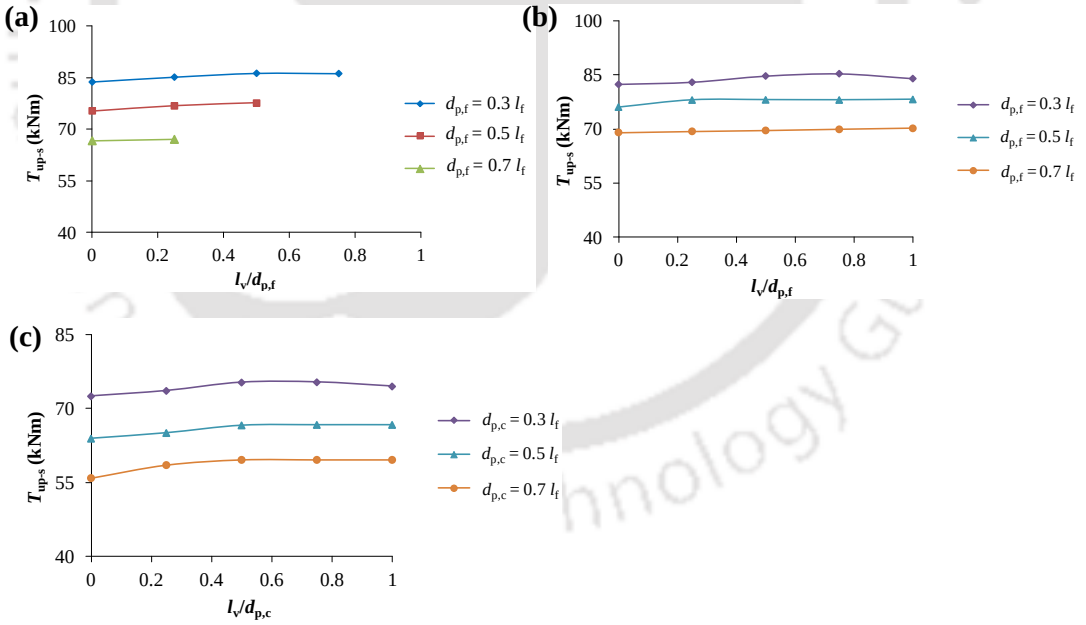

Figure 5.4: Variation of $T_{up\text{-}s}$ with anchorage length (l_v) for (a) vertical and (b) horizontal stiffeners on flat element; (c) horizontal stiffeners on curve element

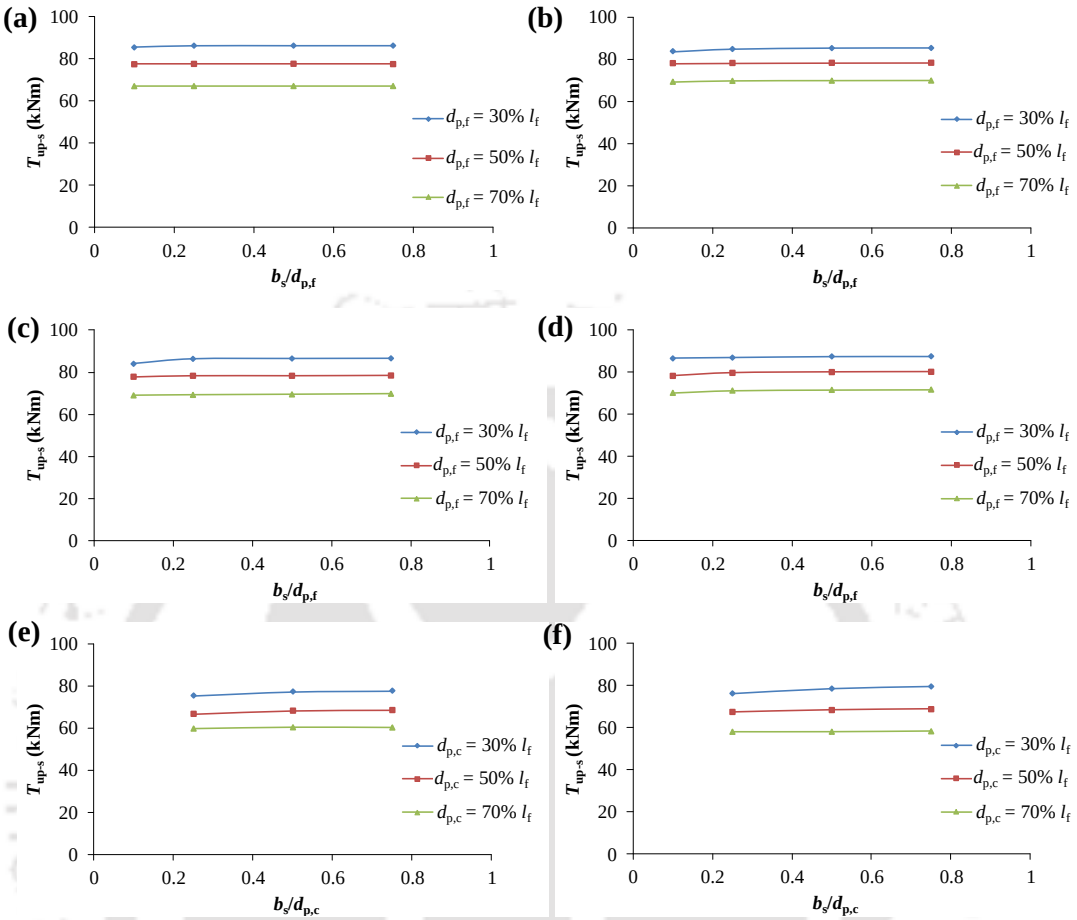

Figure 5.5: Variation of $T_{up\text{-}s}$ with stiffener width (b_s) for (a) Vertical, (b) Horizontal, (c) Square frame and (d) Ring stiffener for perforation on flat element; (e) Horizontal and (f) Ring stiffener for perforation on curve element

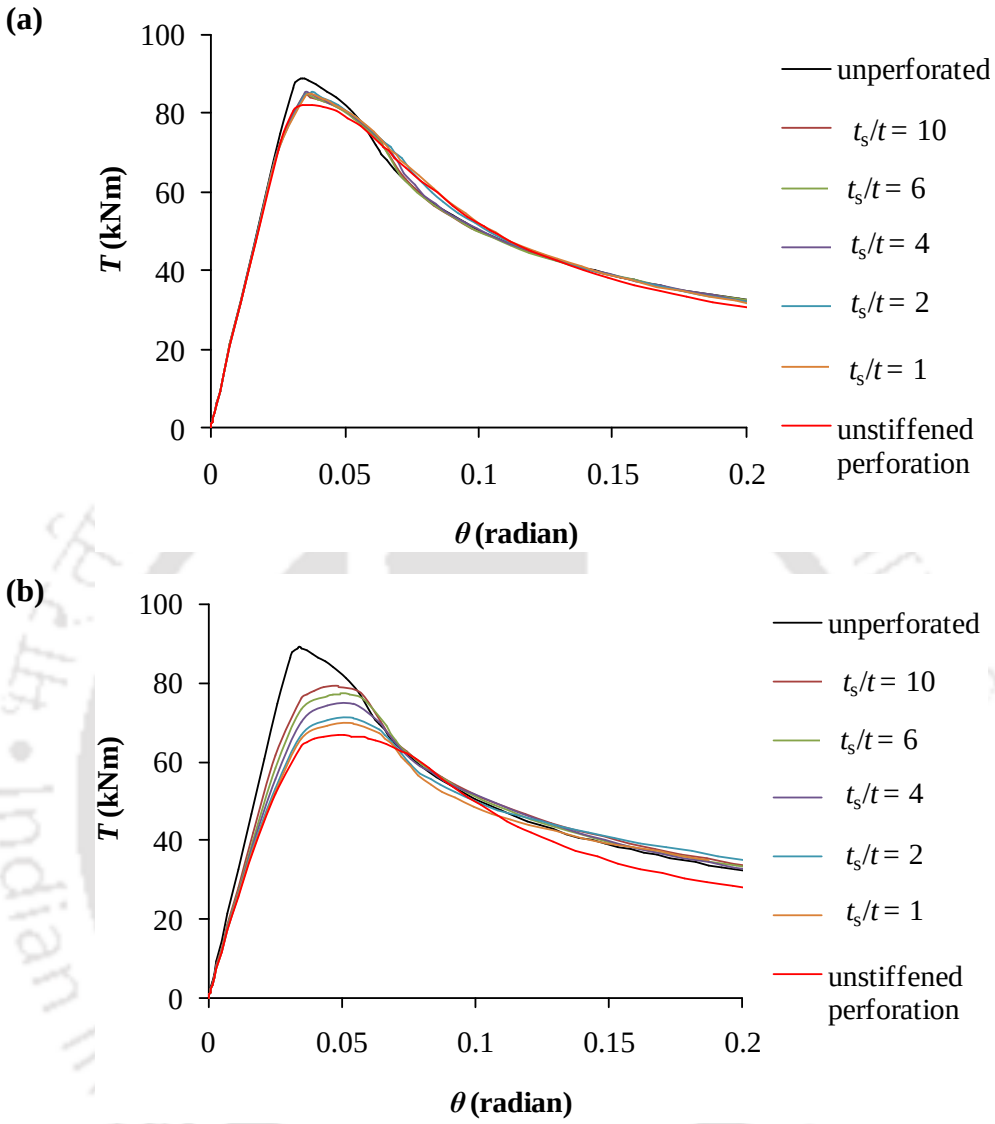

Figure 5.6: Comparison of $T - \theta$ curves of member with no perforation, unstiffened perforation and stiffened perforation (by horizontal stiffeners on flat element) for (a) $d_{p,f}/l_f = 0.3$ and (b) $d_{p,f}/l_f = 0.7$

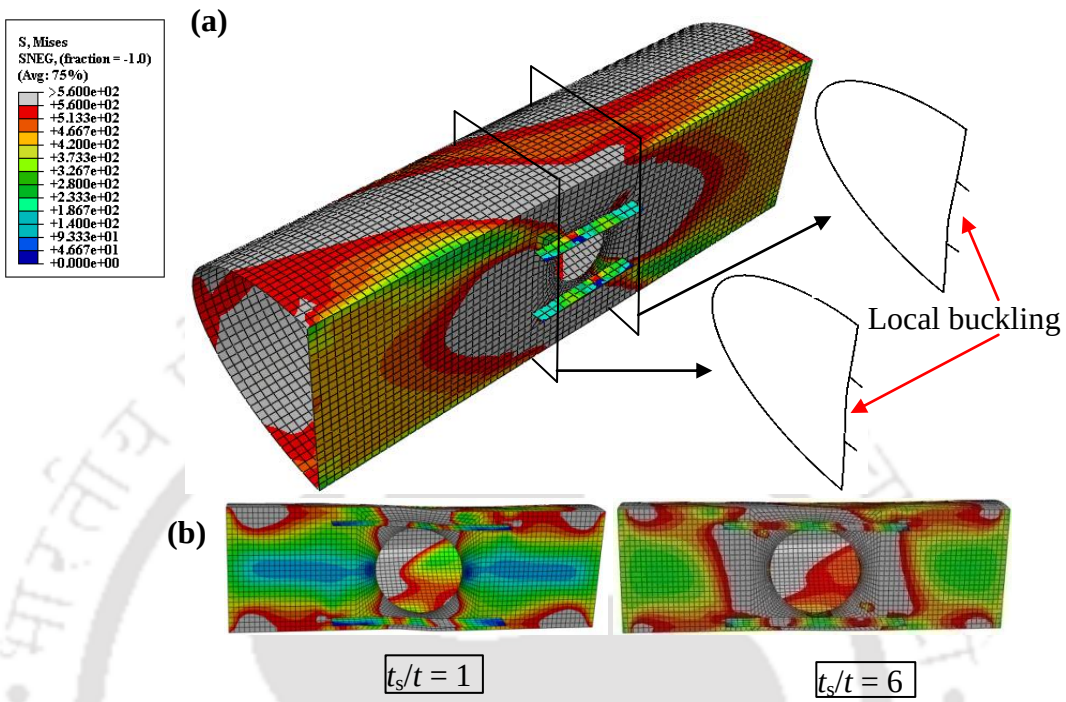

Figure 5.7: Deformed shapes at $T_{up\text{-}s}$ superimposed with Von-Mises stress contour of perforated members with horizontal stiffeners on flat element for (a) $d_{p,f}/l_f$ = 0.3 and (b) $d_{p,f}/l_f$ = 0.7

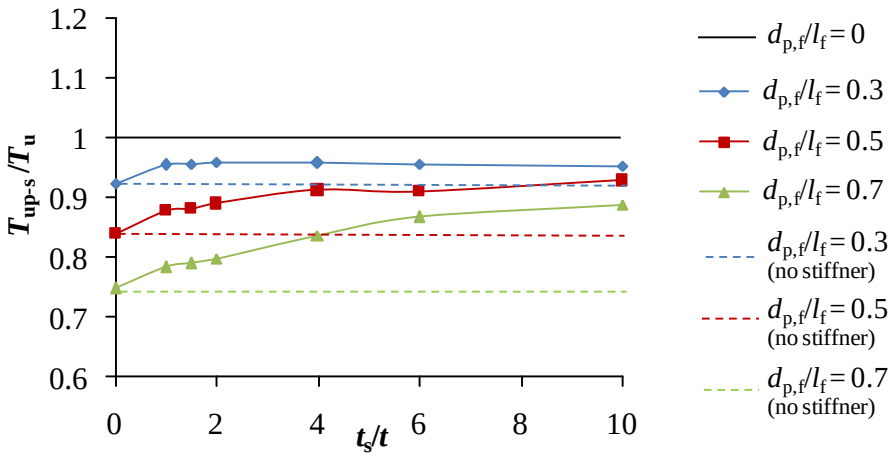

Figure 5.8: Variation of $T_{up\text{-}s}$ with thickness of horizontal stiffener (t_s) on flat element for SEHS members of h/b = 1.8

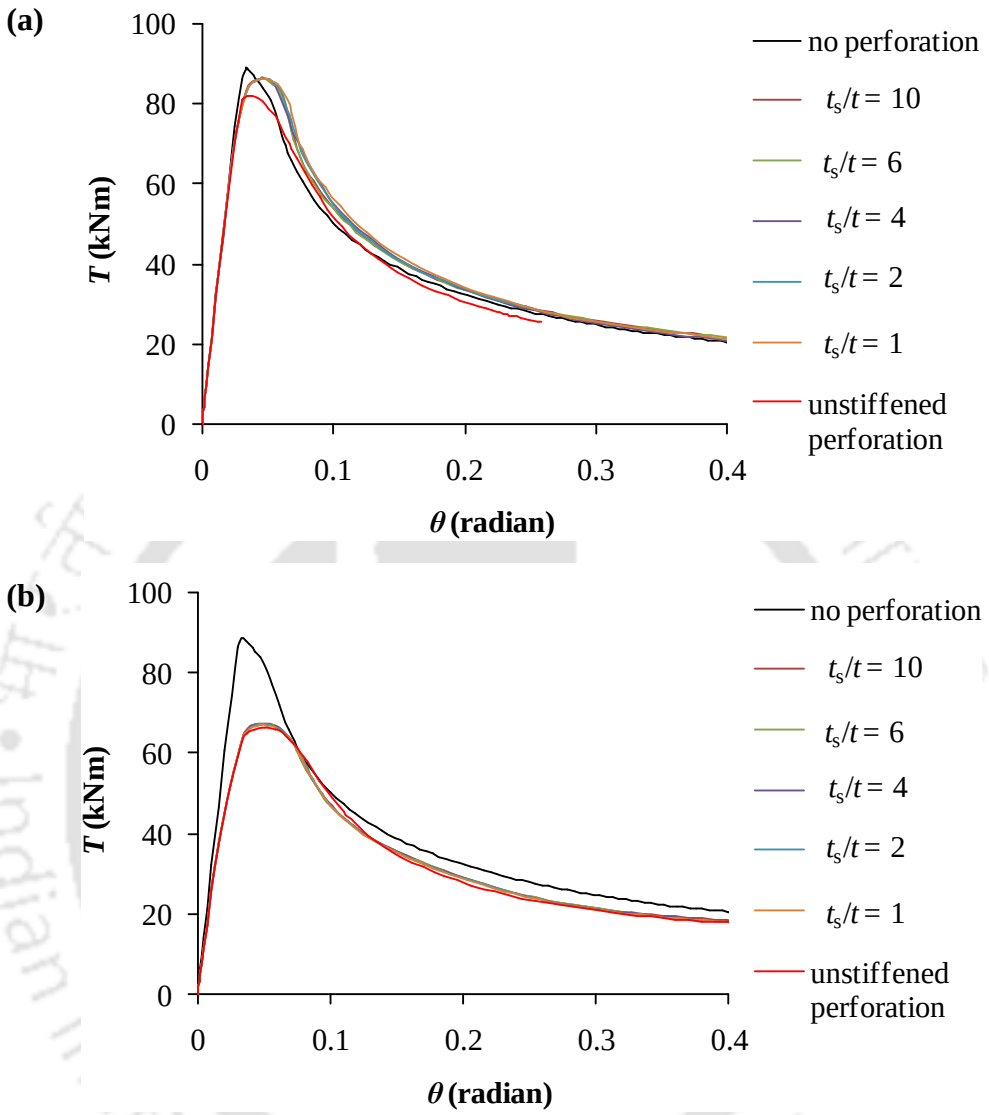

Figure 5.9: Comparison of $T - \theta$ curves of member with no perforation, unstiffened perforation and stiffened perforation (by vertical stiffeners on flat element) for (a) $d_{p,f}/l_f = 0.3$ and (b) $d_{p,f}/l_f = 0.7$

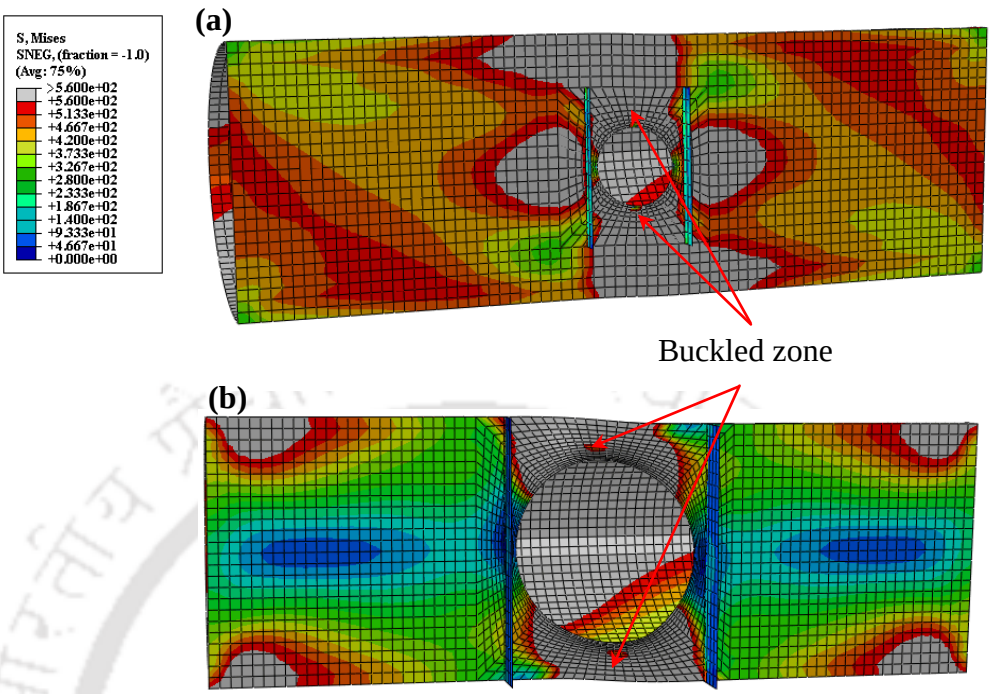

Figure 5.10: Deformed shapes at $T_{up\text{-}s}$ superimposed with Von-Mises stress contour of perforated members with vertical stiffeners on flat element for (a) $d_{p,f}/l_f$ = 0.3 and (b) $d_{p,f}/l_f$ = 0.7

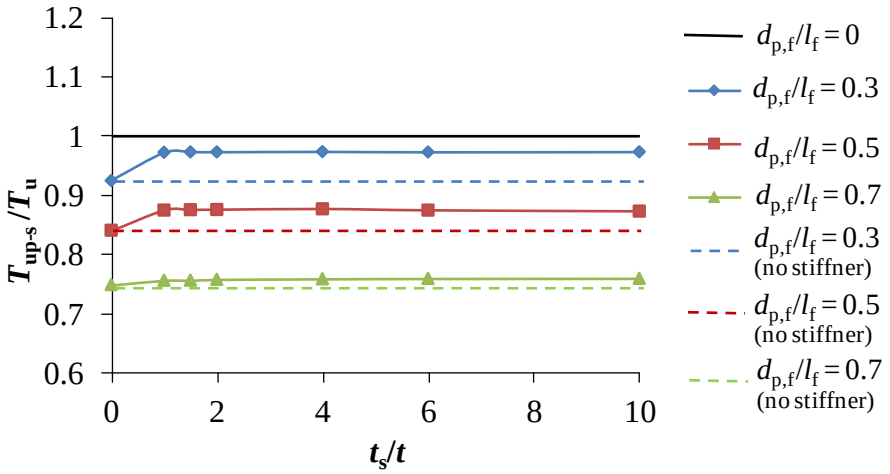

Figure 5.11: Variation of $T_{up\text{-}s}$ with thickness of vertical stiffener (t_s) on flat element for SEHS members of h/b = 1.82

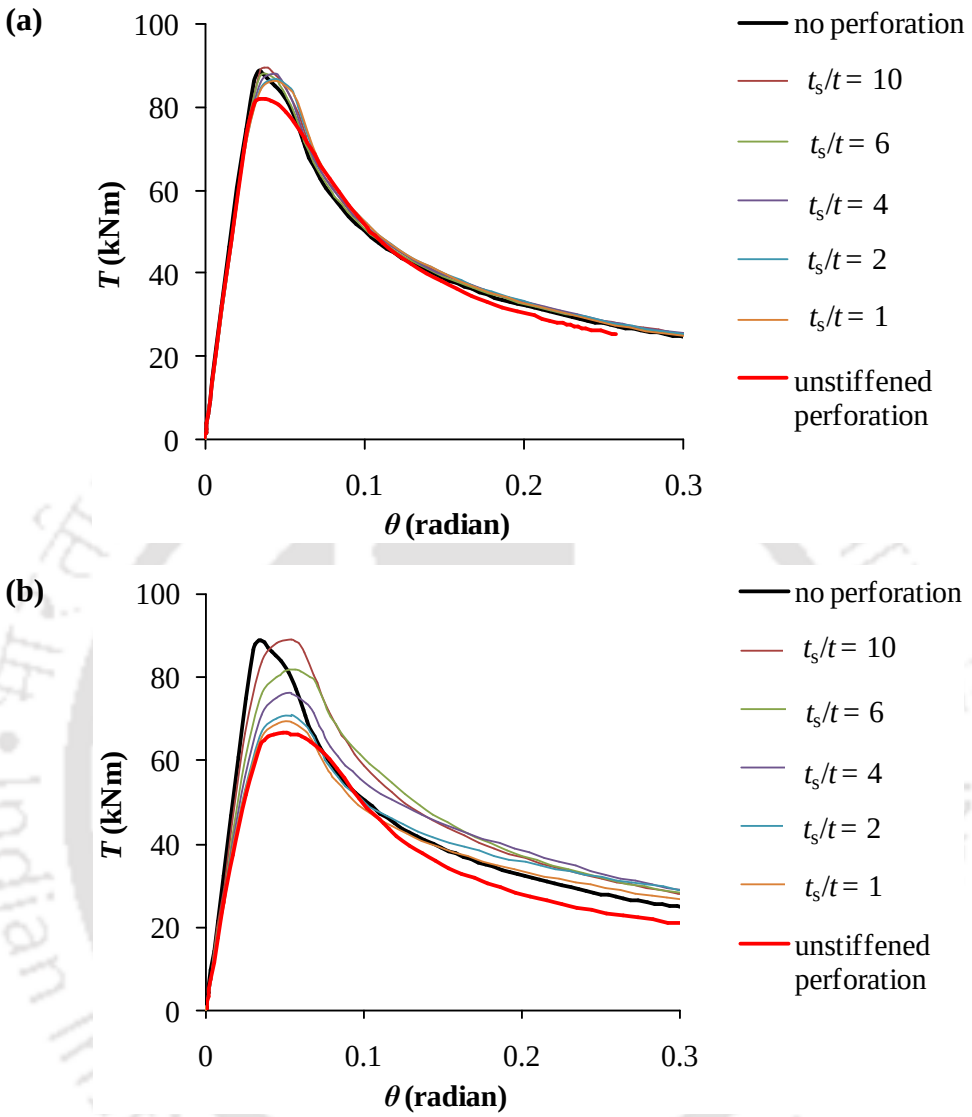

Figure 5.12: Comparison of $T - \theta$ curves of member with no perforation, unstiffened perforation and stiffened perforation (by square frame stiffener on flat element) for (a) $d_{p,f}/l_f = 0.3$ and (b) $d_{p,f}/l_f = 0.7$

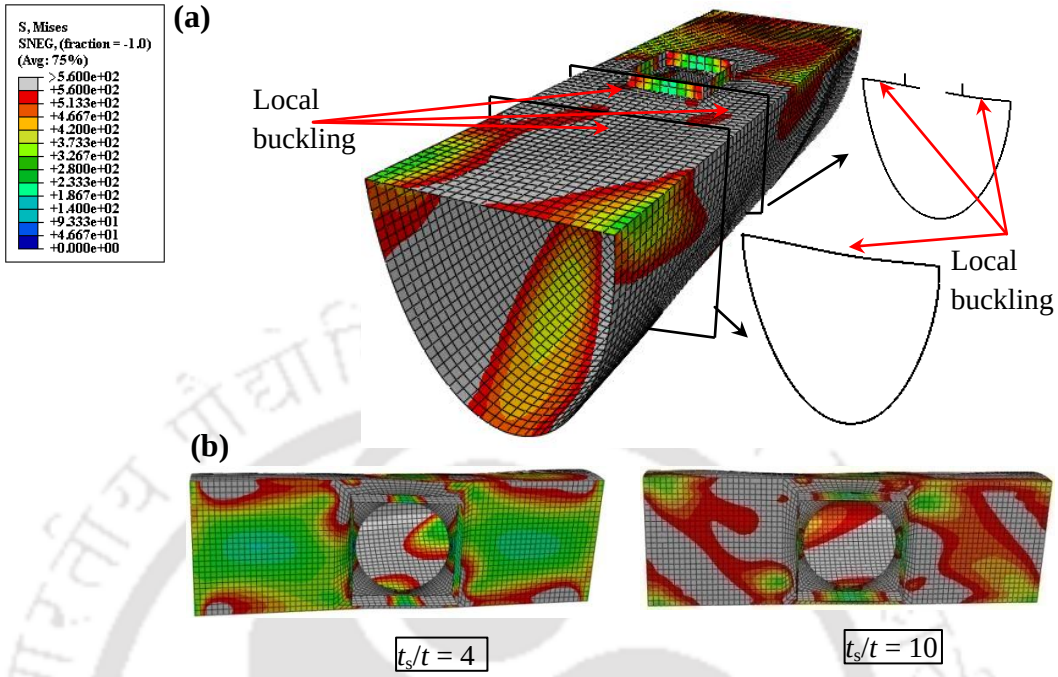

Figure 5.13: Deformed shapes at $T_{up\text{-}s}$ superimposed with Von-Mises stress contour of perforated members with square frame stiffener on flat element for (a) $d_{p,f}/l_f$ = 0.3 and (b) $d_{p,f}/l_f$ = 0.7

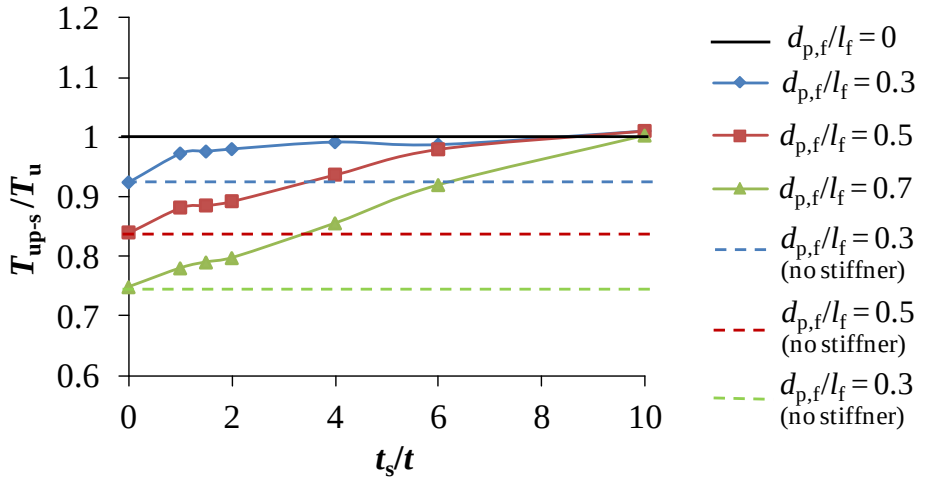

Figure 5.14: Variation of $T_{up\text{-}s}$ with thickness of square frame stiffener (t_s) on flat element for SEHS members of h/b = 1.82

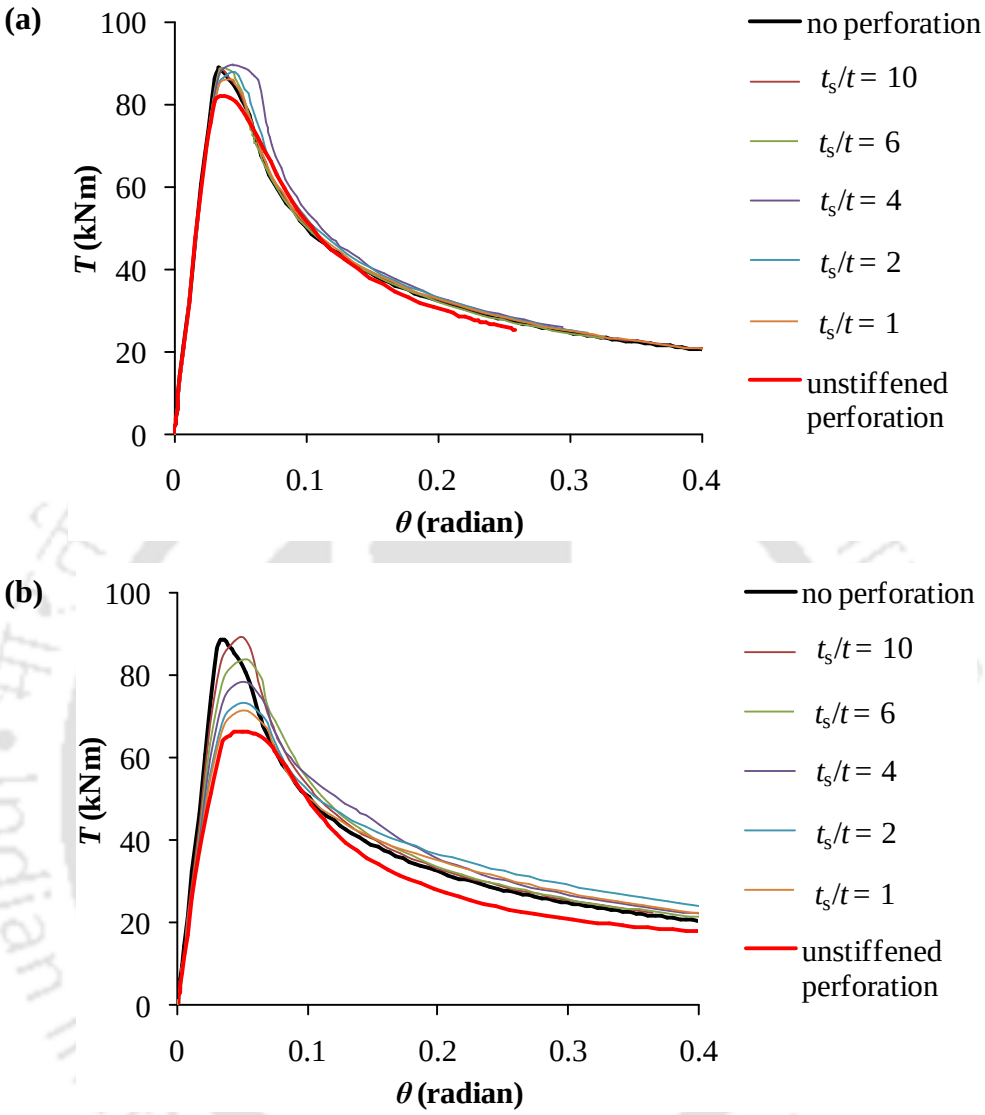

Figure 5.15: Comparison of T – θ curves of member with no perforation, unstiffened perforation and stiffened perforation (by ring stiffener on flat element) for (a) $d_{p,f}/l_f$ = 0.3 and (b) $d_{p,f}/l_f$ = 0.7

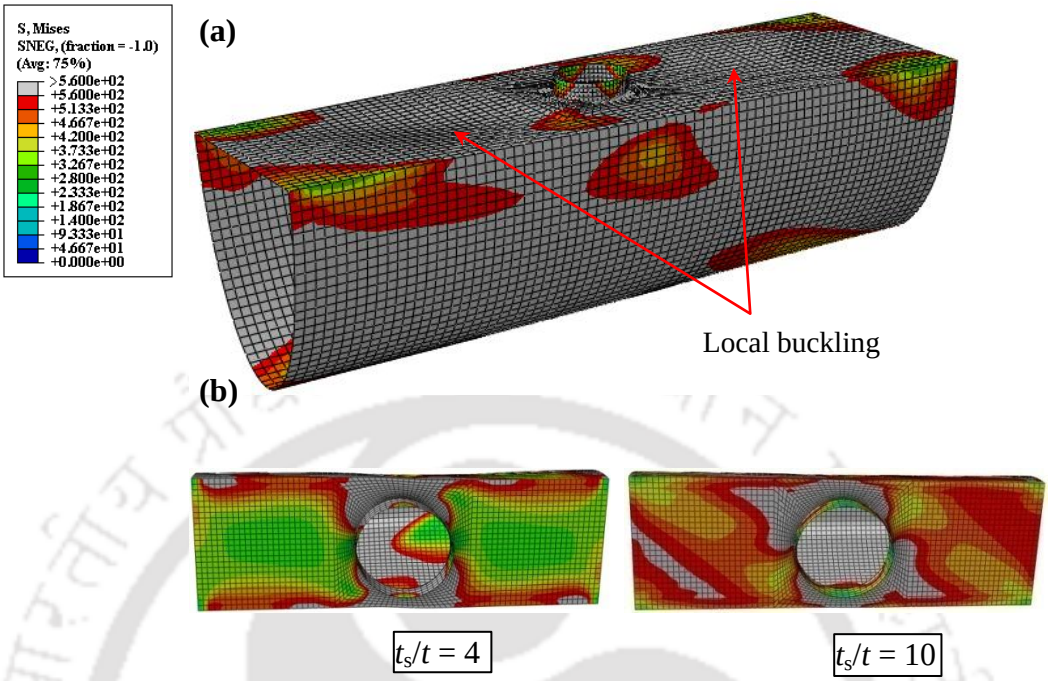

Figure 5.16: Deformed shapes at $T_{up\text{-}s}$ superimposed with Von-Mises stress contour of perforated members with ring stiffener on flat element for (a) $d_{p,f}/l_f$ = 0.3 and (b) $d_{p,f}/l_f$ = 0.7

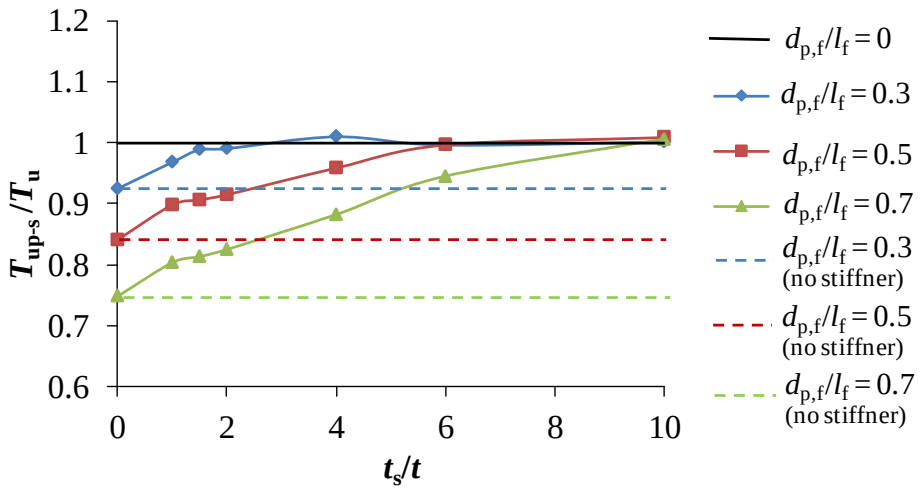

Figure 5.17: Variation of $T_{up\text{-}s}$ with thickness of ring stiffener (t_s) on flat element for SEHS members of h/b = 1.82

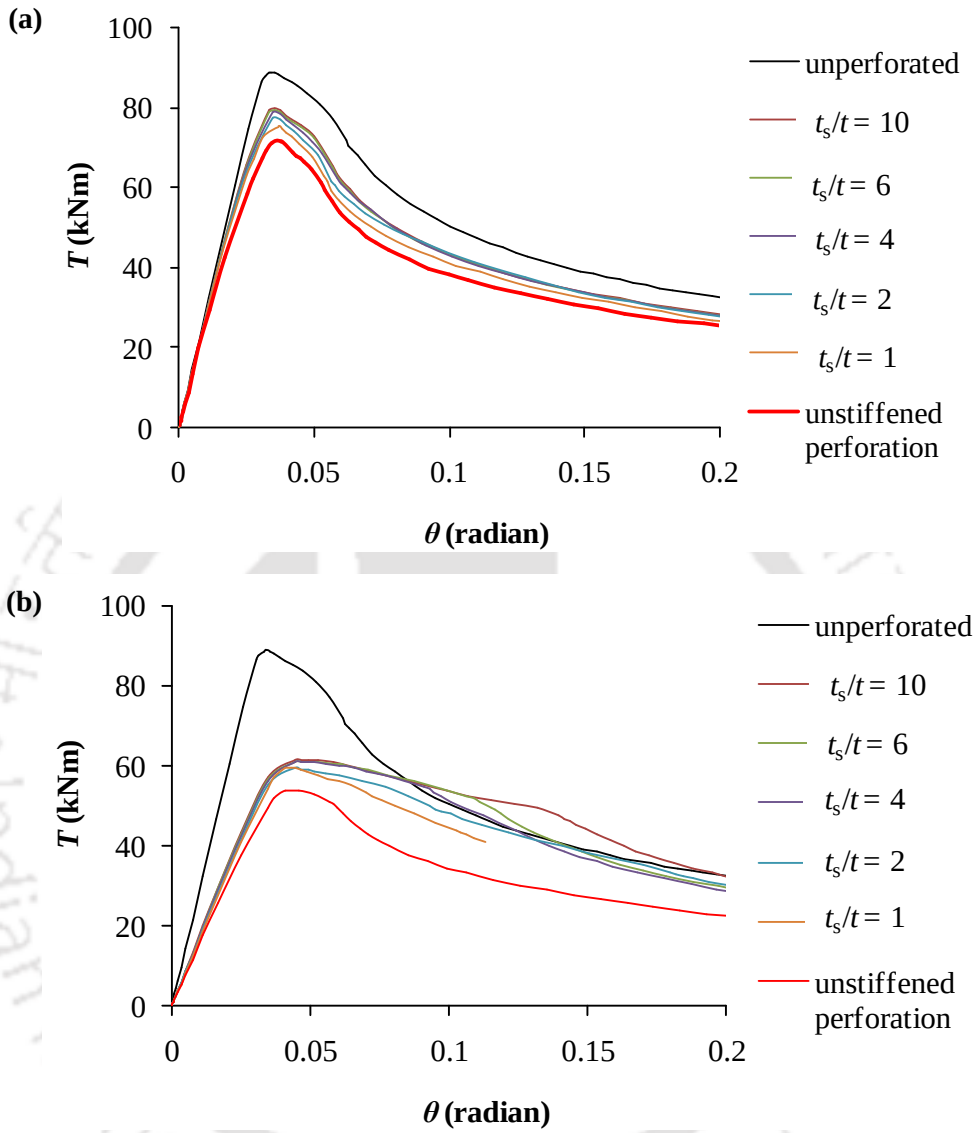

Figure 5.18: Comparison of $T - \theta$ curves of member with no perforation, unstiffened perforation and stiffened perforation on curve element (by horizontal stiffeners) for (a) $d_{p,c}/l_f = 0.3$ and (b) $d_{p,c}/l_f = 0.7$

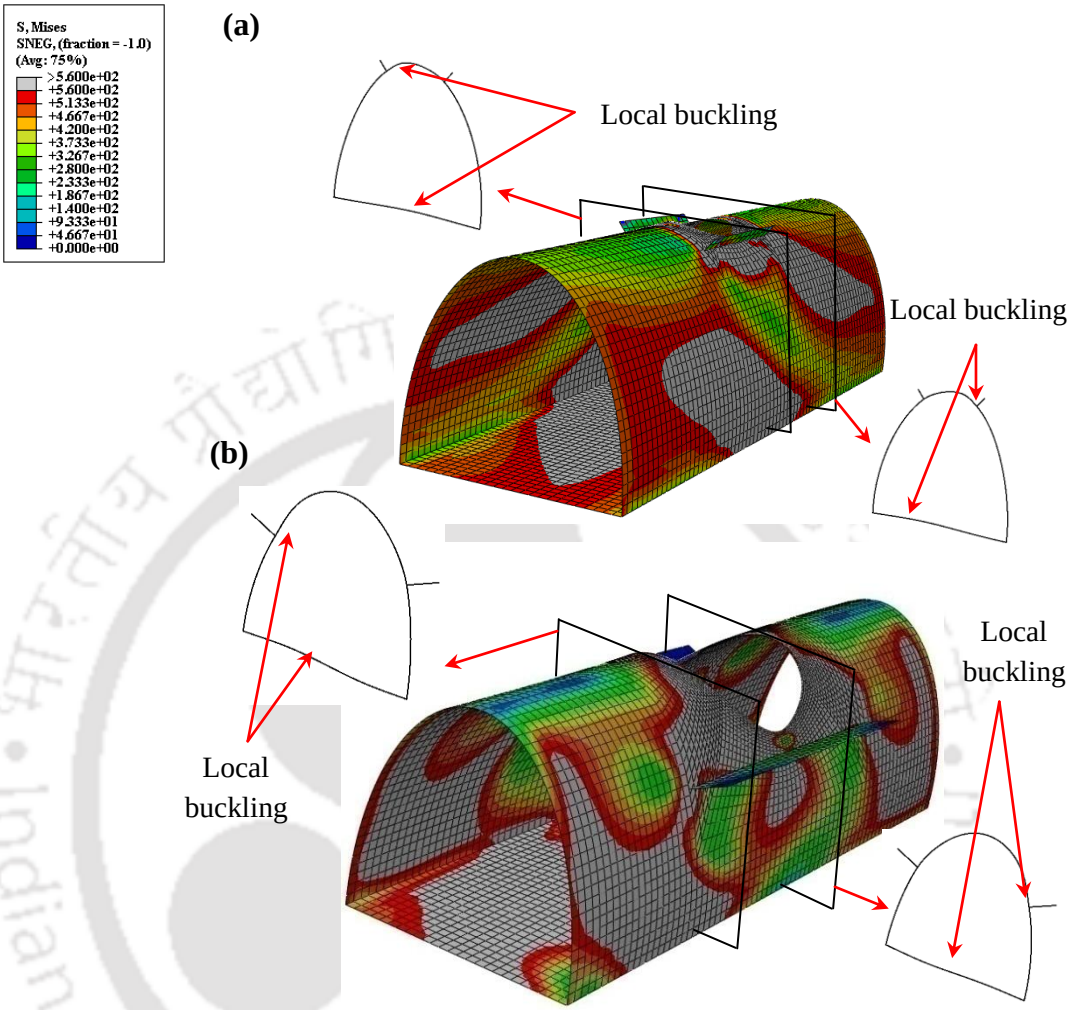

Figure 5.19: Deformed shapes at $T_{up\text{-}s}$ superimposed with Von-Mises stress contour of perforated members with horizontal stiffeners on curve element for (a) $d_{p,c}/l_f$ = 0.3 and (b) $d_{p,c}/l_f$ = 0.7

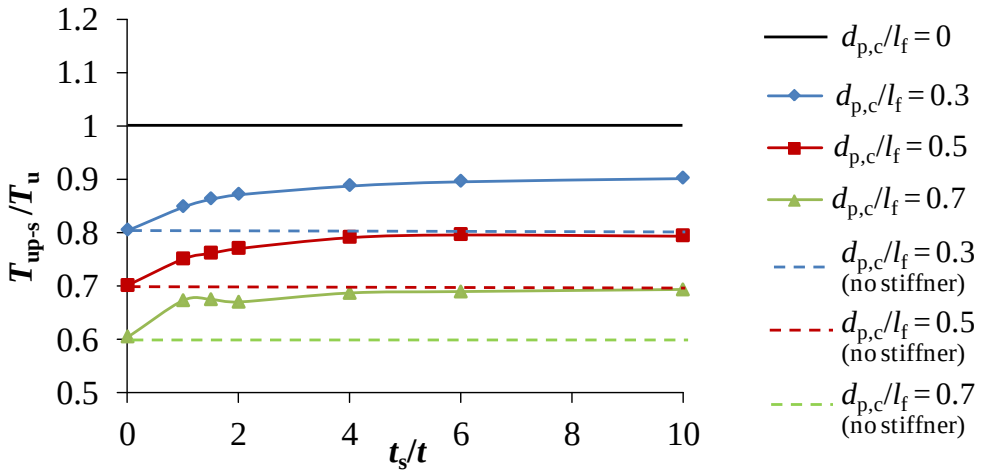

Figure 5.20: Variation of $T_{up\text{-}s}$ with thickness of horizontal stiffener (t_s) on curve element for SEHS members of h/b = 1.82

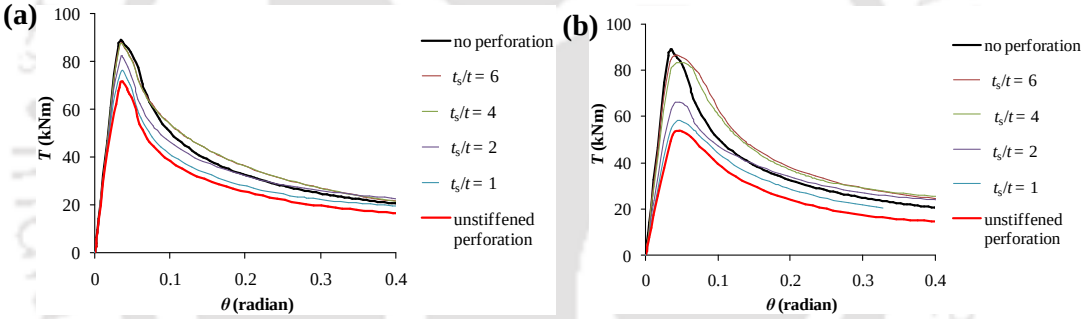

Figure 5.21: Comparison of T – θ curves of member with no perforation, unstiffened perforation and stiffened perforation on curve element (by ring stiffener) for (a) $d_{p,c}/l_f$ = 0.3 and (b) $d_{p,c}/l_f$ = 0.7

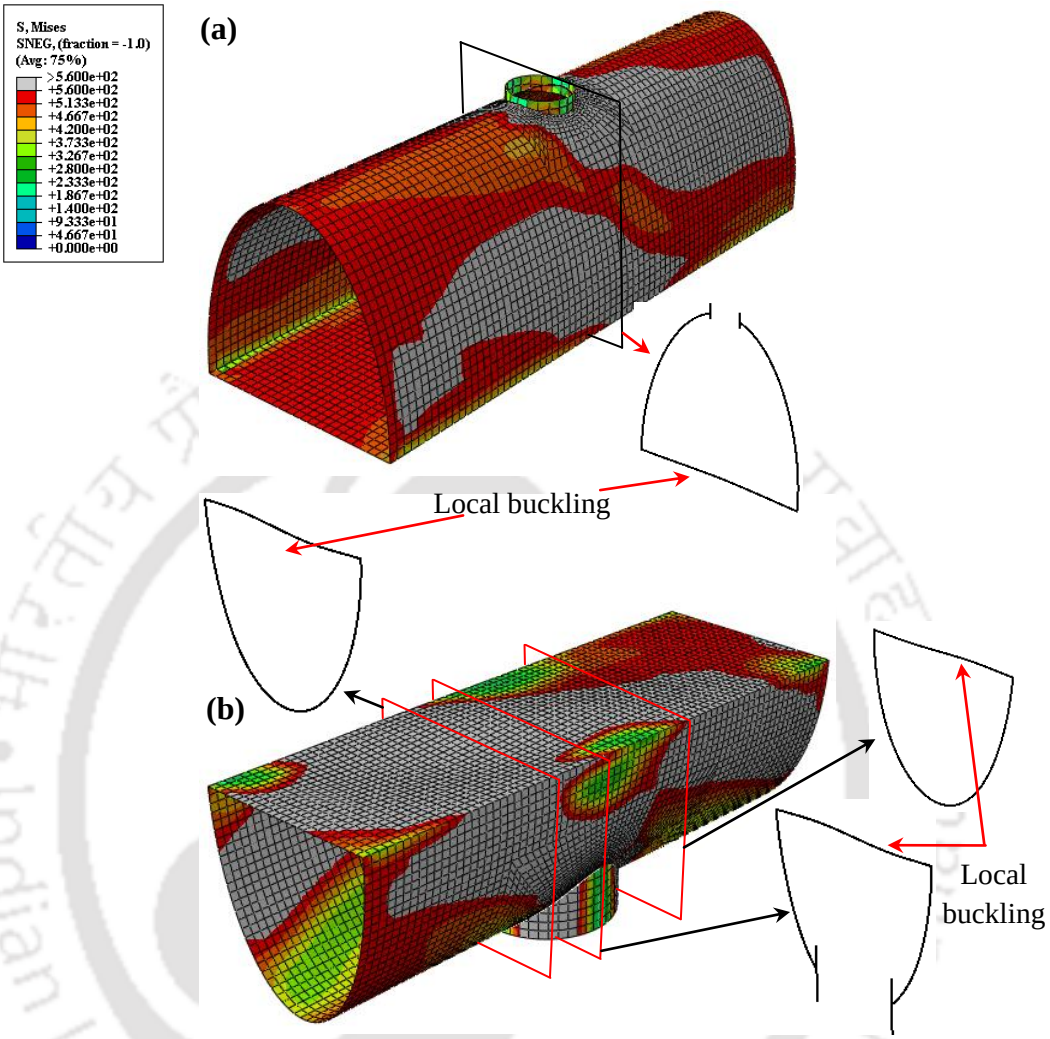

Figure 5.22: Deformed shapes at $T_{up\text{-}s}$ superimposed with Von-Mises stress contour of perforated members with ring stiffener on curve element for (a) $d_{p,c}/l_f$ = 0.3 and (b) $d_{p,c}/l_f$ = 0.7

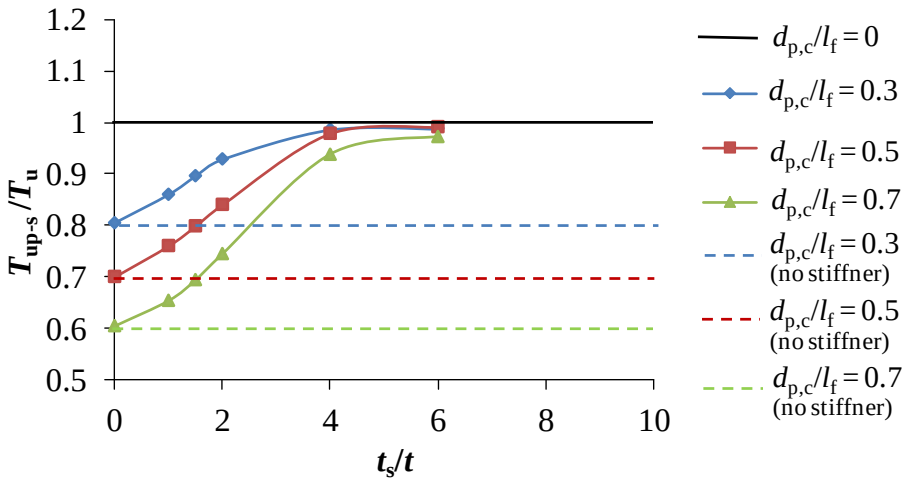

Figure 5.23: Variation of $T_{up\text{-}s}$ with thickness of ring stiffener (t_s) on curve element for SEHS members of h/b = 1.82

CHAPTER 6

CONCLUSIONS AND FUTURE SCOPE

6.1 Introduction

To derive the significant advantages of LDSS mentioned in the beginning of this thesis, structural LDSS member has been investigated under compression (e.g. Anbarasu & Ashraf, 2017; Huang & Young, 2013b; Sachidananda & Singh, 2017; Theofanous & Gardner, 2009), bending (e.g. Huang & Young, 2013a; Sonu & Singh, 2017b; Theofanous & Gardner, 2010) and combined loading (e.g. Huang & Young, 2014a; Zhao et al., 2015). However, structural performance of LDSS closed hollow section (or tubular) members under torsion have not been investigated yet, to the best of author's knowledge. In general, studies reported on torsional behaviour of cold-formed steel closed hollow section members are limited (e.g. Ridley-Ellis, 2000). Considering the lack in study reported on behaviour of closed hollow members under action of pure torsion, an attempt has been made in this thesis to investigate torsional behaviour of lean duplex stainless steel semi-elliptical hollow section members. Parametric study has been carried out on both unperforated and perforated members using the commercial finite element software, Abaqus. Effectiveness of various stiffeners around perforation in restoring member torsional capacity has also been assessed. Important conclusions

derived from the present study are enumerated below. Possible extensions of the current study in future are also suggested at the end of this chapter.

6.2 Conclusions

6.2.1 Torsional capacity of unperforated LDSS SEHS member

A systematic parametric study has been conducted on lean duplex stainless steel (LDSS) semi-elliptical hollow tubular members under torsion using finite element analyses. Effects of various cross-section parameters such as curve length (l_c), aspect ratio (h/b), section size and member length (L) on ultimate torsional capacity have been studied considering a wide range of cross-section slenderness. The following observations have been made from the parametric study:

1. Torsional capacity (T_u) of semi-elliptical hollow section member (SEHS) has been found to increase with increase in curve length (l_c), in a near linear manner. Also, rate of increase in T_u was seen to be more in stocky sections as compared to slender sections.
2. Sections of higher aspect ratio (h/b) have been observed to have higher torsional capacity, in contrast to twist at maximum torque.
3. Reduction in section size resulted in decreasing its torque carrying capacity. With increasing section size, the initial stiffness of T-θ response has been found to increase.
4. It has been observed that member length do not to have significant effect on T_u although θ_u has been found to increase significantly with increase in member length. In general, no apparent change in T_u was seen with increasing member length, although for very short lengths ($L/l_f < 3$), a decrease in T_u has been observed with increasing member length.
5. Initial stiffness in T-θ curve has been found to reduce significantly as l_c (curve element length), h/b (aspect ratio) and cross-section size reduces, and

L (member length) increases. Design equations have been proposed for LDSS SEHS members under torsion, adapted to three different formats – Direct Strength Method (DSM), Eurocode (EN 1993-1-4:2006+A1, 2015) and Deformation Based Method (DBM). The proposed equations have been assessed by reliability analysis and observed to satisfy the target reliability index.

6.2.2 Torsional capacity of perforated LDSS SEHS member

A finite element numerical investigation has been carried out on perforated LDSS semi-elliptical hollow tubular members under torsion, to investigate effects of perforation on its torsional capacity. A single circular perforation of various sizes ($d_{p,f}$ or $d_{p,c}$) at mid length of member has been employed on flat or curve elements of SEHS members of various aspect ratios. Based on the parametric study, the following observations have been made:

1. In comparison to flat element perforation, introducing perforation on curve element has been found to have higher effect in reducing torsional capacity of LDSS SEHS member.
2. Different failure modes (such as local buckling at periphery of perforation, Vierendeel failure mechanism, failure due to yielding etc.) have been identified for members with varying perforation size and cross-section slenderness.
3. Torsional capacity of member has been observed to reduce with increasing perforation size. Also, rate of reduction in the torsional capacity was seen to vary with cross-section slenderness (higher rate of reduction in slender cross-section).
4. Design equations for torsional capacity of perforated LDSS SEHS members have been proposed, based on the torsional capacity of unperforated member using a perforation reduction factor (R_f).

6.2.3 Stiffening effects of stiffeners on torsional capacity of perforated LDSS SEHS members

A parametric study on LDSS slender SEHS members with stiffened perforation using FE software Abaqus has been presented. Several stiffener arrangements were considered for stiffening perforation on flat or curve element of SEHS member. The optimum dimensions of stiffener (width (b_s), thickness (t_s) etc.) for partial or full recovery of reduced torsional capacity have been determined. The following conclusions have been drawn from the FE analyses:

1. Stiffener width (b_s) and anchorage length (l_v) have been observed to show negligible effect on torsional capacity of stiffened perforated member ($T_{up\text{-}s}$) and torsional capacity recovery of perforated member. On the other hand, stiffener thickness (t_s) has been found to contribute significantly in recovering torsional capacity. Torsional capacity of stiffened perforated member was seen to increase with increase in t_s, leading to partial or full recovery of torsional capacity for the stiffeners considered.
2. In case of horizontal stiffeners (on flat and curve elements) and vertical stiffeners (on flat element) placed on two opposite sides of perforation, torsional capacity have been observed to recover partially. Further, percentage of this recovery has been found to be higher for members with small perforation size compared to large perforation size.
3. In case of ring stiffener (on flat and curve elements) and square frame stiffener (on flat element), full recovery of torsional capacity has been seen at relatively lower (or slender) stiffener thickness for members with small perforation size as compared to large perforation size.
4. In general, ring and square frame stiffeners with stiffener thickness greater than six times that of member thickness and stiffener width equal to one-fourth of perforation diameter have been seen to provide good stiffening effects for slender SEHS members, considered in this study.

6.3 Future scope

The current work resulted from ~ 590 finite element models covered the structural behaviour of unperforated, perforated and stiffened perforated lean duplex stainless steel semi-elliptical hollow section members subjected to pure torsion loading, considering various parameters such as cross-section aspect ratio, curve element length, section size, member length, circular perforation size and location, various arrangements of stiffener and stiffener dimensions etc. Although several geometrical aspects of SEHS LDSS have been covered in the present study, there remains possibility of extending the study i.e. there are scopes of further extension to this investigation, e.g. in terms of loading conditions, other sections, including infill etc.; some of which are presented herein.

6.3.1 Loading condition

The present study is limited to the case of pure torsion static loading on SEHS members. It may be extended to other loading scenarios such as cyclic torsion, combination of torsion with compression or bending, torsion with compression and bending etc. Additionally, other cases of loadings like impact and blast may also be considered.

6.3.2 Geometric and material parameter

The current investigation was carried out specifically on SEHS members subjected to torsion. Similar study may be carried out for other cross-section shapes such as channel, I, hollow flange beams, elliptical, flat-oval, tunnel etc. Moreover, the study is limited to cold-formed LDSS material. Hence, it may be extended to other grades of stainless steel, carbon steel, exhibiting different material behaviour to lean duplex stainless steel. Further, torsional behaviour with elevated temperature and post-fire material properties can also be investigated.

6.3.3 Infill material

Addition of infill material to hollow tubular members has been known to enhance member capacity. Therefore, the present study can be extended to tubular members with infill material such as ordinary concrete, fibre reinforced concrete, geopolymer concrete etc. Hollow tubes may be fully filled with the infill material or infill may be sandwiched between an outer and an inner tube (i.e. double skin). Various shapes such as square, circular, elliptical etc. can also be considered for the outer and the inner tubes.

6.3.4 Types of perforation

Only single central circular perforation has been considered in the present study. There are scopes of extension to other shapes of perforation such as square, rectangular, elliptical etc. Location of perforation may also be varied and its effect on torsional capacity investigated. The study can also be extended to multiple perforation and their interaction effects on torsional capacity of member.

6.3.5 Design guidelines

Torsion design guidelines provided in the present study are based on results obtained for cold-formed lean duplex stainless steel semi-elliptical hollow section members. Extension of these proposed equations to other grades of stainless steel such as duplex, austenitic, ferritic etc. may be investigated. Applicability of these torsion design guidelines may also be assessed to other closed hollow section such as elliptical, tunnel etc.

References

Abaqus. (2009). *Abaqus/standard user's manual volumes I-III and ABAQUS CAE manual, Version 6.9-EF1, Dassault Systemes Corp., Providence, USA*.

Afshan, S., Francis, P., Baddoo, N. R. & Gardner, L. (2015). Reliability analysis of structural stainless steel design provisions. *Journal of Constructional Steel Research*, *114*, 293–304.

Afshan, S. & Gardner, L. (2013). The continuous strength method for structural stainless steel design. *Thin-Walled Structures*, *68*, 42–49.

Ahmed, S., Ashraf, M. & Anwar-Us-Saadat, M. (2016). The Continuous Strength Method for slender stainless steel cross-sections. *Thin-Walled Structures*, *107*, 362–376.

AISI S100-16-C. (2016). *Commentary on North American Specification for the Design of Cold-Formed Steel Structural Members*. American Iron and Steel Institute, Washington, DC.

AISI S100-16. (2016). *North American Specification for the Design of Cold-Formed Steel Structural Members*. American Iron and Steel Institute, Washington, DC.

Aisyah Mohd Zaifuddin, S., Chen, D. H. & Ushijima, K. (2017). Estimation of maximum torsional moment for multicorner tubes. *Thin-Walled Structures*, *112*, 66–77.

Alsalah, A., Holloway, D. & Ghazijahani, T. G. (2017). Recovery of capacity lost due to openings in cylindrical shells under compression. *Journal of Constructional Steel Research*, *137*, 169–179.

Anbarasu, M. & Ashraf, M. (2017). Interaction of local-flexural buckling for cold-formed lean duplex stainless steel hollow columns. *Thin-Walled Structures*, *112*, 20–30.

ANSI/AISC 360. (2016). *Specification for Structural Steel Buildings*. American Institute of Steel Construction.

Anumolu, S., Abdelkarim, O. I. & ElGawady, M. A. (2016). Behavior of hollow-core steel-concrete-steel columns subjected to torsion loading. *Journal of Bridge Engineering*, *21*(10), 4016070.

Arrayago, I., Rasmussen, K. J. R. & Real, E. (2017). Full slenderness range DSM approach for stainless steel hollow cross-sections. *Journal of Constructional Steel Research*, *133*, 156–166.

AS/NZS 4600. (2005). *Cold-formed steel structures*. Australian / New Zealand Standard, Sydney, Australia.

AS/NZS 4673. (2001). *Cold-formed stainless steel structures*. Standards Australia, Sydney.

ASCE 8-02. (2002). *Specification for the Design of Cold-Formed Stainless Steel Structural Members*. American Society of Civil Engineers.

ASTM. (2015). *Standard Test Methods for Tension Testing of Metallic Materials, E8/E8M-15a*. American Society for Testing and Materials.

Baddoo, N. R. (2008). Stainless steel in construction: A review of research, applications, challenges and opportunities. *Journal of Constructional Steel Research*, *64*(11), 1199–1206.

Basler, K. (1960). *Strength of plate girders in shear, Fritz Engineering Laboratory Report No. 251 (20)*.

Batdorf, S. B., Stein, M. & Schildcrout, M. (1947). *Critical stress of thin-walled cylinders in torsion, Technical Note No. 1344, National Advisory Committee for Aeronautics, Washington, DC*.

Beck, J. & Kiyomiya, O. (2003). Fundemental pure torsional properties of concrete filled circular steel tubes. *Doboku Gakkai Ronbunshu*, *60*, 285–296.

Becque, J., Lecce, M. & Rasmussen, K. J. R. (2008). The direct strength method for stainless steel compression members. *Journal of Constructional Steel Research*, *64*(11), 1231–1238.

Bennett, J. G., Dove, R. C. & Butler, T. A. (1982). An investigation of buckling of steel cylinders with circular reinforced cutouts. *Nuclear Engineering and Design*, *69*(2), 229–239.

Bian, G., Peterman, K. D., Torabian, S. & Schafer, B. W. (2016). Torsion of cold-formed steel lipped channels dominated by warping response. *Thin-Walled Structures*, *98*, 565–577.

Chan, T. M. & Gardner, L. (2008). Bending strength of hot-rolled elliptical hollow sections. *Journal of Constructional Steel Research*, *64*(9), 971–986.

Chen, G. & Trahair, N. S. (1992). Inelastic nonuniform torsion of steel I-beams. *Journal of Constructional Steel Research*, *23*(1–3), 189–207.

Chen, M.-T. & Young, B. (2018). Experimental and numerical investigation on cold-formed steel semi-oval hollow section compression members. *Journal of Constructional Steel Research*, *151*, 174–184.

Chen, W. & Wierzbicki, T. (2000). Torsional collapse of thin-walled prismatic columns. *Thin-Walled Structures*, *36*(3), 181–196.

Cheng, B. & Li, C. (2012). Buckling behavior of strengthened perforated plates under shear loading. *Steel and Composite Structures*, *13*(4), 367–382.

Cooper, P. B. & Roychowdhury, J. (1990). Shear strength of plate girders with web openings. *Journal of Structural Engineering*, *116*(7), 2042–2048.

Dimopoulos, C. A. & Gantes, C. J. (2012). Experimental investigation of buckling of wind turbine tower cylindrical shells with opening and stiffening under bending. *Thin-Walled Structures*, *54*, 140–155.

Dimopoulos, C. A. & Gantes, C. J. (2013). Comparison of stiffening types of the cutout in tubular wind turbine towers. *Journal of Constructional Steel Research*, *83*, 62–74.

Donnell, L. H. (1933). *Stability of thin-walled tubes under torsion, Report No. 479, National Advisory Committee for Aeronautics, Washington, DC*.

EN 1993-1-1. (2005). *Eurocode 3: Design of steel structures - Part 1-1: General rules and rules for buildings*. CEN.

EN 1993-1-4:2006+A1. (2015). *Eurocode 3: Design of Steel Structures–Part 1-4: General Rules–Supplementary Rules for Stainless Steel*. CEN.

EN 1993-1-4. (2006). *Eurocode 3: Design of steel structures–Part 1.4: General rules–Supplementary rules for stainless steels*. CEN.

Feng, R. & Young, B. (2015). Experimental investigation of aluminum alloy stub columns with circular openings. *Journal of Structural Engineering*, *141*(11), 4015031.

Galambos, T. V. (1998). *Guide to stability design criteria for metal structures*. John Wiley & Sons.

Gardner, L. (2002). *A New Approach to Structural Stainless Steel Design, PhD Thesis*. Imperial College London, UK.

Gardner, L. (2005). The use of stainless steel in structures. *Progress in Structural Engineering and Materials*, *7*(2), 45–55.

Gardner, L. & Ashraf, M. (2006). Structural design for non-linear metallic materials. *Engineering Structures*, *28*(6), 926–934.

Gardner, L. & Nethercot, D. A. (2004a). Experiments on stainless steel hollow sections—Part 1: Material and cross-sectional behaviour. *Journal of Constructional Steel Research*, *60*(9), 1291–1318.

Gardner, L. & Nethercot, D. A. (2004b). Numerical Modeling of Stainless Steel Structural Components—A Consistent Approach. *Journal of Structural Engineering*, *130*(10), 1586–1601.

Hagen, N. C., Larsen, P. K. & Aalberg, A. (2009). Shear capacity of steel plate girders with large web openings, Part I: Modeling and simulations. *Journal of Constructional Steel Research*, *65*(1), 142–150.

Han, L.-H., Yao, G.-H. & Tao, Z. (2007). Performance of concrete-filled thin-walled steel tubes under pure torsion. *Thin-Walled Structures*, *45*(1), 24–36.

Hassanein, M. F. (2011). Finite element investigation of shear failure of lean duplex stainless steel plate girders. *Thin-Walled Structures*, *49*(8), 964–973.

Hassanein, M. F., Kharoob, O. F. & Liang, Q. Q. (2013). Circular concrete-filled double skin tubular short columns with external stainless steel tubes under axial compression. *Thin-Walled Structures*, *73*, 252–263.

Hassanein, M. F. & Silvestre, N. (2013). Flexural behavior of lean duplex stainless steel girders with slender unstiffened webs. *Journal of Constructional Steel Research*, *85*, 12–23.

Hill, H. N. (1944). *Determination of stress-strain relations from" offset" yield strength values, Technical Note No 927, National Advisory Committee for*

Aeronautics, Washington, DC.

Huang, H., Han, L.-H. & Zhao, X.-L. (2013). Investigation on concrete filled double skin steel tubes (CFDSTs) under pure torsion. *Journal of Constructional Steel Research*, *90*, 221–234.

Huang, Y. & Young, B. (2012). Material properties of cold-formed lean duplex stainless steel sections. *Thin-Walled Structures*, *54*, 72–81.

Huang, Y. & Young, B. (2013a). Experimental and numerical investigation of cold-formed lean duplex stainless steel flexural members. *Thin-Walled Structures*, *73*, 216–228.

Huang, Y. & Young, B. (2013b). Tests of pin-ended cold-formed lean duplex stainless steel columns. *Journal of Constructional Steel Research*, *82*, 203–215.

Huang, Y. & Young, B. (2014a). Experimental investigation of cold-formed lean duplex stainless steel beam-columns. *Thin-Walled Structures, 76*, 105–117.

Huang, Y. & Young, B. (2014b). The art of coupon tests. *Journal of Constructional Steel Research*, *96*, 159–175.

Huang, Y. & Young, B. (2018). Structural performance of cold-formed lean duplex stainless steel beams at elevated temperatures. *Thin-Walled Structures*, *129*, 20–27.

Jiao, P., Chen, Z., Xu, F., Tang, X. & Su, W. (2018). Effects of ringed stiffener on the buckling behavior of cylindrical shells with cutout under axial compression: Experimental and numerical investigation. *Thin-Walled Structures*, *123*, 232–243.

Keerthan, P. & Mahendran, M. (2012). New design rules for the shear strength of LiteSteel beams with web openings. *Journal of Structural Engineering*,

139(5), 640–656.

Keerthan, P. & Mahendran, M. (2013). Experimental studies of the shear behaviour and strength of lipped channel beams with web openings. *Thin-Walled Structures, 73,* 131–144.

Kim, K. & Yoo, C. H. (2008). Ultimate strengths of steel rectangular box beams subjected to combined action of bending and torsion. *Engineering Structures, 30*(6), 1677–1687.

LaBoube, R. A., Yu, W. W., Langan, J. E. & Shan, M. Y. (1997). Cold-formed steel webs with openings: Summary report. *Thin-Walled Structures, 27*(1), 79–84.

Lauwens, K., Debruyne, D. & Rossi, B. (2018). Stainless Steel I beams with slender webs submitted to torsion. *Eighth International Conference on Thin Walled Structures, Lisbon, Portugal*.

Lawson, R. M., Basta, A. & Uzzaman, A. (2015). Design of stainless steel sections with circular openings in shear. *Journal of Constructional Steel Research, 112,* 228–241.

Lawson, R. M. & Hicks, S. J. (2011). *Design of composite beams with large web openings: in accordance with Eurocodes and the UK National Annexes*. Steel Construction Institute.

Lundquist, E. E. (1932). *Strength tests on thin-walled duralumin cylinders in torsion, Technical Note No. 427, National Advisory Committee for Aeronautics, Washington, DC.*

Mahendran, M. & Keerthan, P. (2013). Experimental studies of the shear behavior and strength of LiteSteel beams with stiffened web openings. *Engineering Structures, 49,* 840–854.

Mahendran, M. & Murray, N. W. (1990). Ultimate load behaviour of box-columns under combined loading of axial compression and torsion. *Thin-Walled Structures*, *9*(1–4), 91–120.

McMahon, B., Peach, T. L., Spear, N. & Wilkinson, T. (2008). Shear capacity of LiteSteel beams with circular web openings. *Proc. of the Fifth International Conference on Thin-Walled Structures, Brisbane, Australia*, 419–424.

Mirambell, E. & Real, E. (2000). On the calculation of deflections in structural stainless steel beams: an experimental and numerical investigation. *Journal of Constructional Steel Research*, *54*(1), 109–133.

Moen, C. D. & Schafer, B. W. (2008). Experiments on cold-formed steel columns with holes. *Thin-Walled Structures*, *46*(10), 1164–1182.

Moen, C. D. & Schafer, B. W. (2010). Direct strength method for design of cold-formed steel columns with holes. *Journal of Structural Engineering*, *137*(5), 559–570.

Mohareb, M. & Nowzartash, F. (2003). Exact Finite Element for Nonuniform Torsion of Open Sections. *Journal of Structural Engineering*, *129*(2), 215–223.

Nadjai, A. & Johnson, D. (1998). Torsion in tall buildings by a discrete force method. *The Structural Design of Tall Buildings*, *7*(3), 217–231.

Nakai, H., Kitada, T. & Murayama, Y. (1990). On ultimate strength of horizontally curved box girder bridges. *JSCE, 36A*, 63–70.

Narayanan, R. & Chow, F. Y. (1985). Experiments on perforated plates subjected to shear. *The Journal of Strain Analysis for Engineering Design*, *20*(1), 23–34.

Narayanan, R. & Der-Avanessian, N. G.-V. (1985). Design of slender webs having rectangular holes. *Journal of Structural Engineering*, *111*(4), 777–787.

Narayanan, R. & Der Avanessian, N. G. V. (1984). Elastic buckling of perforated plates under shear. *Thin-Walled Structures*, *2*(1), 51–73.

Nie, J., Wang, Y. & Fan, J. (2012). Experimental study on seismic behavior of concrete filled steel tube columns under pure torsion and compression–torsion cyclic load. *Journal of Constructional Steel Research*, *79*, 115–126.

Nowzartash, F. & Mohareb, M. (2010). Plastic interaction relations for semi-elliptical hollow sections. *Thin-Walled Structures*, *48*(1), 42–54.

Omidvari, A. & Hematiyan, M. R. (2015). Approximate closed-form formulae for buckling analysis of rectangular tubes under torsion. *International Journal of Engineering-Transactions B: Applications*, *28*(8), 1226–1232.

Patton, M. L. & Singh, K. D. (2012). Numerical modeling of lean duplex stainless steel hollow columns of square, L-, T-, and+-shaped cross sections under pure axial compression. *Thin-Walled Structures*, *53*, 1–8.

Pellegrino, C., Maiorana, E. & Modena, C. (2009). Linear and non-linear behaviour of steel plates with circular and rectangular holes under shear loading. *Thin-Walled Structures*, *47*(6–7), 607–616.

Pham, C. H. (2017). Shear buckling of plates and thin-walled channel sections with holes. *Journal of Constructional Steel Research*, *128*, 800–811.

Pham, C. H. & Hancock, G. J. (2012). Direct strength design of cold-formed C-sections for shear and combined actions. *Journal of Structural Engineering*, *138*(6), 759–768.

Ramberg, W. & Osgood, W. R. (1943). *Description of stress-strain curves by three parameters, Technical Note No. 902, National Advisory Committee for Aeronautics, Washington, DC*.

Rasmussen, K. J. R. (2003). Full-range stress–strain curves for stainless steel

alloys. *Journal of Constructional Steel Research, 59*(1), 47–61.

Ridley-Ellis, D. (2000). *Rectangular hollow sections with circular web openings: fundamental behaviour in torsion, bending and shear, PhD thesis*. University of Nottingham.

Rossi, B. (2014). Discussion on the use of stainless steel in constructions in view of sustainability. *Thin-Walled Structures, 83*, 182–189.

Rossi, B. & Rasmussen, K. J. R. (2012). Carrying capacity of stainless steel columns in the low slenderness range. *Journal of Structural Engineering, 139*(6), 1088–1092.

Sachidananda, K. & Singh, K. D. (2015). Numerical study of fixed ended lean duplex stainless steel (LDSS) flat oval hollow stub column under pure axial compression. *Thin-Walled Structures, 96*, 105–119.

Sachidananda, K. & Singh, K. D. (2017). Structural behaviour of fixed ended stocky Lean Duplex Stainless Steel (LDSS) flat oval hollow column under axial compression. *Thin-Walled Structures, 113*, 47–60.

Saliba, N. & Gardner, L. (2013b). Cross-section stability of lean duplex stainless steel welded I-sections. *Journal of Constructional Steel Research, 80*, 1–14.

Saliba, N. & Gardner, L. (2013a). Experimental study of the shear response of lean duplex stainless steel plate girders. *Engineering Structures, 46*, 375–391.

Saliba, N., Real, E. & Gardner, L. (2014). Shear design recommendations for stainless steel plate girders. *Engineering Structures, 59*, 220–228.

Schafer, B. W. & Pekoz, T. (1998). Direct strength prediction of cold-formed steel members using numerical elastic buckling solutions. *14th International Specialty Conference on Cold-Formed Steel Structures*. St. Louis, Missouri.

Schwerin, E. (1924). Torsional stability of thin-walled tubes. *Proceedings of First*

International Congress for Applied Mechanics, 255–265.

Sezawa, K. & Kubo, K. (1931). *The Buckling of a Cylindrical Shell under Torsion, Report No. 76, Aeronautical Research Institute, Tokyo Imperial University* (Vol. 6).

Shakerley, T. M. & Brown, C. J. (1996). Elastic buckling of plates with eccentrically positioned rectangular perforations. *International Journal of Mechanical Sciences*, *38*(8–9), 825–838.

Shanmugam, N. E. (1997). Openings in thin-walled steel structures. *Thin-Walled Structures*, *28*(3–4), 355–372.

Shen, K., Wan, S., Mo, Y. L., Song, A. & Li, X. (2018). Behavior of single-box multi-cell box-girders with corrugated steel webs under pure torsion. Part I: Experimental and numerical studies. *Thin-Walled Structures*, *129*, 542–557.

Singh, T. G. & Singh, K. D. (2018). Experimental investigation on performance of perforated cold–formed steel tubular stub columns. *Thin-Walled Structures*, *131*, 107–121.

Sivakumaran, K. S. (2008). *Reinforcement schemes for CFS joists having web openings*. American Iron and Steel Institute.

Sonu, J. K. (2016). *Shear Behaviour of Lean Duplex Stainless Steel (LDSS) Rectangular Hollow Beams – a Finite Element Study, PhD thesis*. Indian Institute of Technology Guwahati.

Sonu, J. K. & Singh, K. D. (2017a). Shear behaviour of single perforated lean duplex stainless steel (LDSS) rectangular hollow beams. *Thin-Walled Structures*, *119*, 851–867.

Sonu, J. K. & Singh, K. D. (2017b). Shear characteristics of Lean Duplex Stainless Steel (LDSS) rectangular hollow beams. *Structures*, *10*, 13–29.

Tallin, A. & Ellingwood, B. (1985). Analysis of torsional moments on tall buildings. *Journal of Wind Engineering and Industrial Aerodynamics*, *18*(2), 191–195.

Theofanous, M. & Gardner, L. (2009). Testing and numerical modelling of lean duplex stainless steel hollow section columns. *Engineering Structures*, *31*(12), 3047–3058.

Theofanous, M. & Gardner, L. (2010). Experimental and numerical studies of lean duplex stainless steel beams. *Journal of Constructional Steel Research*, *66*(6), 816–825.

Toda, S. (1983). Buckling of cylinders with cutouts under axial compression. *Experimental Mechanics*, *23*(4), 414–417.

Trahair, N. S., Bradford, M. A., Nethercot, D. & Gardner, L. (2007). *The behaviour and design of steel structures to EC3*. CRC Press.

Umbarkar, K. R., Patton, L. M. & Singh, K. D. (2013). Effect of single circular perforation in lean duplex stainless steel (LDSS) hollow circular stub columns under pure axial compression. *Thin-Walled Structures*, *68*, 18–25.

Vilnay, O. & Burt, C. (1988). The shear effective width of aluminium plates. *Thin-Walled Structures*, *6*(2), 119–128.

Von Karman, T. (1932). The strength of thin plates in compression. *Trans. ASME*, *54*, 53–57.

Wan, H.-X. & Mahendran, M. (2015). Bending and torsion of hollow flange channel beams. *Engineering Structures*, *84*, 300–312.

Wanniarachchi, K. S., Mahendran, M. & Keerthan, P. (2017). Shear behaviour and design of Lipped Channel Beams with non-circular web openings. *Thin-Walled Structures*, *119*, 83–102.

Wardenier, J., Packer, J. A., Zhao, X. L. & Van der Vegte, G. J. (2002). *Hollow sections in structural applications*. Bouwen met staal Rotterdam,, The Netherlands.

White, G. J., Grzebieta, R. H. & Murray, N. W. (1993). Maximum strength of square thin-walled sections subjected to combined loading of torsion and bending. *International Journal of Impact Engineering*, *13*(2), 203–214.

Yamaki, N. & Matsuda, K. (1976). Postbuckling Behavior of Circular Cylindrical Shells Under Torsion. *Archive of Applied Mechanics*, *45*(2), 79–89.

Yu, W.-W. & Davis, C. S. (1973). Cold-formed steel members with perforated elements. *Journal of the Structural Division*, *99*(10), 2061–2077.

Zhang, X. & Han, Q. (2007). Buckling and postbuckling behaviors of imperfect cylindrical shells subjected to torsion. *Thin-Walled Structures*, *45*(12), 1035–1043.

Zhao, O., Afshan, S. & Gardner, L. (2017). Structural response and continuous strength method design of slender stainless steel cross-sections. *Engineering Structures*, *140*, 14–25.

Zhao, O., Gardner, L. & Young, B. (2016). Structural performance of stainless steel circular hollow sections under combined axial load and bending - Part 1: Experiments and numerical modelling. *Thin-Walled Structures*, *101*, 231–239.

Zhao, O., Rossi, B., Gardner, L. & Young, B. (2015). Behaviour of structural stainless steel cross-sections under combined loading–Part I: experimental study. *Engineering Structures*, *89*, 236–246.

Zhu, A., Zhu, H., Zhang, X. & Lu, Y. (2016). Experimental study and analysis of inner-stiffened cold-formed SHS steel stub columns. *Thin-Walled Structures*, *107*, 28–38.

Zhu, J.-H. & Young, B. (2010). Cold-formed-steel oval hollow sections under axial compression. *Journal of Structural Engineering*, *137*(7), 719–727.

Zhu, J.-H. & Young, B. (2012). Design of cold-formed steel oval hollow section columns. *Journal of Constructional Steel Research*, *71*, 26–37.

Appendix A

Design example of torsional capacity of LDSS SEHS member

Calculation of torsional capacity of LDSS SEHS member based on different design equation format - DSM, Eurocode and DBM are provided below for i) slender and ii) stocky section.

A1 ***Section 1***

A1.1 ***Cross-section dimensions***

h = 213.6 mm

b = 106.8 mm

t = 4 mm

l_f = 2 × b = 213.6 mm

L = 641 mm

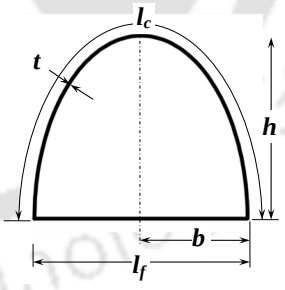

$$\lambda = \frac{l_f - 2\times t}{t}\sqrt{\frac{f_y \times 210000}{235 \times E}} = 81.67$$

Since λ > 46.8, the cross-section is slender section.

A1.2 *LDSS material property*

f_y = 560 MPa

$$\tau_y = \frac{f_y}{\sqrt{3}} = \frac{560}{\sqrt{3}} = 323.3\,\text{MPa}$$

E = 198200 MPa

$$G = \frac{E}{2\times(1+\nu)} = \frac{198200}{2\times(1+0.3)} = 76231\,\text{MPa}$$

υ = 0.3

A1.3 *Design torsional capacity*

A1.3.1 *Direct Strength Method (DSM)*

The torsional slenderness of the member can be calculated as

$$\lambda_T = \sqrt{\frac{\tau_y}{\tau_{cr}}}$$

where τ_{cr} = 486.94 N/mm^2 (obtained from FE analysis). Substituting the value, we get

$$\lambda_T = \sqrt{\frac{323.3}{486.94}} = 0.815$$

Yield torque (T_y) of the member is calculated using the following equation:

$$T_y = 2\times A_e \times t \times \tau_y$$

where A_e = area enclosed by mid line of cross-section and is calculated as

$$A_e = \frac{1}{2}\times\left[\pi\times\left(h-2\times\frac{t}{2}\right)\times\left(b-\frac{t}{2}\right)\right]$$

$$A_e = \frac{1}{2}\times\left[\pi\times\left(213.6-2\times\frac{4}{2}\right)\times\left(106.8-\frac{4}{2}\right)\right] = 34504\,\text{mm}^2$$

Substituting values in the above equation of T_y, we get

$T_y = 2 \times 34504 \times 4 \times 323.3 = 89.24$ kNm

The predicted design torsional capacity ($T_{us,DSM}$) based on DSM format is given by the following equations

$$T_{us,DSM} / T_y = 1 + (0.13 - 0.27 \times \lambda_T) \qquad \lambda_T \le 0.548$$

$$= 1.18 - 0.35 \times \lambda_T \qquad 0.548 < \lambda_T \le 0.91$$

$$= \frac{3.42}{\lambda_T^{0.38}} - \frac{2.61}{\lambda_T^{0.27}} \qquad \lambda_T > 0.91$$

Since calculated λ_T = 0.815, which is greater than 0.548 but less than 0.91, $T_{us,DSM}$ can be calculated as

$$T_{us,DSM} / T_y = 1.18 - 0.35 \times \lambda_T = 1.18 - 0.35 \times 0.815 = 0.895$$

Therefore,

$$T_{us,DSM} = 0.895 \times T_y = 0.895 \times 89.24 = 79.87 \text{ kNm}$$

A1.3.2 *Modified Eurocode*

The proposed torsional design strength ($T_{us,EN\text{-}modified}$) based on modified Eurocode format is as given below:

$$T_{us,EN-\text{modified}} = \chi_w \times T_y$$

where

χ_w = 1.2 $\qquad \bar{\lambda}_w \le 0.14$

$$= \frac{0.883}{\bar{\lambda}_w^{0.155}} \qquad 0.14 < \bar{\lambda}_w < 0.72$$

$$= \frac{1.023}{0.377 + \bar{\lambda}_w} \qquad \bar{\lambda}_w \geq 0.72$$

For the member considered,

$$\bar{\lambda}_w \left(or \lambda_T \right) = \sqrt{\frac{\tau_y}{\tau_{cr}}} = 0.815$$

Since $\bar{\lambda}_w > 0.72$, $\chi_w = \frac{1.023}{0.377 + \bar{\lambda}_w} = \frac{1.023}{0.377 + 0.815} = 0.858$

Therefore, $T_{us,EN-\mathrm{modified}} = 0.858 \times 89.24 = 76.56\,\mathrm{kNm}$

A1.3.3 *Deformation based method*

Rotation capacity (θ_c) in terms of torsional slenderness (λ_T) is proposed as below:

$$\frac{\theta_c}{\theta_y} = \frac{0.581}{\lambda_T^{1.41}} \qquad \lambda_T \leq 0.68$$

$$= \frac{1}{\lambda_T^{1.05}} \left(1 - \frac{0.222}{\lambda_T^{1.05}} \right) \qquad \lambda_T > 0.68$$

where $\theta_y = \frac{T_y \times L}{G \times J}$, J = torsional moment of inertia

$$J = \frac{4 \times A_e^2 \times t}{p}$$

$$p = \pi \times \left(h + b - t \right) \times \left[1 + 0.25 \times \left(\frac{h - b}{h + b - t} \right)^2 \right] + \left(2 \times b - t \right)$$

Substituting the values, we get

$$J = \frac{4 \times 34504^2 \times 4}{\pi \times (213.6 + 106.8 - 4)\left[1 + 0.25 \times \left(\frac{213.6 - 106.8}{213.6 + 106.8 - 4}\right)^2\right] + (2 \times 106.8 - 4)}$$

$$J = 15.46 \times 10^6 \text{ mm}^4$$

Since $\lambda_T > 0.68$ for the member considered,

$$\frac{\theta_c}{\theta_y} = \frac{1}{\lambda_T^{1.05}}\left(1 - \frac{0.222}{\lambda_T^{1.05}}\right)$$

$$= \frac{1}{0.815^{1.05}}\left(1 - \frac{0.222}{0.815^{1.05}}\right)$$

$$= 0.898 \quad (< 1)$$

For $\frac{\theta_c}{\theta_y} < 1$,

$$\frac{T_{us,DBM}}{T_y} = \left(\frac{\theta_c}{\theta_y}\right) = 0.898$$

$$T_{us,DBM} = 0.898 \times T_y = 0.898 \times 89.24 = 80.13 \text{ kNm}$$

A2 ***Section 2***

A LDSS SEHS member similar to Section 1 but with a member thickness of 10 mm was considered as Section 2 for strength calculation.

$$\lambda = \frac{l_f - 2 \times t}{t}\sqrt{\frac{f_y \times 210000}{235 \times E}} = \frac{213.6 - 2 \times 10}{10}\sqrt{\frac{560 \times 210000}{235 \times 198200}} = 30.76$$

Since $\lambda < 46.8$, the cross-section can be classified as stocky section.

A2.1 *Design torsional capacity*

A2.1.1 *Direct Strength Method (DSM)*

The torsional slenderness of the member can be calculated as

$$\lambda_T = \sqrt{\frac{\tau_y}{\tau_{cr}}}$$

where τ_{cr} = 2661.72 N/mm^2 (obtained from FE analysis). Substituting the value, we get

$$\lambda_T = \sqrt{\frac{323.3}{2661.72}} = 0.348$$

For calculation of T_y,

$$A_e = \frac{1}{2} \times \left[\pi \times \left(h - 2 \times \frac{t}{2} \right) \times \left(b - \frac{t}{2} \right) \right]$$

$$A_e = \frac{1}{2} \times \left[\pi \times \left(213.6 - 2 \times \frac{10}{2} \right) \times \left(106.8 - \frac{10}{2} \right) \right] = 32557 \text{ mm}^2$$

Substituting values in the equation of T_y, we get

$$T_y = 2 \times 32557 \times 10 \times 323.3 = 210 \text{ kNm}$$

Since calculated $\lambda_T \leq 0.548$,

$$T_{us,DSM} / T_y = 1 + \left(0.13 - 0.27 \times \lambda_T \right) = 1 + \left(0.13 - 0.27 \times 0.348 \right) = 1.036$$

Therefore,

$T_{us,DSM} = 1.036 \times T_y = 1.036 \times 210 = 217.56\,\text{kNm}$

A2.1.2 *Modified Eurocode*

For the member considered,

$$\bar{\lambda}_w \left(or \lambda_T\right) = \sqrt{\frac{\tau_y}{\tau_{cr}}} = 0.348$$

Since $0.14 < \bar{\lambda}_w < 0.72$, $\chi_w = \frac{0.883}{\bar{\lambda}_w^{0.155}} = \frac{0.883}{0.348^{0.155}} = 1.039$

Therefore, $T_{us,EN-\text{modified}} = 1.039 \times 210 = 218.19\,\text{kNm}$

A2.1.3 *Deformation based method*

For calculation of θ_y

$$p = \pi \times \left(h + b - t\right) \times \left[1 + 0.25 \times \left(\frac{h-b}{h+b-t}\right)^2\right] + \left(2 \times b - t\right)$$

$$= \pi \times \left(213.6 + 106.8 - 10\right) \times \left[1 + 0.25 \times \left(\frac{213.6 - 106.8}{213.6 + 106.8 - 10}\right)^2\right] + \left(2 \times 106.8 - 10\right)$$

= 1207.6 mm

Substituting the values, we get

$$J = \frac{4 \times 32557^2 \times 10}{1207.6} = 35.1 \times 10^6\, mm^4$$

Since $\lambda_T \le 0.68$ for the member considered,

$$\frac{\theta_c}{\theta_y} = \frac{0.581}{\lambda_T^{1.41}} = \frac{0.581}{0.348^{1.41}} = 2.57$$

For $\frac{\theta_c}{\theta_y} \geq 1$, the design strength is calculated as

$$\frac{T_{us,DBM}}{T_y} = \left(\frac{\theta_c}{\theta_y}\right)^{0.1} = 2.57^{0.1} = 1.098$$

$$T_{us,DBM} = 1.098 \times T_y = 1.098 \times 210 = 230.58 \text{ kNm}$$

Appendix B

Design example of torsional capacity of perforated LDSS SEHS member

Torsional capacity of perforated members (T_{up}) can be calculated as a factor of corresponding unperforated member via a reduction factor (R_f) as given below:

$$T_{up} = R_f \times T_{us}$$

B1 ***Section 1 member with a perforation on flat element***

B1.1 ***Reduction factor***

For Section 1 member ($\lambda_T = 0.815$) with perforation on flat element with perforation diameter ($d_{p,f}$) equal to 0.3 × l_f, reduction factor for perforation on flat element ($R_{f,f}$) can be calculated as

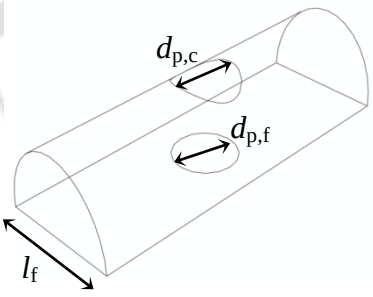

$R_{f,f} = A \times \lambda^2 + B \times \lambda + C$, where $\lambda = \lambda_T$ or $\bar{\lambda}_w$

For $\lambda \leq 1$,

$$A = -0.388\left(\frac{d_{p,f}}{l_f}\right)^2 + 0.646\left(\frac{d_{p,f}}{l_f}\right) = -0.388 \times 0.3^2 + 0.646 \times 0.3 = 0.158$$

$$B = 0.349\left(\frac{d_{p,f}}{l_f}\right)^2 - 0.756\left(\frac{d_{p,f}}{l_f}\right) = 0.349\times 0.3^2 - 0.756\times 0.3 = -0.195$$

$$C = -0.204\left(\frac{d_{p,f}}{l_f}\right)^2 - 0.076\left(\frac{d_{p,f}}{l_f}\right) + 1.002 = -0.204\times 0.3^2 - 0.076\times 0.3 + 1.002 = 0.96$$

Hence,

$$R_{f,f} = 0.158\times 0.815^2 - 0.195\times 0.815 + 0.96 = 0.906$$

B1.2 ***Design torsional strength***

Design torsional strength of perforated member can then be calculated as:

a) DSM: $T_{up,DSM} = R_{f,f}\times T_{us,DSM} = 0.906\times 79.87 = 72.36$ kNm

b) Modified EN: $T_{up,EN-\text{modified}} = R_{f,f}\times T_{us,EN-\text{modified}} = 0.906\times 76.56 = 69.36$ kNm

c) DBM: $T_{up,DBM} = R_{f,f}\times T_{us,DBM} = 0.906\times 80.13 = 72.59$ kNm

B2 ***Section 1 member with a perforation on curve element***

B2.1 ***Reduction factor***

Reduction factor for perforation on curve element ($R_{f,c}$) for Section 1 member with perforation diameter ($d_{p,c}$) equal to 0.5 × l_f is calculated as below:

$R_{f,c} = A\times\lambda^2 + B\times\lambda + C$, where $\lambda = \lambda_T$ or $\bar{\lambda}_w$

Since $\lambda > 0.75$,

$$A = -0.159\left(\frac{d_{p,c}}{l_f}\right)^2 + 0.165\left(\frac{d_{p,c}}{l_f}\right) = -0.159\times 0.5^2 + 0.165\times 0.5 = 0.043$$

$$B = 1.033\left(\frac{d_{p,c}}{l_f}\right)^2 - 1.026\left(\frac{d_{p,c}}{l_f}\right) = 1.033\times 0.5^2 - 1.026\times 0.5 = -0.255$$

$$C = -1.033\left(\frac{d_{p,c}}{l_f}\right)^2 + 0.274\left(\frac{d_{p,c}}{l_f}\right) + 1.00 = -1.033\times 0.5^2 + 0.274\times 0.5 + 1.00 = 0.878$$

Therefore, $R_{f,c} = 0.043\times 0.815^2 - 0.255\times 0.815 + 0.878 = 0.698$

B2.2 ***Design torsional strength***

Design torsional strength of perforated member can then be calculated as:

a) DSM: $T_{up,DSM} = R_{f,f}\times T_{us,DSM} = 0.698\times 79.87 = 55.75$ kNm

b) Modified EN: $T_{up,EN-\mathrm{modified}} = R_{f,f}\times T_{us,EN-\mathrm{modified}} = 0.698\times 76.56 = 53.43$ kNm

c) DBM: $T_{up,DBM} = R_{f,f}\times T_{us,DBM} = 0.698\times 80.13 = 55.93$ kNm

List of Publications

Journals

1. **Devi, S. V., Singh, T. G. & Singh, K. D.** (2019). Cold-formed steel square hollow members with circular perforations subjected to torsion. ***Journal of Constructional Steel Research***, *162*, 105730.
2. **Devi, S. V. & Singh, K. D.** (2019). Numerical investigation on torsional behaviour of lean duplex stainless steel semi elliptical hollow section members. (***Under review***)
3. **Devi, S. V. & Singh, K. D.** (2019). Finite element study of lean duplex stainless steel semi-elliptical hollow section members with circular perforation subjected to torsion. (***Under review***)
4. **Devi, S. V. & Singh, K. D.** (2019). Stiffening effects on torsional capacity of perforated stainless steel slender semi elliptical hollow section members. (***Manuscript prepared***)

Conferences

1. **Devi, S. V., Singh, T. G. & Singh, K. D.** (2019). Perforated cold formed YSt 310 steel hollow members under pure torsion. ***Ninth International Conference on Steel and Aluminium Structures***, Bradford, UK.

2. **Devi, S. V.** & **Singh, K. D.** (2019). Effect of geometric parameters on torsional behaviour of lean duplex stainless steel semi-elliptical hollow section members. ***Seventeenth International Symposium on Tubular Structures***, Singapore (***Accepted***).